

707

POLARISATION CORRELATION IN THE TWO-PHOTON DECAY OF METASTABLE
ATOMIC DEUTERIUM AND A TEST OF BELL'S INEQUALITY.

W. Perrie

Atomic Physics Laboratory, University of Stirling,

May 1985

3/86

UNIVERSITY OF STIRLING

NAME OF CANDIDATE: W. Perrie

Abstract of thesis entitled:

POLARISATION CORRELATION IN THE TWO-PHOTON DECAY OF METASTABLE
ATOMIC DEUTERIUM AND A TEST OF BELL'S INEQUALITY.

Submitted for the degree of Ph.D.

Atomic Physics Laboratory, May 1985

ABSTRACT

A 1-keV metastable atomic deuterium [D(2S)] beam of density about 10^4 atoms cm^{-3} has been produced by charge-exchange, in caesium vapour, of deuterons extracted from a radio-frequency ion source. The linear and circular polarisation correlation of the two photons emitted spontaneously by metastable atomic deuterium in a true second order radiative process have been measured for the first time. While the circular polarisation results confirm the conservation of angular momentum along the common axis of detection, the correlation in linear polarisation has been applied in a test of Bell's Inequality which allows a quantitative distinction to be made between the predictions of Quantum Mechanics and local realistic ("hidden variable") theories. The results are in agreement with Quantum Mechanics and violate Bell's Inequality by almost two standard deviations.

ACKNOWLEDGEMENTS

I would like to gratefully acknowledge the support and guidance of my principal supervisor, Professor H. Kleinpoppen, whose encouragement and constant enthusiasm was instrumental in bringing this project to a successful conclusion.

I also want to express my sincere appreciation to Dr. A.J. Duncan, whose active involvement at all stages of the work helped overcome many of the experimental difficulties and clarified some of the conceptual problems.

I would like to thank my colleagues at Stirling, in particular, Dr. H.J. Beyer, Dr. I. McGregor and Dr. M. Roberts for many helpful discussions.

Assistance from the staff of Shared Technical Services is greatly appreciated and in particular the technical expertise of the department staff, Mr. A.J. Duncan, and Mr. A. Sherman was invaluable.

Finally, I would like to express my deep appreciation to my family whose unswerving support and encouragement has been a source of inspiration, and in particular to my wife, who typed the thesis.

I acknowledge the financial assistance of the University of Stirling.

CONTENTS

<u>SECTION</u>	<u>PAGE</u>
INTRODUCTION	vi
CHAPTER I	1
I.1 Decay of the 2S state.....	1
I.2 Theory of Two-Photon Emission.....	2
I.2.1 Perturbation Theory.....	2
I.2.2 Emission of Two Photons.....	6
I.2.3 Characteristics of Two-Photon Radiation.....	8
I.3 Two-Photon State Vector for $\alpha = \pi$	10
I.4 Experimental Observations on the Hydrogenic 2S State..	12
CHAPTER II	16
II.2.1 Introduction.....	16
II.2.2 QM and the Copenhagen Interpretation.....	16
II.2.3 Search for Hidden Variables.....	19
II.2.4 Discovery of Bell's Theorem.....	20
II.2.5 The Einstein-Podolsky-Rosen-Bohm Gedanken experiment.	22
II.2.6 Non-Localilty Paradox and Furry's Hypothesis.....	24
II.3 Bell's Inequalities; Proof of Clauser and Horne.....	25
II.3.1 Objective Local Theories.....	25
II.3.2 Experimental Consequencies.....	28
II.3.3 Considerations of Symmetry.....	29
II.3.4 Incompatibility with Quantum Mechanics.....	30
II.3.5 Consequencies with a Supplementary Assumption.....	32
II.3.6 Symmetry Conditions.....	34
II.3.7 Bell's Inequalities in terms of Coincidence Rates....	34
II.3.8 Freedman's Simplified Form.....	35
II.4.1 Quantum Mechanical Coincidence Rates; Ideal Case....	36
II.4.2 Predictions for a particular Local Deterministic Model.....	36

II.4.3	Quantum Mechanical Coincidence Rate; Actual Experiment.....	37
CHAPTER III	Apparatus.....	39
III.3	Introduction.....	39
III.3.1	Vacuum System	39
III.3.2	Rectangular Tank.....	41
III.3.3	Pumping Speed at Source.....	42
III.4.1	The Ion Source.....	43
III.4.2	Extraction, Acceleration and Focussing.....	45
III.4.3	Observations on Extracted Ion Beam.....	46
III.4.4	Magnetic Separation.....	48
III.5.1	Caesium Cell.....	48
III.5.2	Production of Metastable Beam.....	50
III.5.3	Charge-Exchange Observations.....	51
III.6	System Interlock.....	54
III.7	Metastable Monitor System.....	56
III.8	Pre-Quench Plates.....	58
III.9	Coincidence Photomultipliers.....	59
III.9.1	Detection Electronics.....	61
III.9.2	Switch Unit.....	63
III.10	Background Radiation.....	64
III.11.1	Optical System.....	66
III.11.2	Focal Length of Lenses in UV.....	68
III.11.3	Effective Observation Volume.....	68
III.11.4	Pile-of-Plates Polarisers.....	70
III.11.5	Angular Acceptance of Polariser.....	72
III.11.6	Transverse Ray Displacements.....	73
III.11.7	Measured Transmittances ϵ_M, ϵ_m at $\lambda = 254\text{nm}$	73
III.11.8	Quarter Wave Plates.....	76

CHAPTER 4	Results.....	77
IV.4.1	Measurement Method.....	77
IV.4.2	Optimum Conditions for Best Statistical Accuracy.....	77
IV.4.3	Linear Polarisation Correlation.....	78
IV.4.4	Test of Bell's Inequality.....	79
IV.4.5	Circular Polarisation Correlation.....	82
IV.4.6	Check for Rotational Symmetry of Optical System.....	87
IV.4.7	Normalisation Procedure.....	87
IV.4.8	Spurious (Background) Coincidence Rate.....	89
CHAPTER V	Discussion and Conclusions.....	92
Appendix 1	Von Neumann's Assumption.....	96
Appendix 2	QM Predictions for Detection Probabilities and Geometrical Factors.....	97
Appendix 3	Data for Linear Polarisation Correlation.....	99
References	101

101
102
103
104
105
106
107
108
109
110
111
112
113
114
115
116
117
118
119
120
121
122
123
124
125
126
127
128
129
130
131
132
133
134
135
136
137
138
139
140
141
142
143
144
145
146
147
148
149
150
151
152
153
154
155
156
157
158
159
160
161
162
163
164
165
166
167
168
169
170
171
172
173
174
175
176
177
178
179
180
181
182
183
184
185
186
187
188
189
190
191
192
193
194
195
196
197
198
199
200

INTRODUCTION

The interest in polarisation correlation measurements between photon pairs goes back over three decades. Following a suggestion by Wheeler,¹ Wu and Shakhnov² in 1950 measured the linear polarisation correlation of the two photons emitted from the annihilation of singlet positronium, confirming a prediction of pair theory that these quanta, when detected, have orthogonal polarisations. Yang³ pointed out that such measurements could be important in nuclear physics in deciding the symmetry nature of mesons which decay into two photons.

More recently, attention has been focussed on the polarisation correlation of pairs of visible photons emitted from certain atomic cascades. The motivation for such experiments has been to test the now famous Bell's Inequalities⁴ which provide a quantitative criterion for comparing the predictions of so-called "Hidden Variable" theories with those of Quantum Mechanics (QM). The first suggestion (almost 50 years ago) that quantum mechanics was fundamentally incomplete and that its statistical features might be described by an underlying substructure was proposed by Einstein, Podolsky and Rosen⁵. Bohr⁶ vigorously defended the completeness of QM and his views appeared to be confirmed by the publication of von Neumann's⁷ proof on the mathematical impossibility of a hidden variable completion of QM. However, the realisation that von Neumann's proof is of limited relevance was put forward by Bohm⁸, and that the axioms on which the theorem is based are unreasonable, by Bell.⁹

In 1965, in fact, it was shown by J.S. Bell¹⁰ for the Gedanken experiment of Bohm¹¹ (involving spatially separated but correlated systems) that deterministic hidden variable theories satisfying a physically realistic locality condition can reproduce some, but not all of the statistical predictions of quantum mechanics.

Bell's analysis, which applied to ideal systems was extended by Clauser et al⁴ to cover actual systems and they specifically proposed an atomic cascade in which an excited atomic level decays to a state of lower energy via an intermediate state with a finite lifetime, as the area for a decisive test. They also pointed out that the results of two previous related experiments (Wu and Shaknov² on the 0.5 MeV gamma rays from positronium, and that of Kocher and Commins¹² on the photon pairs in the $6^1S_0 - 4^1P_1 - 4^1S_0$ cascade in calcium) were not sufficient to test Bell's Inequalities directly. However, they indicated that a simple extension of the Kocher-Commins experiment would allow for such a test.

This suggestion led to a remarkable series of experiments culminating in the most recent sophisticated experiments of Aspect and his collaborators¹³⁻¹⁵. Although the outcome of these experiments clearly favours QM, the debate regarding a causal completion of QM still continues and in the view of some has not yet been finally settled.¹⁶⁻²⁰

The work in this thesis reports for the first time the observation of the polarisation correlation of photon pairs emitted simultaneously from an atom. These measurements of such a fundamental process, interesting as they are in their own right, gain added significance when used as a test for the existence of hidden variables and of the idea of local realism.

The plan of the thesis is as follows; Chapter I discusses the decay modes of the hydrogenic 2S state, and presents the theory and characteristics of two-photon emission. Chapter II introduces briefly the reasons for considering the existence of hidden variables and the subtle Einstein-Podolsky-Rosen-Bohm¹¹ argument which led Bell to discover his famous theorem. A proof of Bell's theorem then follows.

Chapter III discusses the apparatus and experimental details. In Chapter IV, the experimental results and comparison with theory are presented. Finally, Chapter V completes the thesis with a discussion and conclusions.

CHAPTER I

I.1 Decay of the Hydrogenic 2S state

It is well known that the unperturbed hydrogenic $2^2S_{1/2}$ state decays predominantly, at low atomic number Z by the simultaneous emission of two electric dipole photons (2E1) and, at high Z by the emission of a single magnetic dipole (M1) photon. In the non-relativistic limit, decay of the $2S_{1/2}$ state to the ground $1S_{1/2}$ state by the emission of a single electric dipole or quadrupole photon is completely forbidden.

The non-relativistic calculations of the two-photon decay rate in hydrogen began with the early estimates of Breit and Teller²¹ who applied the pioneering multi-photon theory of Maria GÜppert Mayer²². Over the years, the 2E1 decay rates have been obtained with progressively greater accuracy²³⁻²⁷ culminating in the most recent relativistic calculations of Goldman and Drake²⁸ and confirmed by Parpia and Johnson²⁹. At low Z , they obtain for the 2E1 and M1 decay rates;

$$W_{1S}^{2S} (2E1) = 8.229 Z^6 s^{-1}$$

$$W_{1S}^{2S} (M1) = 2.496 \cdot 10^{-6} Z^{10} s^{-1}$$

Hence, the decay of the $2S_{1/2}$ state in hydrogen is determined by two-photon emission, with a lifetime $\tau(2S_{1/2}) = 8.229^{-1} = 0.1215s$, while the contribution from single photon M1 decay is negligible, with a lifetime $\sim 4 \cdot 10^5 s$ (Fig.1). In addition, since the energy of the $2S_{1/2}$ state lies above that of the $2P_{1/2}$ state by a small amount (the Lamb shift), there is the possibility of a cascade via the $2P_{1/2}$ level. This process however, is negligible due to the small energy separation of these states and has a lifetime of around $5 \cdot 10^9 s$.²⁴

Goldman and Drake²⁷ have also shown that the contribution to

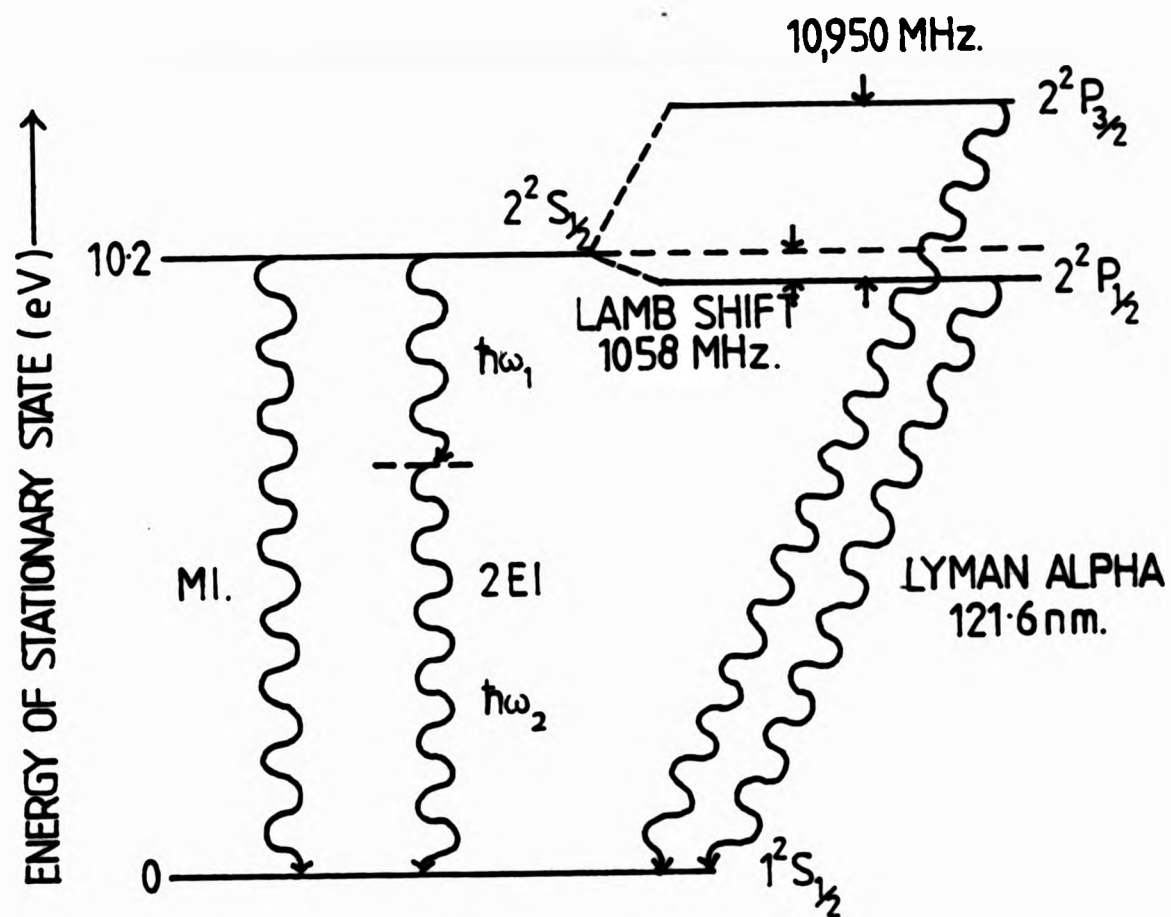


Fig. 1 ENERGY LEVEL DIAGRAM OF THE FIRST TWO LEVELS OF ATOMIC HYDROGEN IN THE ABSENCE OF HYPERFINE STRUCTURE. THE IMPORTANT DECAY MODES ARE SHOWN. THE 2P STATES HAVE A LIFETIME $\tau=1.6 \cdot 10^{-9}$ s. IN CONTRAST THE 2S STATE IS METASTABLE WITH A LIFETIME $\sim 1/8$ s AND DECAYS PREDOMINANTLY BY THE SPONTANEOUS EMISSIONS OF TWO PHOTONS.

the decay of the 2S state from higher order two-photon multipole modes such as E1-M2, 2M1, 2E2 etc. are negligible.

I.2 Theory of Two-Photon Emission

We now consider the relevant theory for the two-photon decay of the $2S_{1/2}$ state in hydrogen from which the spectral distribution, lifetime, angular correlation and most importantly the polarisation correlation can be deduced.

I.2.1 Perturbation Theory

The interaction of electrons and photons, in the Schrödinger picture, can be described by the equation of motion for the state vectors, the Schrödinger equation,

$$i\hbar \frac{\partial |\psi\rangle}{\partial t} = H|\psi\rangle$$

I.1

where $|\psi\rangle$ and H are the state vector and Hamiltonian, respectively of the complete system. H can be written as a sum of unperturbed and interaction Hamiltonians,

$$H = H_0 + H_{int} \\ = (H_1 + H_2) + H_{int} \quad \text{I.2}$$

where H_1 represents the Hamiltonian of the electrons alone, H_2 the Hamiltonian of the photons alone, and H_{int} their mutual interaction.

When H_{int} is small compared to H_0 , it can be regarded as a perturbation of H_0 , in which case the electrons and photons are described independently by the two Schrödinger equations,

$$i\hbar \frac{\partial}{\partial t} |\phi\rangle = H_1 |\phi\rangle \quad \text{electrons} \\ i\hbar \frac{\partial}{\partial t} |\omega\rangle = H_2 |\omega\rangle \quad \text{photons} \quad \text{I.3}$$

The state vectors of the Hamiltonian H_0 , which represent stationary states, are products of the state vectors of the non interacting parts of the system, $|\phi\rangle$ and $|\omega\rangle$,

$$|\psi\rangle = |\phi\rangle |\omega\rangle \quad \text{I.4}$$

and H causes transitions between these stationary states.

The Schrödinger equation can be transformed into the interaction picture by introducing the state vector in the interaction picture,

$$|\psi_i\rangle = e^{-i(H_0/\hbar)t} |\psi\rangle \quad \text{I.5}$$

and the interaction Hamiltonian in the interaction picture,

$$H_{int}^i = e^{i(H_0/\hbar)t} H_{int} e^{-i(H_0/\hbar)t} \quad \text{I.6}$$

to give the Schrödinger equation in the interaction picture,

$$i\hbar \frac{d}{dt} |\psi_i\rangle = H_{int}^i |\psi_i\rangle \quad \text{I.7}$$

If we formally integrate equation I.7 remembering that $|\psi_i\rangle = |\psi_i(t)\rangle$, then make a first order approximation by replacing $|\psi_i(t)\rangle$ by $|\psi_i(0)\rangle$, we obtain,

$$|\psi_i(t)\rangle = \left[1 + \frac{1}{i\hbar} \int_0^t H_{int}^i(\tau) d\tau \right] |\psi_i(0)\rangle \quad \text{I.8}$$

This technique of iteration can be continued indefinitely to yield an infinite series for $|\psi_i(t)\rangle$.

We now introduce a new operator, the scattering operator S whose matrix elements form the scattering matrix and write;

$$|\psi_i(t)\rangle = S |\psi_i(0)\rangle \quad \text{I.9}$$

S transforms the state vector at $t = 0$ to that at time t and is thus given by,

$$\begin{aligned} S = & 1 + \int_0^t \frac{1}{i\hbar} H_{int}^i(\tau) d\tau \\ & + \frac{1}{(i\hbar)^2} \int_0^t d\tau_1 \int_0^{\tau_1} H_{int}^i(\tau_1) H_{int}^i(\tau_2) d\tau_2 \\ & + \frac{1}{(i\hbar)^3} \int_0^t d\tau_1 \int_0^{\tau_1} d\tau_2 \int_0^{\tau_2} H_{int}^i(\tau_1) H_{int}^i(\tau_2) H_{int}^i(\tau_3) d\tau_3 \\ & + \dots \end{aligned} \quad \text{I.10}$$

The interaction Hamiltonian between an electron and radiation field described by the classical vector potential \underline{A} is given, in the Schrödinger picture by,³⁰

$$H_{int} = -\frac{e}{m} \underline{p} \cdot \underline{A} + \frac{e^2}{2m} |\underline{A}|^2 \quad \text{I.11}$$

where $-e$ is the electronic charge and \underline{p} is the electron's canonical momentum. The second term in equation I.11, which is quadratic in the vector potential, is small due to the presence of e^2 . Moreover, the A^2 term does not alter the state of tightly bound electrons when the wavelength of the radiation being considered, 121.6nm, is large compared with the dimensions of the region over which the electron wave functions are appreciably different from zero (a_0 , the Bohr radius). The A^2 term in this case does not excite transitions. We therefore ignore this term and make the approximation,

$$H_{int} = -\frac{e}{m} \underline{p} \cdot \underline{A} \quad \text{I.12}$$

The vector potential \underline{A} can be decomposed into radiation modes of the

electromagnetic field and in terms of travelling wave modes,³¹

$$\underline{A} = \sum_{\sigma=1}^2 \sum_n \sqrt{\frac{\hbar}{2\epsilon_0 \omega_n V}} \hat{e}_{n\sigma} (a_{n\sigma}^+ e^{-i\mathbf{k}_n \cdot \mathbf{r}} + a_{n\sigma} e^{i\mathbf{k}_n \cdot \mathbf{r}}) \quad \text{I.13}$$

In this equation, $a_{n\sigma}^+$, $a_{n\sigma}$ are creation and annihilation operators, $\hat{e}_{n\sigma}$ is a unit vector in the direction of polarisation where σ determines the two polarisation states, ϵ_0 is the permittivity of free space, ω_n and \mathbf{k}_n the angular frequency and wave-vector of the n 'th mode, and V is the "box" volume used to ensure periodic boundary conditions. This description regards the radiation field as dynamically equivalent to an infinite set of uncoupled harmonic oscillators, one for each mode of the electromagnetic field.

The probability that a system in an initial state $|\psi_i\rangle$ at $t = 0$ makes a transition to a final state $|\psi_f\rangle$ (at time t) in the energy range dE_f is just,³¹

$$P_f = |\langle \psi_f | \psi_i(t) \rangle|^2 = |\langle \psi_f | S | \psi_i(0) \rangle|^2 \quad \text{I.14}$$

Hence, the first term of equation I.10 for S does not give rise to any transitions since the initial and final states are orthogonal. The second term, which involves the vector potential once gives rise to single photon transitions. The third term, in which the vector potential appears twice, couples the electron to the radiation field twice and so gives rise to two-photon transitions. The fourth and higher terms correspond to higher multiphoton transitions.

The number of states occurring in the neighbourhood of E_f is usually large so that we sum over these states to obtain the total transition probability per unit time, given by,

$$W = \frac{1}{t} \int_f P_f \rho_f dE_f \quad \text{I.15}$$

where ρ_f is the density of final states function. In the case of single photon emission, this is given by,

$$\rho_f = \frac{2V}{(2\pi)^3} \frac{\omega^2}{\hbar c^3} \cdot 4\pi \quad \text{I.16}$$

I.2.2 Emission of Two photons

Emission (and absorption) of two photons is possible provided that the frequencies ω_1, ω_2 of these photons are related to the energy difference of the 2S and 1S levels by,

$$W_i - W_f = \hbar(\omega_1 + \omega_2) \quad \text{I.17}$$

The simultaneous emission of two photons of frequencies ω_1 and ω_2 must be described by the second order of perturbation theory (where the $\underline{p} \cdot \underline{A}$ term occurs twice in the matrix element for the scattering operator). The probability of finding the atom in the final state is now,

$$P_f = |\langle \psi_f | S' | \psi_i \rangle|^2 \quad \text{I.18}$$

where, from equation I.10,

$$S' = \frac{1}{(i\hbar)^2} \int_0^t d\tau_1 \int_0^{\tau_1} d\tau_2 H_{int}^i(\tau_1) H_{int}^i(\tau_2) \quad \text{I.19}$$

Hence, changing the Hamiltonian to the Schrödinger picture and performing the integrations,

$$P_f = 4 \left(\frac{e}{m}\right)^4 \left| \sum_j \frac{\langle \psi_f | \underline{p} \cdot \underline{A} | \psi_j \rangle \langle \psi_j | \underline{p} \cdot \underline{A} | \psi_i \rangle}{E_i - E_j} \right|^2 \quad \text{I.20}$$

where $|\psi_j\rangle \langle \psi_j|$ is the unit operator and the $|\psi_j\rangle$'s form a complete set of basis states.

Designating the state of the atom by $|\phi\rangle$ and the photon state by $|\omega\rangle$, the initial state of the physical system is,

$$|\psi_i\rangle = |\phi_i\rangle |0\rangle \quad \text{I.21}$$

where $|0\rangle$ represents the initial state of the radiation field i.e. no photons; and the final state,

$$|\psi_f\rangle = |\phi_f\rangle |\omega_1\rangle |\omega_2\rangle \quad \text{I.22}$$

where two photons of angular frequencies ω_1 and ω_2 have been added to the radiation field. The vector potential representing the creation of two photons is,

$$\underline{A} = \sqrt{\frac{\hbar}{2\epsilon_0 V}} \left[\sum_{\mathbf{k}_1} \frac{\underline{e}_{\mathbf{k}_1}}{\sqrt{\omega_1}} a_1^\dagger e^{-i\mathbf{k}_1 \cdot \underline{r}} + \sum_{\mathbf{k}_2} \frac{\underline{e}_{\mathbf{k}_2}}{\sqrt{\omega_2}} a_2^\dagger e^{-i\mathbf{k}_2 \cdot \underline{r}} \right] \quad \text{I.23}$$

Substituting this form of the vector potential which has two terms, into equation I.20, we have in the electric dipole approximation, ($e^{-ik \cdot r} \approx 1$),

$$P_f = \frac{\hbar^2}{\epsilon_0^2 V^2 \omega_1 \omega_2} \left(\frac{e}{m}\right)^4 \left| \sum_j \frac{\langle \phi_f | \hat{e}_1 \cdot p | \phi_j \rangle \langle \phi_j | \hat{e}_2 \cdot p | \phi_i \rangle}{E_i - E_j'} + \frac{\langle \phi_f | \hat{e}_2 \cdot p | \phi_j \rangle \langle \phi_j | \hat{e}_1 \cdot p | \phi_i \rangle}{E_i - E_j''} \right|^2 \quad \text{I.24}$$

These two terms can be illustrated by Feynman diagrams, Fig.2. The two photons can be emitted in "either order" and the decay can proceed by either diagram so that the probabilities are summed. If the W's represent the electron energies, then,

$$\begin{aligned} E_i &= W_i & E_j' &= W_j + \hbar \omega_1 \\ E_j'' &= W_j + \hbar \omega_2 & E_f &= W_f + \hbar \omega_1 + \hbar \omega_2 \end{aligned} \quad \text{I.25}$$

hence

$$E_i - E_j' = \hbar(\omega_{ij} - \omega_1), \quad E_i - E_j'' = \hbar(\omega_{ij} - \omega_2) \quad \text{I.26}$$

where $\hbar \omega_{ij}$ is the energy difference between the states W_i and W_j . The density of states with two photons present is given by,

$$\rho_f = \rho_1 \rho_2 \hbar d\omega_1 \quad \text{I.27}$$

Changing the matrix element of equation I.24 from the dipole velocity to dipole length form, then the transition probability per unit time, (provided t is large enough,) is given by, (using I.24, I.26, and I.27),

$$\begin{aligned} W &= \frac{2\pi}{\hbar} P_f \rho_f \\ &= \frac{2e^4}{\epsilon_0^2 \hbar^2 c^6 \pi^3} \left\langle \left| \sum_j \frac{\langle \phi_f | \hat{e}_1 \cdot r | \phi_j \rangle \langle \phi_j | \hat{e}_2 \cdot r | \phi_i \rangle}{\omega_{ij} - \omega_1} + \frac{\langle \phi_f | \hat{e}_2 \cdot r | \phi_j \rangle \langle \phi_j | \hat{e}_1 \cdot r | \phi_i \rangle}{\omega_{ij} - \omega_2} \right|^2 \right\rangle_{av.} \omega_1^3 \omega_2^3 d\omega_1 \\ &= A(\omega) d\omega_1 \end{aligned} \quad \text{I.28}$$

Once the average is taken over the directions of propagation and polarisation of the photons, the total transition probability is obtained by integrating I.29 to give,

$$W_{if}^{25} = \frac{1}{2} \int_0^{\omega_{if}} A(\omega) d\omega_1 \quad \text{I.30}$$

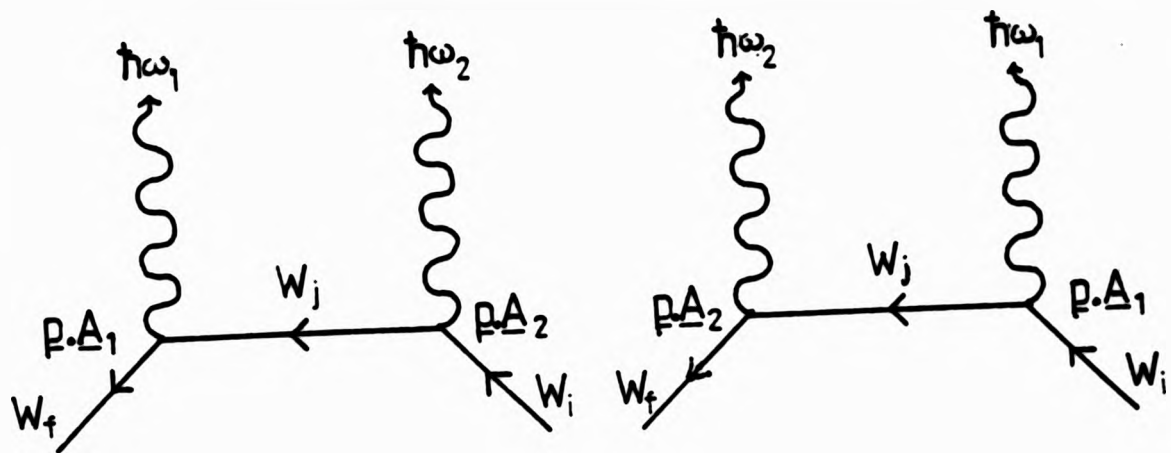


FIG. 2. FEYNMAN DIAGRAMS REPRESENTING THE SIMULTANEOUS EMISSION OF TWO PHOTONS. THE SOLID LINES REPRESENT THE ENERGIES WHILE THE VERTICES REPRESENT THE INTERACTIONS.

where the factor $\frac{1}{2}$ avoids counting each pair of photons twice.

The virtual states $|\psi_j\rangle$ which have opposite parity* are the P states of atomic hydrogen (both discrete and continuum) since the transitions are electric dipole and the summation in the matrix element includes integration over the continuum.

I.2.3 Characteristics of Two-Photon Radiation

As a consequence of the above theoretical considerations, the two photon process has the following characteristics;

- (1) The energies of the photons satisfy,

$$\hbar\omega_1 + \hbar\omega_2 = 10.2 \text{ eV} \quad \text{I.31}$$

- (2) Each photon can have any energy from zero to 10.2 eV, with the spectral distribution shown in fig. 3. On a frequency scale, the distribution is symmetric about 5.1 eV, or equivalently 243 nm. This fact is particularly fortunate since these photons fall in a wavelength range accessible to conventional polarisation analysis. Since the hydrogenic 2S state energy scales as Z^2 , then all such decays for higher Z yield photons of much shorter wavelength, in the x-ray region of the spectrum where direct polarisation measurements are very difficult.

- (3) The electric dipole length operator \underline{r} in the matrix element of

* i.e. odd

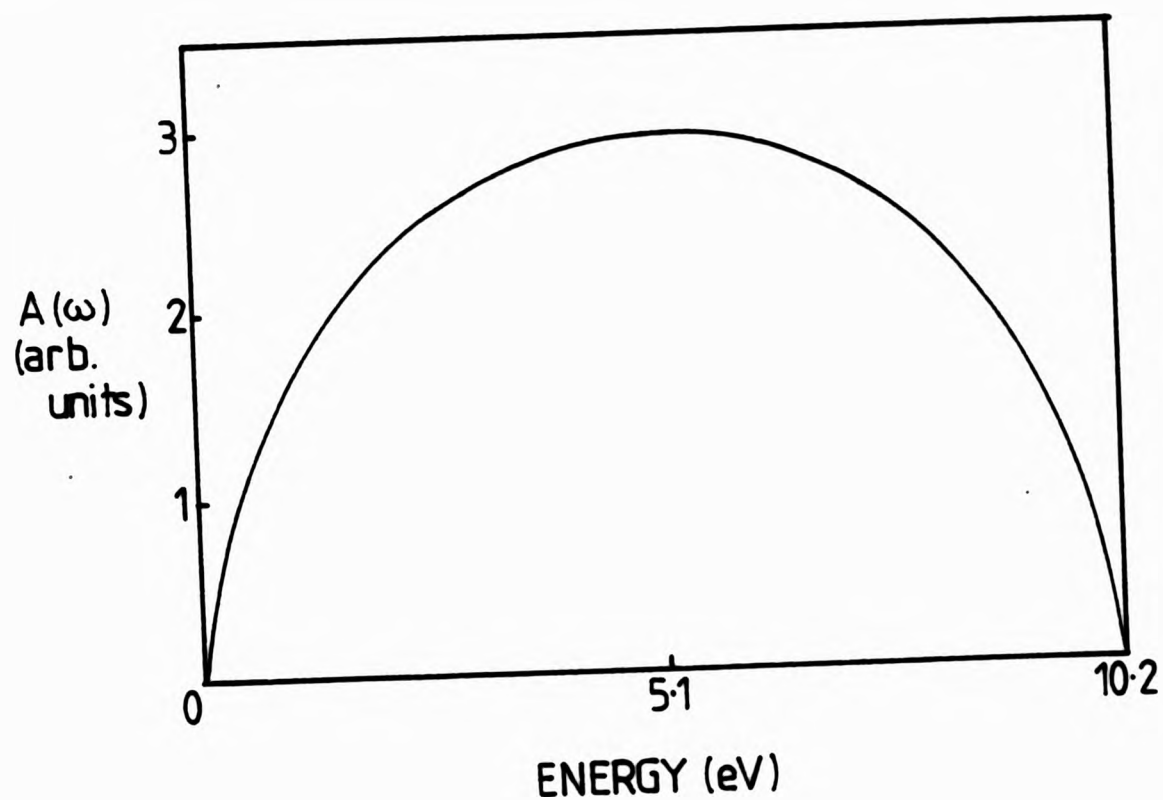


FIG. 3 THEORETICALLY PREDICTED TWO-PHOTON SPECTRAL DISTRIBUTION FOR METASTABLE HYDROGEN ON AN ENERGY SCALE.

equation I.29 is diagonal in both electronic and nuclear spin so the effects of fine and hyperfine structure may be neglected.

- (4) Breit and Teller²¹ have shown that the sum over intermediate states in equation I.29 is proportional to,

$$\hat{\mathbf{e}}_1 \cdot \hat{\mathbf{e}}_2 \sum_{n=2}^{\infty} \left[\frac{1}{\omega_{in} - \omega_1} + \frac{1}{\omega_{in} - \omega_2} \right] \quad \text{I.32}$$

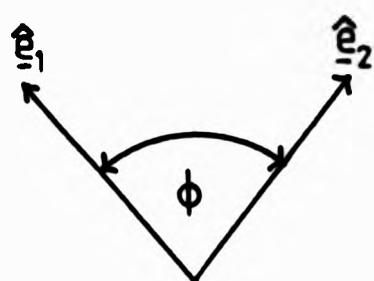
where n is the principal quantum number of the intermediate state.

Hence the transition probability,

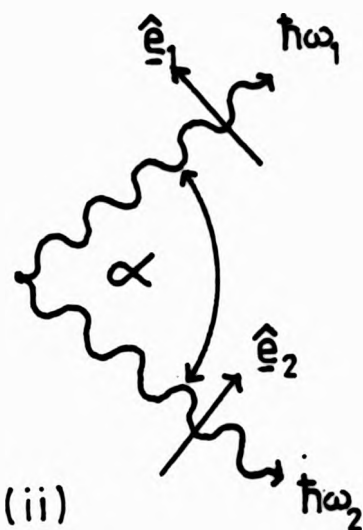
$$w_{1s}^{2s} \propto (\hat{\mathbf{e}}_1 \cdot \hat{\mathbf{e}}_2)^2 = \cos^2 \phi \quad \text{I.33}$$

where ϕ is the relative angle between the directions of linear polarisation of the photons and $\hat{\mathbf{e}}_1, \hat{\mathbf{e}}_2$ are unit vectors in the direction of linear polarisation, Fig. 4 (i). Thus, in an experiment with linear polarisers, one would expect to measure a two-photon polarisation correlation proportional to $\cos^2 \phi$, where ϕ is now the relative angle between the polariser transmission axes. By averaging over photon polarisation, one obtains the angular correlation factor, proportional to;

$$\langle (\hat{\mathbf{e}}_1 \cdot \hat{\mathbf{e}}_2)^2 \rangle_{av.} \propto (1 + \cos^2 \alpha) \quad \text{I.34}$$



(i)



(ii)

FIG. 4. DIAGRAM ILLUSTRATING THE ANGLES INVOLVED IN TWO-PHOTON EMISSION FROM THE 2S STATE. \hat{e}_1 AND \hat{e}_2 ARE UNIT VECTORS IN THE DIRECTION OF LINEAR POLARISATION.

where α is the angle between the propagation vectors of the photons, Fig. 4 (ii).

1.3 Two-Photon State Vector for $\alpha = \pi$

The form of the state vector for the case in which the photons travel in opposite directions is particularly interesting and follows from consideration of conservation of angular momentum and parity under inversion at the source.

Consider Fig. 5. in which we take the position of the emitting atom as the origin and assume that the apparatus is set to respond to pairs of photons travelling in the + z and - z directions (i.e. the detectors subtend infinitesimal solid angles).

The source emission is assumed isotropic, in which case the response of the detectors should be independent of the detectors joint rotation about the source centre or about their common axis.

Since the atom is initially and finally in a state of zero (orbital) angular momentum, then the two photons must carry away in total no net angular momentum along their common axis. Hence, in terms of right and left handed circular polarisation basis states, the photon pairs (travelling in opposite directions) can be represented by the ket vectors,

$$|R_1\rangle|R_2\rangle \quad \text{or} \quad |L_1\rangle|L_2\rangle$$

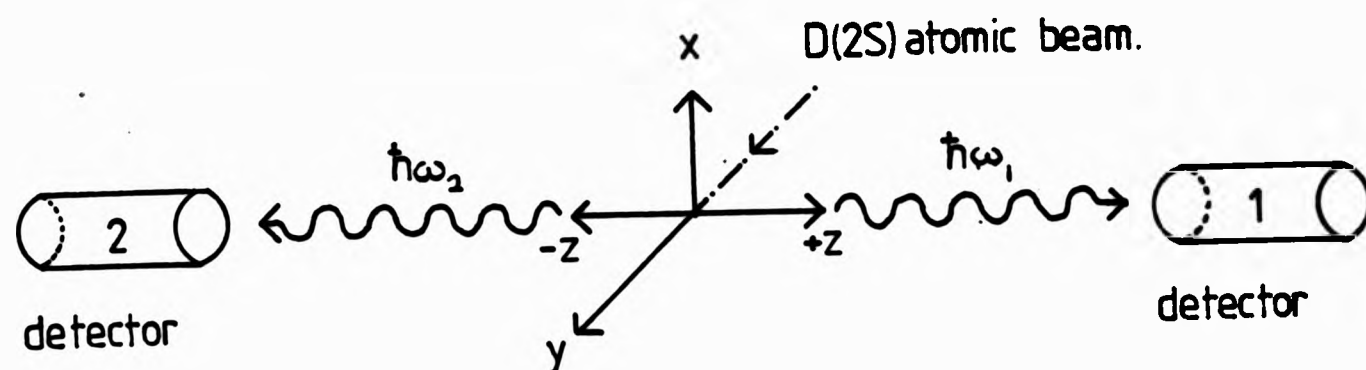


FIG.5 GEOMETRY FOR DETERMINING THE TWO-PHOTON STATE VECTOR WHEN PHOTONS TRAVEL IN OPPOSITE DIRECTIONS.

or by a superposition of these,

$$|R_1\rangle|R_2\rangle \pm |L_1\rangle|L_2\rangle \quad \text{I.36}$$

where $|R_1\rangle$ represents a right hand circularly polarised photon propagating in the $+z$ direction and $|R_2\rangle$ represents a right hand circularly polarised photon travelling in the $-z$ direction. Similarly for $|L_1\rangle$ and $|L_2\rangle$. The kets $|R_1\rangle|L_2\rangle$ and $|R_2\rangle|L_1\rangle$ can be excluded since these would imply a total angular momentum about the axis of $\pm 2\hbar$, inconsistent with momentum conservation and with the assumed isotropy of the source emission.

In addition, since the initial and final atomic states have even parity ($l = 0$) then the two-photon state vector must also have even parity. If P is the parity operator, then

$$P|R_1\rangle|R_2\rangle = |L_1\rangle|L_2\rangle \quad \text{I.37}$$

$$P|L_1\rangle|L_2\rangle = |R_1\rangle|R_2\rangle$$

and so the required form of the two-photon state vector in the case of the two-photon decay of metastable atomic hydrogen and deuterium is,

$$|\psi_+\rangle = \frac{1}{\sqrt{2}} (|R_1\rangle|R_2\rangle + |L_1\rangle|L_2\rangle) \quad \text{I.38}$$

where the normalisation $\langle\psi_+|\psi_+\rangle = 1$ has been included. Clearly, $|\psi_+\rangle$ has even parity since $P|\psi_+\rangle = |\psi_+\rangle$.

The above arguments are very general and hence in the case of a two-photon $J = 0-1-0$ atomic cascade, yields an identical state-vector. In contrast, in the case of the singlet state of positronium, where a

change of parity takes place, the appropriate state vector is,

$$|\psi_{-}\rangle = \frac{1}{\sqrt{2}} (|R_{1}\rangle|R_{2}\rangle - |L_{1}\rangle|L_{2}\rangle) \quad \text{I.39}$$

and accordingly, $P|\psi_{-}\rangle = -|\psi_{-}\rangle$. This state vector would also apply to a $J = 1-1-0$ atomic cascade. Note that as we should expect, the expression for $|\psi_{\pm}\rangle$ are invariant under a rotation, since,

$$\begin{aligned} R(\phi)|R_{1}\rangle &= e^{i\phi}|R_{1}\rangle \\ R(\phi)|L_{1}\rangle &= e^{-i\phi}|L_{1}\rangle \\ R(\phi)|R_{2}\rangle &= e^{-i\phi}|R_{2}\rangle \\ R(\phi)|L_{2}\rangle &= e^{i\phi}|L_{2}\rangle \end{aligned} \quad \text{I.40}$$

where $R(\phi)$ is the rotation operator. The basis states $|R\rangle$ and $|L\rangle$ are of course eigenvectors of both the spin and rotation matrices.

Finally, the state vector I.38 can be expressed in terms of linear polarisation basis states through the relations,

$$\begin{aligned} |R_{1}\rangle &= \frac{1}{\sqrt{2}} (|x_{1}\rangle + i|y_{1}\rangle), \quad |L_{1}\rangle = \frac{1}{\sqrt{2}} (|x_{1}\rangle - i|y_{1}\rangle) \\ |R_{2}\rangle &= \frac{1}{\sqrt{2}} (|x_{2}\rangle - i|y_{2}\rangle), \quad |L_{2}\rangle = \frac{1}{\sqrt{2}} (|x_{2}\rangle + i|y_{2}\rangle) \end{aligned} \quad \text{I.41}$$

Substituting these expressions into equation I.38 yields,

$$|\psi_{+}\rangle = \frac{1}{\sqrt{2}} (|x_{1}\rangle|x_{2}\rangle + |y_{1}\rangle|y_{2}\rangle) \quad \text{I.42}$$

as the appropriate two-photon state vector. This is a remarkable state in which neither photon has a definite polarisation prior to measurement, and yet, at the instant of detection both photons will be found to be either $|x\rangle$ polarised or $|y\rangle$ polarised when analysed using linear polarisers, hence the photon polarisations are highly correlated.

The implications of this type of state vector will be discussed in Chapter II more fully.

I.4 Experimental Observations on the Hydrogenic 2S State

For an appreciation of the accuracy of the theoretical predictions regarding the hydrogenic 2S state, we review briefly the experimental observations. The decay rates for example have been measured

for a number of Z in the range $1 \leq Z \leq 18$ where excellent agreement has been found throughout. The most recent highly accurate measurements (within 1%) have been carried out on He^+ (2S) by Hinds et al and on Ar^{+17} (2S) by Gould and Marrus. In the latter case, the accuracy obtained was sufficiently precise to observe the contribution to the total decay rate from the relativistic single photon M1 decay mode which, in hydrogenlike argon, makes a contribution of 3.2% to the total decay rate.

The first observation of two-photon emission was carried out by Lipeles et al in 1965 on He^+ (2S) using a coincidence counting technique. Since the photons were expected to have a continuous spectral distribution, centred around 20.1eV (608 Å), two "hard" u.v. windowless photomultipliers sensitive to photons in the range 200 - 1200 Å were used as detectors. They measured the coincidence signal as a function of angle between the detectors confirming the expected $(1 + \cos^2 \alpha)$ angular correlation.

In 1969, in the same laboratory, Artura, Novick and Tolk re-observed the two-photon decay in He^+ (2S) this time using one "hard" and one "soft" phototube. They confirmed the continuous nature of the spectral distribution by placing various broad band filters over the face of the "soft" u.v. phototube, sensitive from 1050 to 3500 Å.

In 1970, Schneider and Marrus observed the two-photon decay of the 2S_{1/2} state in hydrogenlike Argon (Ar^{+17}) using a beamfoil experiment. They observed a broad continuous single photon spectrum between the detector threshold and energy $E \sim 3\text{keV}$ in general agreement with the theoretical predictions for the spectral distribution. The spectrum of the sum energy $\hbar\omega_1 + \hbar\omega_2$ of the photons observed as true coincidences was shown to be a single peak at 3.3keV which is equal to the 2S - 1S energy separation. Further, by using a time-of-flight

method in which decay photons were monitored as the foil-detector separation was varied, the first lifetime measurement of a hydrogenic 2S state was carried out.

The first observations of two-photon emission in metastable atomic hydrogen was carried out by O'Connell et al in 1974, using a fast coincidence counting technique. The angular correlation of the coincidence count rate was investigated and results were in agreement with the predicted $(1 + \cos^2 \alpha)$ angular correlation.

Oed and Krüger³⁹ also observed this emission, estimating the decay rate over a narrow window of the spectral distribution and confirmed its continuous nature.

In 1983, Gould and Marrus, using a beam foil technique, re-observed the two-photon decay in hydrogenlike argon, Ar^{+17} , confirming in great detail the continuous nature of the spectral distribution. By taking into account very carefully a number of important systematic effects, their accurate measurements of the two-photon decay rate allowed them to derive the Lamb shift from the electric field quenching rate of the $2S_{1/2}$ state, in agreement with theory.

However, although the above observations on decay rates, spectral distributions, and angular correlations confirm the theory of two-photon emission for the 2S state to a high degree, and the angular correlations, which involve averaging over photon polarisations, have been confirmed in H (2S) and He^+ (2S), no direct polarisation correlation measurements have previously been reported for the two-photon decay of a hydrogenic 2S state which is a true second order emission process.

Since atomic hydrogen is unique in the hydrogenic isoelectronic sequence in producing two optical photons from the decay of the 2S state, the motivation for observing such a fundamental process in greater detail is quite clear.

In addition, since the photon polarisations are highly correlated the results bear on a well known and interesting problem in the quantum theory of measurement, first described by Einstein, Podolsky and Rosen,⁵ and elucidated by Bohr⁶ and Bohm.¹¹ This relates to the completeness or otherwise of the quantum mechanical interpretation, and Chapter II discusses the relevant theoretical and experimental developments which have led to the idea that observations on certain two-photon polarisation correlations can be used as a test of the range of validity of quantum mechanics in an area where it could, conceivably, break down.⁴⁵

CHAPTER II

II 2.1 Introduction

Quantum Mechanics is one of two major revolutionary physical theories developed this century (the other, of course is Relativity). There can be no doubt that QM is a tremendously successful theory which has increased greatly our understanding of nature on the atomic and nuclear level, giving highly accurate predictions regarding the structure of matter, electromagnetic radiation and their mutual interaction*.

Since QM was developed, however, there have been repeated suggestions that its statistical features possibly might be described by an underlying deterministic substructure, a quantum state representing a statistical ensemble of "hidden variable" states. The stimulus for such ideas arose mainly from the dissatisfaction with the presently accepted interpretation of the quantum theory, known as the Copenhagen-Göttingen interpretation, due mainly to the efforts of Bohr, Heisenberg and Born.⁴⁷

It is well known that a number of eminent physicists who contributed to the development of quantum theory, most notably, Planck, Einstein, Schrödinger and de Broglie, expressed deep concern over its final formulation.

We now review briefly the QM formalism and describe the main philosophy behind the Copenhagen interpretation.

II 2.2 QM and the Copenhagen Interpretation

Quantum mechanics makes quantitative predictions about the outcome of a large number of identically conducted experiments on an ensemble of identically prepared microscopic physical systems.

* Interestingly, atomic hydrogen has played a central role in this development since this simple atomic system has often been used as the testing ground for ever greater refinements of the theory.⁴⁶

In a QM system, physical 'observables' are represented by Hermitian operators in a complex linear vector space. Observables with commuting operators can be measured simultaneously while those with non-commuting operators cannot. Every measurement of an observable yields one of the eigenvalues of the corresponding operator. The QM state is represented by a state vector $|\psi\rangle$ in the linear vector space (whose time variation satisfies the Schrödinger equation) and the statistical expectation value of an observable A is given by;

$$\begin{aligned}\langle A \rangle &= \langle \psi | A | \psi \rangle / \langle \psi | \psi \rangle \\ &= \langle \psi | A | \psi \rangle\end{aligned}\tag{2.1}$$

Alternatively, if the ensemble of the system is described by a density operator ρ (a Hermitian matrix) which acts in a Hilbert space, then the expectation value of A is given by,⁴⁸

$$\langle A \rangle = \text{trace}(\rho A)\tag{2.2}$$

where, for the pure case, $\rho = |\psi\rangle\langle\psi|$, so that

$$\rho^2 = \rho\tag{2.3}$$

and expresses the fact that ρ is "idempotent".

Regarding the microscopic systems of interest, one rejects the notion that objective physical properties can be attributed to them. QM therefore concerns the interaction of microsystems with experimental apparatus and not their intrinsic character.⁴⁹

One divides microscopic/macroscopic systems arbitrarily. For example, if $|\psi\rangle = \alpha|a_1\rangle + \beta|a_2\rangle + \gamma|a_3\rangle$ is the state vector of a given QM system, then when a system in state $|\psi\rangle$ enters an apparatus designed to measure an observable A, the apparatus randomly records one of the eigenvalues a_1, a_2, a_3 , with probabilities $|\alpha|^2, |\beta|^2, |\gamma|^2$ respectively. For an ensemble of identical systems all in the pure state $|\psi\rangle$, the result of a series of measurements for observable A turns the ensemble into a mixture i.e.

$$\rho_{\text{before}} = |\psi\rangle\langle\psi| = \begin{pmatrix} \alpha^*\alpha & \beta^*\alpha & \gamma^*\alpha \\ \alpha^*\beta & \beta^*\beta & \gamma^*\beta \\ \alpha^*\gamma & \beta^*\gamma & \gamma^*\gamma \end{pmatrix} \quad 2.4$$

$$\text{while } \rho_{\text{after}} = \begin{pmatrix} \alpha^*\alpha & 0 & 0 \\ 0 & \beta^*\beta & 0 \\ 0 & 0 & \gamma^*\gamma \end{pmatrix} \quad 2.5$$

i.e. all off-diagonal 'interference terms' disappear. This process, in which a change of state occurs (reduction of the wave-packet) is not describable by the Schrödinger equation. Rather, the state vector reduction has already taken place at the time when we consider any definite experimental set-up and so is not really a physical event. If it were, it would be in contradiction with relativity since the probability amplitude at the moment of detection would have to become zero instantaneously at other points in space.

In principal, no causal description can be given why a particular eigenvalue results in a given measurement. The state vector, therefore, is used merely as a tool for predicting the relative probability for the different outcomes when the given quantum system interacts with the measurement apparatus.

This interpretation clearly requires a radical departure from classical notions on causality, determinism, physical reality,* and in particular on the nature of measurement. (In classical mechanics, the measurement process yields information on an already existing state of affairs, while in QM an observable acquires a

*This interpretation has far reaching consequences regarding the nature of physical reality since the microscopic system of interest and the measuring device constitutes from this point of view an indivisible whole.

definite value as a result of a measurement).

In particular, the inability of QM to predict with certainty the behaviour of a single microscopic system (which has been found unsatisfying to many individuals) stimulated the search for a more complete picture of the measurement process. This effort has resulted in theories with further degrees of freedom not contained in QM and known as "hidden variable" theories. (For a survey of such theories, the reader is referred to the work of Belinfante⁵⁰).

II 2.3 Search for Hidden Variables

J.S. Bell¹⁰ has described the search for hidden variables in the following manner; "It is interesting to ask if the statistical element (in QM) be thought of as arising, as in classical statistical mechanics because the states in question are averages over better defined states for which individually, the results would be quite determined".

These hypothetical states, termed "dispersion free" would be specified not only by the QM state vector $|\psi\rangle$ but also by further parameters or "hidden variables" λ whose function is to reproduce the measurable peculiarities of QM when averaged over.

The real impetus to search for hidden variables, without doubt, came from a classic paper by Einstein, Podolsky and Rosen⁵ in 1935 (EPR) in which they questioned the completeness of the QM description of physical reality. By considering a system of two spatially separated but QM correlated particles and making some assumptions about the nature of reality, they showed that the results of various experiments are predetermined but that this fact is not part of the QM description and hence that description is incomplete. They concluded that QM should be supplemented by postulating the existence of additional variables, the specification of which would pre-

determine the result of measuring any observable of a system. As a result, the complete theory would provide a causal description for all those processes that quantum theory treated as acausal. They believed the predictions of QM to be correct, but only as consequence of the statistical distributions of the hidden variables.

Bohr^b replied to EPR defending the completeness of QM and criticised EPR's argument on the basis that their formulation of a "criterion of physical reality" contained an essential ambiguity when applied to a quantum system. He concluded that the whole realistic viewpoint is inapplicable to microscopic systems. This view was further strengthened by the publication of a famous paper by von Neumann⁷ on the mathematical impossibility of such a hidden variable completion of QM. This theory could not tolerate "dispersion free ensembles" and had to be considered objectively false if hidden variables existed. He stated that, "we need not go any further into the mechanism of the hidden parameters since we now know that the established results of quantum mechanics can never be re-derived with their help". This claim stifled any progress in the search for hidden variable theories for nearly two decades.

It was first realised by Bohm⁸ that von Neumann's theorem in fact did not have the generality and exhaustiveness attributed to it. Bell⁹ was first to pinpoint the axiom (discussed in appendix I) by which von Neumann's formulation violated the elementary principles of any realistic hidden variables theory. He also demonstrated in this paper that the assumptions contained in the impossibility proofs of Jauch and Piron⁵¹ and Gleason⁵² were unreasonable. The way was then open for a causal completion of QM.

II.2.4 Discovery of Bell's Theorem

In 1965 a major discovery took place. J.S. Bell¹⁰ showed that for the Gedanken experiment of Bohm¹¹ in which one considers the quantum

mechanical correlations between spatially separated particles), that no deterministic hidden variable theory, satisfying a reasonable condition of locality, could reproduce all of the statistical predictions of quantum mechanics. In particular, he discovered an upper bound set on the strength of the correlations allowed by such theories expressed in the now celebrated Bell Inequality and that in certain situations, quantum mechanical predictions violate this inequality.

In fact, it is the requirement of locality, or more precisely, that the result of a measurement on one system be unaffected by operations (measurements) on a distant system with which it has interacted in the past that creates the essential difficulty.

Bell's original analysis assumed ideal apparatus and systems and so was stated in a form not directly applicable to real experiments. His analysis was subsequently extended by Clauser et al⁴ to apply to realisable experiments this being possible using a reasonable supplementary assumption. They specifically proposed in this paper an atomic cascade experiment as the experimental area where a decisive test could be made, and derived the conditions for such an experiment.

Bell's theorem has subsequently been generalized and shown to apply to a much broader family of hidden variable theories, termed local realistic theories⁵³ (stochastic theories) of which deterministic hidden variable theories are a sub-group. Hence, it would appear that it is the objectivity of the associated systems and their locality which produces the incompatibility with quantum mechanics, not their deterministic character. The great importance of Bell's theorem lies in the fact that it points to a single experimental arrangement in which all such hidden variable theories can be tested against quantum mechanics.

$$|\psi\rangle = \frac{1}{\sqrt{2}} (|x_1\rangle|x_2\rangle + |y_1\rangle|y_2\rangle)$$

The Gedanken experiment of Bohm¹¹ is central to Bell's theorem and consequently, we now present this important argument along with the assumptions therein.

II 2.5 The Einstein - Podolsky-Rosen-Bohm Gedanken experiment

There are four premises on which the important argument of EPR rests;

- (i) In a complete theory, there is an element corresponding to each element of reality.
- (ii) A sufficient condition for the the reality of a physical quantity is the possibility of predicting it with certainty (i.e with probability equal to unity) without disturbing the system.
- (iii) Some of the quantum mechanical predictions concerning observations on a system of two spatially separated particles are correct.
- (iv) Action-at-a-distance has no meaning in nature.

With these premises, EPR showed that for spatially separated particles which have previously interacted, two physical quantities described by non-commuting operators can have simultaneous reality, contrary to the QM description. A conceptually equivalent but simpler form of their argument was stated by Bohm¹¹ in terms of discrete states, in which a source emits pairs of spin $\frac{1}{2}$ particles prepared in the singlet $S = 0$ state.

We consider the optical transposition of Bohm's Gedanken experiment first described by Bohm and Aharonov⁵⁴ since this has more relevance to the present experiment, and the experimental situation envisaged is shown in Fig 6.

A source emits correlated pairs of photons which counter propagate along $\pm Oz$. Suppose that the two-photon state vector is described by;

$$|\psi\rangle = \frac{1}{\sqrt{2}} (|x_1\rangle|x_2\rangle + |y_1\rangle|y_2\rangle)$$

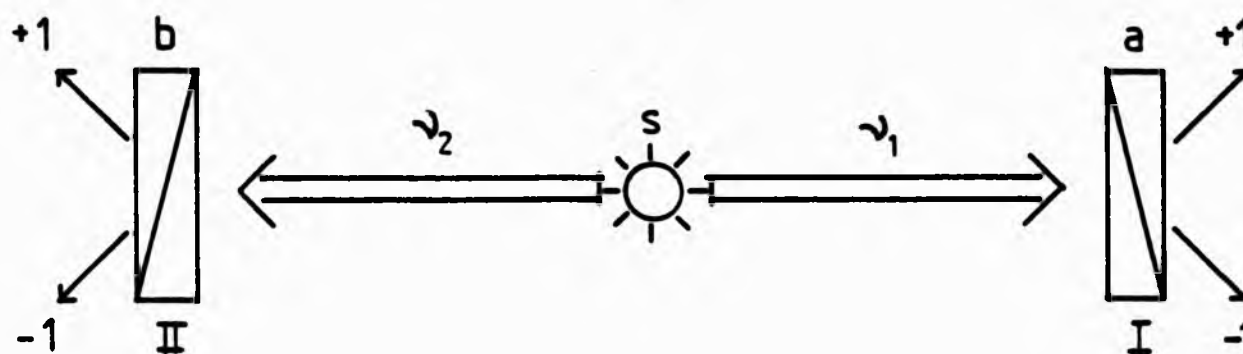


FIG. 6 EPR-BOHM GEDANKEN EXPERIMENT WITH CORRELATED PAIRS OF PHOTONS. ANALYSER I IN ORIENTATION a IS FOLLOWED BY TWO DETECTORS AND A RESULT $+1$ (-1) CORRESPONDS TO A LINEAR POLARISATION FOUND PARALLEL (PERPENDICULAR) TO a . ANALYSER II IN ORIENTATION b ACTS SIMILARLY.

where $|x_1\rangle$, $|x_2\rangle$, $|y_1\rangle$, $|y_2\rangle$ are linear polarisation basis states. We have shown previously (section I.3) that such a state vector describes the two photons emitted in a $J = 0-1-0$ atomic cascade and also the two photons emitted from the spontaneous decay of metastable atomic deuterium.

After the photons have separated far enough so that they cease to interact, one performs correlated measurements of their states of linear polarisations along arbitrary directions a and b with analysers I, II.

Suppose photon 1, as a result of a measurement is found to be polarised along the x -axis (y -axis) the probability of which is 50%, then one can predict with certainty and without disturbing photon 2 that it will be polarised along the x -axis (y -axis) if it is also measured, (EPR (ii)). In accordance with the measurement, the reduction of the state vector yields one of the two states $|x_1\rangle |x_2\rangle$ or $|y_1\rangle |y_2\rangle$ and shows that quantum mechanics predicts a strong correlation between the observed photon polarisations. Let us consider that, while the photons are in flight, we decide to rotate the analysers, defining a new rotated x' , y' basis. The two-photon state vector $|\psi\rangle$ is rotationally invariant. Then, a measurement of the state of linear polarisation of photon 1 with respect to the primed axes

yielding $|x'_1\rangle$ or $|y'_1\rangle$ allows one again to predict the linear polarisation state of photon 2. If, as EPR assume that,⁵ "since at the time of measurement the two systems (photons) no longer interact, no real change can take place in system 2 (photon 2) in consequence of any measurement on photon 1", (EPR iv), then photon 2 can be left in different polarisation states $|x\rangle$ or $|x'\rangle$, say depending on what one chooses to measure on photon 1. The specification of photon 2 with respect to both the x, y and x', y' axes is more than is allowed by quantum mechanics since in general, these observables do not commute. EPR conclude that the polarisation of photon 2 and hence photon 1 must have been determined beforehand, contrary to the quantum mechanical description, hence, quantum mechanics at least in this particular situation, would appear to be incomplete.

II 2.6 Non-Locality "Paradox" and Furry's Hypothesis

⁵⁴ Bohm and Aharonov first pointed to an interesting interpretation of the EPR argument in terms of a non-locality "paradox", related to the observed strong correlations between the separated systems. The non-factorisable form of the state vector, equation 2.6 represents a highly correlated state of photon polarisation involving interference between the two terms. This polarisation interference persists, even when the photons are remote from each other and have different frequencies, hence the term non-local. If, as a result of a measurement on photon 1 the wave function collapses so that photon 2 instantaneously assumes the polarisation state corresponding to that of photon 1, then one might suppose that there exists instantaneous interactions between the photons or between the photons and the apparatus, responsible for this effect. Clearly such interactions would be outside the scope of quantum theory and would in general be in contradiction with relativity.

It has been shown recently however, that even if such interactions do exist, that no signals (information) can be transmitted from one system to another at speeds less than or greater than the speed of light.⁵⁵ The fact that the outcome of a measurement on photon 1 is intrinsically indeterministic introduces a random element into the system sufficient to destroy any information carrying ability of such a system.

⁵⁶ Schrödinger and Furry suggested that the above "paradox" could be resolved in a suitably modified theory in which the polarisation interference was eliminated. Then, the non-factorising pure state equation 2.6 is assumed to evolve towards a correlated "mixture" of factorising states when the photons separate far enough. This localisation process then occurs over distances of the order of the coherence length of the wave packets associated with the emitted photons. However, this process would lead to a significant reduction in the observed correlation and experimental results in both positron annihilation and atomic cascades to date refute this hypothesis.⁵⁸

II.3 Bell's Inequalities; Proof of Clauser and Horne

Since the original discovery of Bell's theorem, stronger versions which constrain actual systems have been proved by Bell himself and by others.⁵⁹

⁵³ Bell's theorem was modified by Clauser and Horne for a broad class of theories which they designate objective local theories (OLT) including inherently stochastic theories. Their proof is noteworthy in that it defines an experiment which might actually be carried out and which requires no auxiliary assumptions. We follow their derivation closely.

II .3.1 Objective Local Theories

The experimental arrangement used to formulate the proof is shown

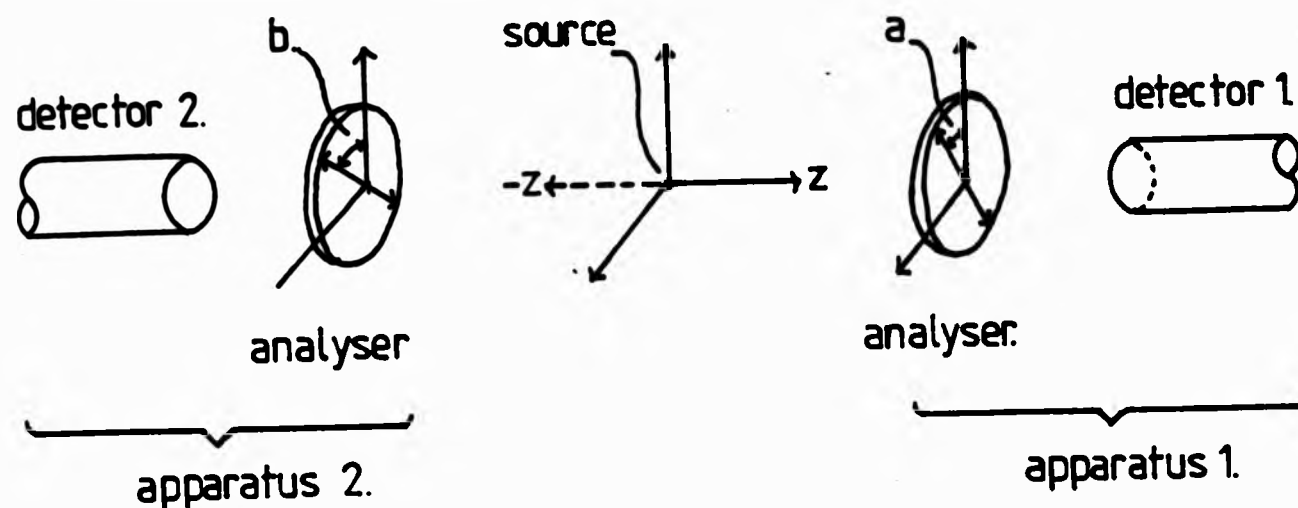


FIG. 7. APPARATUS CONFIGURATION USED FOR A DISCUSSION OF OBJECTIVE LOCAL THEORIES. A SOURCE EMITTING PARTICLE PAIRS IS VIEWED BY TWO APPARATUSES EACH CONSISTING OF AN ANALYSER AND ASSOCIATED DETECTOR. THE ANALYSERS HAVE EXTERNALLY ADJUSTABLE PARAMETERS a AND b WHICH REPRESENT THE ANGLES BETWEEN THE ANALYSER AXES AND A FIXED REFERENCE AXIS.

in fig. 7. A source of coincident two particle emissions is viewed by two analyser-detector assemblies 1 and 2. Each analyser has externally adjustable parameters a and b , respectively. Thus a, b , might represent the orientation axes of linear polarisers for photons or equivalently the directions of the field gradients of Stern-Gerlach magnets for spin $\frac{1}{2}$ particles. Since the relevant source-apparatus geometry is assumed constant and since other additional components (eg. filters, etc) remain in place throughout the experiment, we ignore these in the discussion.

Let the source emit N two-particle systems in a given period of time while the analysers are set to positions a and b . During this period, let $N_1(a)$ and $N_2(b)$ denote the number of counts at detectors 1 and 2, respectively and $N_{12}(a,b)$ the number of coincidence counts from the two detectors. If N is large enough, then the ensemble probabilities of obtaining these results are;

$$P_1(a) = N_1(a) / N$$

$$P_2(b) = N_2(b) / N$$

$$P_{12}(a,b) = N_{12}(a,b) / N$$

Let the state of a particular two-particle system (between emission and detection) be denoted by λ . As it evolves, it may or may not trigger a count at apparatus 1, and similarly for apparatus 2. (CH in fact assume no model regarding the state - it may or may not describe the ultimate essence of the system at the chosen time and so has no special characteristics.) However, λ should at least determine the probabilities of the outcome for these events.

Let $p_1(\lambda, a)$, $p_2(\lambda, b)$ be the probabilities of a count being detected at apparatus 1, 2, respectively and let $p_{12}(\lambda, a, b)$ be the probability that both counts are detected. Since each emission in general may not have the same state, we allow a distribution of states. Accordingly, let $\rho(\lambda)$ be the normalised probability density characterising the ensemble of emissions. The ensemble probabilities, therefore, in equations 2.7 are given by;

$$\begin{aligned} p_1(a) &= \int_{\Gamma} p_1(\lambda, a) \rho(\lambda) d\lambda \\ p_2(b) &= \int_{\Gamma} p_2(\lambda, b) \rho(\lambda) d\lambda \\ p_{12}(a, b) &= \int_{\Gamma} p_{12}(\lambda, a, b) \rho(\lambda) d\lambda \end{aligned} \tag{2.8}$$

where Γ is the space of the states. Note that the formulation 2.8 is quite general and valid also for quantum mechanics. We now make a radical departure from quantum mechanics by introducing a locality assumption, that is, a formulation of 2.8 for which,

$$p_{12}(\lambda, a, b) = p_1(\lambda, a) p_2(\lambda, b) \tag{2.9}$$

Clearly, if one regards each source emission as consisting of a pair of objective particles which have a space-like separation and there is no action-at-a-distance, then the probability p_2 that the second apparatus will be triggered will be independent of any triggering of the

first apparatus, or upon the choice of a , or even on the presence of the first apparatus. A similar assertion of independence holds for p_1 yielding equation 2.9*. CH call any theory for which equation 2.9 holds, a local realistic theory. This class of theories contains deterministic local hidden variable theories discussed by Bell and Clauser et al.⁴ CH drop the term "hidden variable theories", since traditionally this was used to represent theories characterised by dispersion-free states (deterministic theories).

II 3.2 Experimental Consequences

CH introduce the following theorem which is proved by them. If x, x', y, y', x, y , are the real numbers such that $0 \leq x, x' \leq X$; $0 \leq y, y' \leq Y$, then,

$$-XY \leq x_1 y_1 - x_1 y_2 + x_2 y_1 + x_2 y_2 - Yx_2 - Xy_1 \leq 0 \quad 2.10$$

Letting a, a', b, b' , be two orientations of analyser 1 and 2 respectively, then the inequalities,

$$\begin{aligned} 0 &\leq p_1(\lambda, a), p_1(\lambda, a') \leq 1 \\ 0 &\leq p_2(\lambda, b), p_2(\lambda, b') \leq 1 \end{aligned} \quad 2.11$$

must hold for sensible probabilities. Combining these inequalities with the theorem of equation 2.10 yields immediately,

$$\begin{aligned} -1 &\leq p_1(\lambda, a) p_2(\lambda, b) - p_1(\lambda, a) p_2(\lambda, b') + p_1(\lambda, a') p_2(\lambda, b) \\ &+ p_1(\lambda, a') p_2(\lambda, b') - p_1(\lambda, a') - p_2(\lambda, b) \leq 0 \end{aligned} \quad 2.12$$

Multiplying throughout by $\rho(\lambda)$, integrating over λ and using equations 2.8 and 2.9 gives,

$$\begin{aligned} -1 &\leq p_{12}(a, b) - p_{12}(a, b') + p_{12}(a', b) + p_{12}(a', b') \\ &- p_1(a') - p_2(b) \leq 0 \end{aligned} \quad 2.13$$

* More generally, the factored form is a natural expression of a field-theoretical point of view that there is no action at a distance

which constrain the statistical predictions of any OLT. These are one form of Bell's Inequalities. Note that the left side of inequalities 2.13 required an assumption of normalisation, that is,

$$\int_{\Gamma} \rho(\lambda) d\lambda = 1 \quad 2.14$$

and requires knowledge of the absolute magnitude of the probabilities, whereas the right hand inequality can be re-written,

$$\frac{P_{12}(a,b) - P_{12}(a,b') + P_{12}(a',b) + P_{12}(a',b')}{P_1(a') + P_2(b)} \leq 1 \quad 2.15$$

This inequality involves only the ratios of the probabilities and hence, very importantly is independent on N , the actual number of two-particle emissions.

Using equations 2.1 again, and defining $R(a,b)$ as the rate of coincident detections, $r_1(a)$, $r_2(b)$ as the rates of single particle detections by either apparatus, then equation 2.15 can be expressed in terms of experimentally observable count rates as,

$$\frac{R(a,b) - R(a,b') + R(a',b) + R(a',b')}{r_1(a') + r_2(b)} \leq 1 \quad 2.16$$

II 3.3 Considerations of Symmetry

Most experiments involve preparing the particles for detection in an apparatus with cylindrical symmetry since the quantum mechanical predictions for the detection rates and correlations exhibit this symmetry.

We will show later that this indeed is the case in photon correlation experiments. Thus,

$$\begin{aligned} [P_1(a)]_{QM} \text{ and } [r_1(a)]_{QM} & \text{ are independent of } a \\ [P_2(b)]_{QM} \text{ and } [r_2(b)]_{QM} & \text{ are independent of } b \\ [P_{12}(a,b)]_{QM} \text{ and } [R(a,b)]_{QM} & \text{ are functions only of } |a - b| \end{aligned} \quad 2.17 a$$

We assume that the same symmetries apply to local realistic theories, yielding,

$$P_1(a) = P_1, \quad r_1(a) = r_1 \quad \text{are independent of } a$$

$$P_2(b) = P_2, \quad r_2(b) = r_2 \quad \text{are independent of } b$$

$$P_{12}(a,b) = P_{12}(|a-b|); \quad R_{12}(a,b) = R_{12}(|a-b|)$$

2.17b

These relationships in fact need not hold for OLT's since there may be symmetry breaking factors at the hidden variable level. However, such assumptions can always be verified experimentally.

We now choose particular settings of the analysers a, a', b, b' such that

$$|a-b| = |a'-b| = |a'-b'| = \frac{1}{3}|a-b'| = \phi$$

2.18

This choice of settings results in the largest conflict between Bell's Inequalities and the relevant QM predictions. With the assumptions of equations 2.10 and 2.18, equation 2.13 becomes;

$$-1 \leq 3P_{12}(\phi) - P_{12}(3\phi) - P_1 - P_2 \leq 0 \quad 2.19a$$

$$\text{or } -1 \leq 3R(\phi) - R(3\phi) - R_1 - R_2 \leq 0 \quad 2.19b$$

in terms of count rates.

The right hand side of 2.19a yields,

$$S(\phi) = \frac{3P_{12}(\phi) - P_{12}(3\phi)}{P_1 + P_2} \leq 1 \quad 2.20$$

II 3.4 Incompatibility with Quantum Mechanics

We now show that the quantum mechanical predictions for certain experiments described by the configuration of fig 7. violate the above inequalities. The quantum mechanical predictions for such an experiment take the following form, (appendix II).

$$P_{12}(\phi) = \frac{1}{4} \eta_1 \eta_2 f_1 g [\epsilon_+^1 \epsilon_+^2 + \epsilon_-^1 \epsilon_-^2 F \cos(n\phi)]$$

$$P_1 = \frac{1}{2} \eta_1 f_1 \epsilon_+^1$$

$$P_2 = \frac{1}{2} \eta_2 f_2 \epsilon_+^2$$

2.21

These predictions are characteristic for the experiments of interest, for example, the spin $\frac{1}{2}$ - spin $\frac{1}{2}$ Gedanken experiment of Bohm,⁵⁸ the positron annihilation experiments⁵⁹ and for the two-photon-cascade experiments already performed by Freedman and Clauser,⁶⁰ Holt and Pipkin,⁶¹ Clauser,⁶² Fry and Thomson,⁶³ Aspect and his collaborators,¹³⁻¹⁵ The present experiment naturally has similar predictions.

In the above expressions, η_i ($i = 1, 2$) represents the quantum efficiency of detector i , and

$$\epsilon_+^i = \epsilon_M^i + \epsilon_m^i, \quad \epsilon_-^i = \epsilon_M^i - \epsilon_m^i \quad 2.22$$

where $\epsilon_M^i, \epsilon_m^i$ are the maximum and minimum transmissions of the analysers. (For photons, ϵ_M^i (ϵ_m^i) is the transmission efficiency of polariser i for light polarised parallel (perpendicular) to the polariser transmission axis).

The functions f_1, f_2 are the collimator efficiencies, i.e. the probability that an appropriate emission enters apparatus 1,2. The function g is the angular correlation factor, or conditional probability that if emission 1 enters apparatus 1, then emission two will enter apparatus 2; these are actually a function of the collimator acceptance half angle θ .

The function $F = F(\theta)$ is a measure of the initial state purity and hence, the inherent quantum mechanical correlations of the two emissions. The values of n are 1 or 2 depending on whether the "particles" are fermions or bosons (appendix II)

Inserting the QM predictions of equation 2.21 into the inequality 2.20, setting, for simplicity, $\eta_1 = \eta_2 = \eta$, $f_1 = f_2$, $\epsilon_+^1 = \epsilon_+^2 = \epsilon_+$, $\epsilon_-^1 = \epsilon_-^2 = \epsilon_-$, then,

$$S(\phi)_{QM} = \frac{1}{4} \eta g [2\epsilon_+ + 3 \cos 2\phi - \cos 6\phi] F(\epsilon_-^2/\epsilon_+) \quad 2.23$$

Selecting the optimum relative orientation $\phi = \pi/8$, where $\frac{dS}{d\phi} = 0$ (refer to fig. 8) then the condition for a violation of equation 2.20 becomes,

$$\eta g \epsilon_+ [\sqrt{2} (\epsilon_-/\epsilon_+)^2 F + 1] > 2 \quad 2.24$$

This result is very general and shows that any correlation experiment with parameters in the domain specified by equation 2.24 is capable of distinguishing between the predictions of local realistic theories and quantum mechanics. Clearly in the nearly ideal situation, ($\eta \approx g \approx \epsilon_+ \approx \epsilon_- \approx F \approx 1$) the QM predictions violate this inequality. These conditions, however, are so stringent that to date, no experiment has been performed which can violate 2.24 and thus 2.20 directly.

For photon cascade experiments, the angular correlation function $g(\theta) \ll 1$ since such a process is a 3 - body decay; two-photons plus the atom, and also, detection efficiencies are low. For positronium annihilation, $g(\theta) \approx 1$ since the two 0.5 Mev gamma rays travel in opposite directions but even here, the analyser efficiencies are low since the gamma rays have to be Compton scattered before detection. In this process, the direction of Compton scattering is a statistically weak index of the photon's linear polarisation and so neither photon is forced to make a binary decision.⁵⁸

II 3.5 Consequences with a Supplementary Assumption

CH now introduce a physically plausible supplementary assumption which is adequate to allow the results of atomic cascade experiments to test OLT's. This assumption is that, for every emission, the probability of a count with a polariser in place is less than or equal to the probability with the polariser removed. This assumption allows us to replace the probabilities of single counts p_1, p_2 in

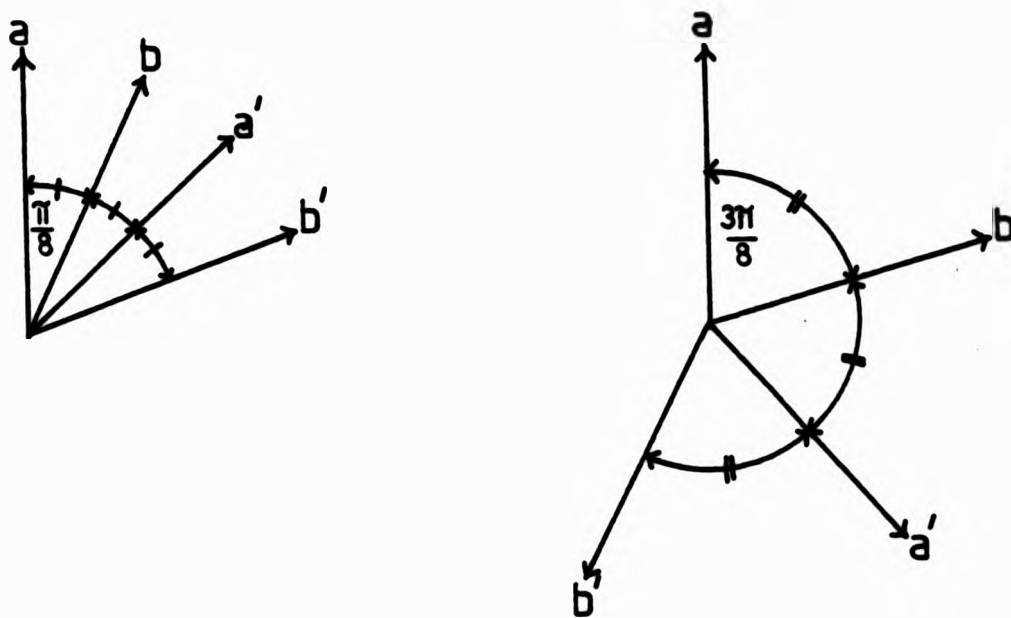


FIG 8 ANALYSER ORIENTATIONS WHICH LEAD TO THE LARGEST CONFLICT BETWEEN BELL'S INEQUALITIES AND QUANTUM MECHANICS.

2.19a by selected coincidence rates. Thus we assume for every λ and all values of a and b ,

$$\begin{aligned} 0 \leq p_1(\lambda, a) \leq p_1(\lambda, \infty) \leq 1 \\ 0 \leq p_2(\lambda, b) \leq p_2(\lambda, \infty) \leq 1 \end{aligned} \quad 2.25$$

where ∞ denotes the absence of the polariser, and so $p_1(\lambda, \infty)$ is the probability of a count from detector 1 when the polariser is absent and the emission state is λ . Similarly for $p_2(\lambda, \infty)$ and apparatus 2. This is called the no-enhancement assumption of Clauser and Horne.⁵³

Inequalities 2.25 with the theorem of 2.10 and using similar arguments that led from 2.8 to 2.13, one obtains,

$$\begin{aligned} -P_{12}(\infty, \infty) \leq P_{12}(a, b) - P_{12}(a, b') + P_{12}(a', b) \\ + P_{12}(a', \infty) - P_{12}(\infty, b) \leq 0 \end{aligned} \quad 2.26$$

where

$$P_{12}(x, y) = \int_{\Gamma} p_1(\lambda, x) p_2(\lambda, y) \rho(\lambda) d\lambda \quad 2.27$$

for all x and y .

Note that all terms in equation 2.26 involve joint probabilities for coincident counts at the two detectors whereas equation 2.13 involved probabilities of single counts at the respective detectors.

II 3.6 Symmetry Conditions

Once again, we invoke a rotational invariance argument, requiring

- (i) $P_{12}(a, \infty)$ is independent of a ; $R_1(a) = R_1$
 (ii) $P_{12}(\infty, b)$ " b ; $R_2(b) = R_2$
 (iii) $P_{12}(a, b) = P_{12}(\phi)$; $R(a, b) = R(\phi)$ where $\phi = |a - b|$

and choose a, a', b, b' so that,

$$|a - b| = |a' - b'| = \frac{1}{2} |a - b'| = \phi,$$

These assumptions along with 2.26 yields,

$$-P_{12}(\infty, \infty) \leq 3P_{12}(\phi) - P_{12}(3\phi) - P_{12}(a', \infty) - P_{12}(\infty, b) \leq 0 \quad 2.29$$

for all a', b , constraining the joint probabilities for coincident counts at the two detectors. The quantum mechanical predictions 2.21, and the other joint probabilities in 2.29, that is,

$$P_{12}(a', \infty) = \frac{1}{2} \eta_1 \eta_2 f(\theta) \cdot g(\theta) \epsilon_+^1 \quad 2.30$$

$$P_{12}(\infty, b) = \frac{1}{2} \eta_1 \eta_2 f(\theta) \cdot g(\theta) \epsilon_+^2$$

$$P_{12}(\infty, \infty) = \eta_1 \eta_2 f(\theta) \cdot g(\theta)$$

result in a violation in the upper bound of 2.29 in a form similar to that of 2.24, but now independent of the detection efficiencies η_i and the angular correlation factor $g(\theta)$,

$$\epsilon_+ \left[\sqrt{2} \left(\frac{\epsilon_-}{\epsilon_+} \right)^2 F(\theta) + 1 \right] \geq 2 \quad 2.31$$

As before, we have used $\phi = \frac{\pi}{8}$, and set $\epsilon_+^1 = \epsilon_+^2 = \epsilon_+$ and $\epsilon_-^1 = \epsilon_-^2 = \epsilon_-$.

This inequality constrains OLT's and shows that photon cascade experiments can be used as a valid test of OLT's versus quantum mechanics if the CH no-enhancement assumption is valid.

II 3.7 Bell's Inequalities in terms of Coincidence Count Rates.

Since the emission rates in the various cascade experiments were

held constant (monitored by auxiliary apparatus) then we can write the ratios of probabilities as the ratios of count rates, i.e.

$$\begin{aligned} P_{12}(\phi) / P_{12}(\infty, \infty) &= R(\phi) / R_0 \\ P_{12}(a', \infty) / P_{12}(\infty, \infty) &= R_1 / R_0 \\ P_{12}(\infty, b) / P_{12}(\infty, \infty) &= R_2 / R_0 \end{aligned} \quad 2.32$$

Inserting 2.32 into 2.29 now yields the inequality,

$$-R_0 \leq 3R(\phi) - R(3\phi) - R_1 - R_2 \leq 0 \quad 2.33$$

In fact, Clauser, Horne, Shimony and Holt⁴ first derived this form of Bell's inequality, but used an alternative supplementary assumption.

II 3.8 Freedman's Simplified Form

Freedman^{60, 64} showed that the above inequality 2.33 can be further reduced to a very simplified and convenient form for comparison with experiment. Let us take the optimal value ($\phi = \frac{\pi}{8}$) for upper limit violation for 2.37 by cascade photon experiments yielding,

$$-R_0 \leq 3R\left(\frac{\pi}{8}\right) - R\left(\frac{3\pi}{8}\right) - R_1 - R_2 \leq 0 \quad 2.34$$

Taking now the optimal value $\phi = \frac{3\pi}{8}$ for the lower limit violation of 2.33, remembering that $3\phi = \frac{9\pi}{8} = \frac{\pi}{8}$, then

$$-R_0 \leq 3R\left(\frac{3\pi}{8}\right) - R\left(\frac{\pi}{8}\right) - R_1 - R_2 \leq 0 \quad 2.35$$

Dividing both inequalities 2.34, 2.35 by R_0 and subtracting 2.35 from 2.34 we obtain,

$$-\frac{1}{4} \leq \frac{R\left(\frac{\pi}{8}\right) - R\left(\frac{3\pi}{8}\right)}{R_0} \leq \frac{1}{4} \quad 2.36$$

or finally,

$$\left| R\left(\frac{\pi}{8}\right) - R\left(\frac{3\pi}{8}\right) \right| / R_0 \leq \frac{1}{4} \quad 2.37$$

This simple statement of Bell's Inequality involves measurements of only three coincidence rates, $R(22.5^\circ)$, $R(67.5^\circ)$ and R_0 the coincidence rate with both polarisers removed.

II 4.1 Quantum Mechanical Coincidence Rates; Ideal Case

The joint linear polarisation measurements made by polarisers oriented at angles ϕ_1 and ϕ_2 to the x-axis, Fig. 7, projects the state of equation 1.42 onto the two linear polarisation states,

$$|\phi_1\rangle = \cos\phi_1 |x_1\rangle + \sin\phi_1 |y_1\rangle \quad 2.38$$

$$|\phi_2\rangle = \cos\phi_2 |x_2\rangle + \sin\phi_2 |y_2\rangle$$

Thus the coincidence probability that one expects to measure in the ideal case considered for the state vector of equation 1.42 is given by, ⁶⁵

$$P_{12}(\phi_1, \phi_2) \propto |\langle\phi_1| \langle\phi_2| \psi_+\rangle|^2 \quad 2.39$$

$$= \left| \frac{1}{\sqrt{2}} (\cos\phi_1 \cos\phi_2 + \sin\phi_1 \sin\phi_2) \right|^2$$

$$= \frac{1}{2} \cos^2(\phi_1 - \phi_2) \quad 2.40$$

$$= \frac{1}{4} (1 + \cos 2\phi)$$

where $\phi = \phi_1 - \phi_2$ is the relative angle between the polariser transmission axes. The $\cos^2\phi$ variation in coincidence count rate derived above is in agreement with that obtained in Chapter I, section 2.3 from the theory of two-photon emission, (see equation 1.33), where in that case the transition probability w_{15}^{25} was shown to depend on a statistical relationship between the electric vectors of the photons, of the form, $(\hat{e}_1 \cdot \hat{e}_2)^2 = \cos^2\phi$.

II 4.2 Predictions for a particular Local Deterministic Model

To emphasise the nature of the QM correlation, we consider a simple deterministic theory following an intuitive line of thought first presented by Holt. ⁶¹

Suppose we have an isotropic source emitting pairs of photons in the $\pm z$ directions which do not always come out in the same state $|\psi\rangle$.

Let the photons have well defined polarisation vectors such that for each pair the directions of linear polarisation are parallel, fig 9. In order to get single rates independent of ϕ_1, ϕ_2 we require the angle of emission with respect to the x - axis, to occur with equal probability from 0 to π .

For a particular pair emitted at angle θ , the coincidence probability,

$$p(\theta, |\phi_1, \phi_2) = \cos^2(\phi_1 - \theta) \cos^2(\phi_2 - \theta)$$

For the whole ensemble, the coincidence rate expected is thus,

$$\begin{aligned} R(\phi_1, \phi_2) &= \frac{1}{\pi} \int_0^\pi \cos^2(\phi_1 - \theta) \cos^2(\phi_2 - \theta) d\theta \\ &= \frac{1}{2} [1 + \frac{1}{2} \cos 2(\phi_1 - \phi_2)] \\ &= \frac{1}{2} [1 + \frac{1}{2} \cos 2\phi] \end{aligned} \quad 2.40'$$

where $\phi = \phi_1 - \phi_2$ is the relative polariser orientation. This correlation function has the same shape as the QM prediction but does not reach the same extremes, fig 10. Other local deterministic models can approach the QM predictions more closely, but all are constrained by Bell's inequality.

II 4. 3 Quantum Mechanical Coincidence Rate; Actual Experiment

The form of the coincidence rate to be expected in a photon correlation experiment such as the present one can easily be obtained from the ratios of the relevant probabilities, equations 2.21 and 2.30. Thus

$$\begin{aligned} \frac{R(\phi)}{R_0} &= \frac{P_{12}(\phi)}{P_{12}(\infty, \infty)} = \frac{1}{4} \left[\epsilon_+^1 \epsilon_+^2 + \epsilon_-^1 \epsilon_-^2 F(\theta) \cos^2 \phi \right] \\ &= \frac{1}{4} \left[(\epsilon_M^1 + \epsilon_m^1) (\epsilon_M^2 + \epsilon_m^2) \right. \\ &\quad \left. + (\epsilon_M^1 - \epsilon_m^1) (\epsilon_M^2 - \epsilon_m^2) F(\theta) \cos 2\phi \right] \end{aligned} \quad 2.41$$

where $\epsilon_M^i, (\epsilon_m^i)$, $i = 1, 2$ are the maximum and minimum transmissions of the polarisers. We shall later test this quantum mechanical prediction when the actual polarisation correlation results are presented in

Chapter IV.

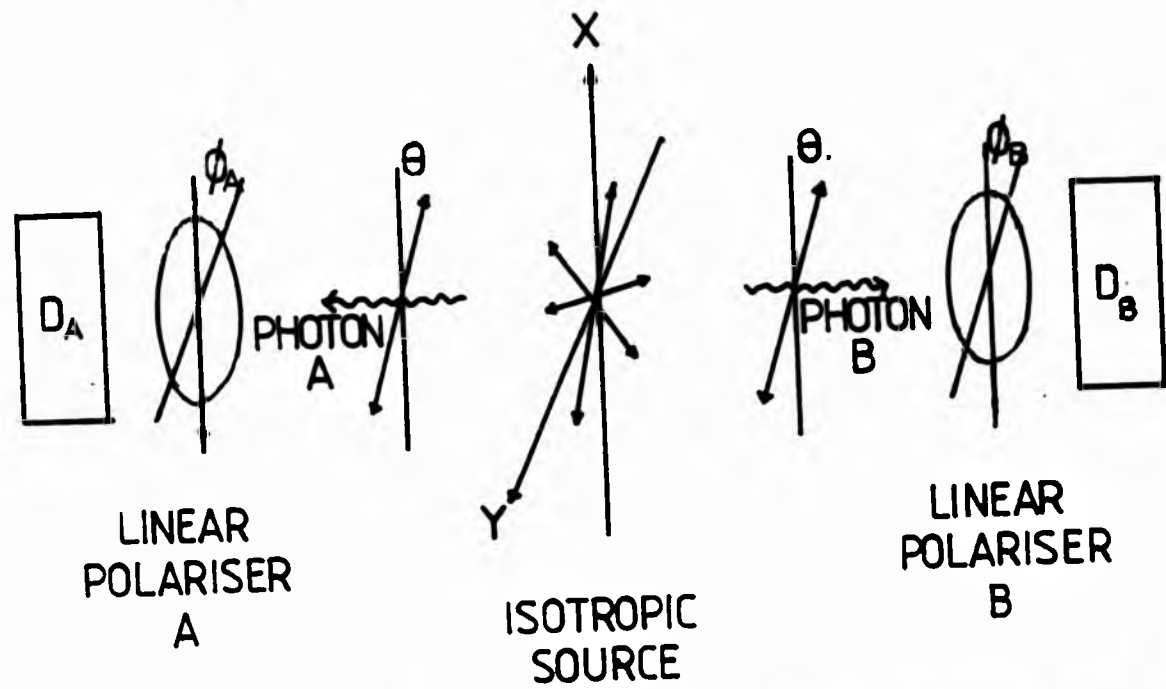


FIG. 9. DIAGRAM TO ILLUSTRATE A LOCAL REALISTIC THEORY IN WHICH PHOTON PAIRS ARE EMITTED ISOTROPICALLY WITH THE SAME DIRECTION OF LINEAR POLARISATION. POLARISERS AND DETECTORS D_A , D_B ARE ASSUMED TO BE 100% EFFICIENT.

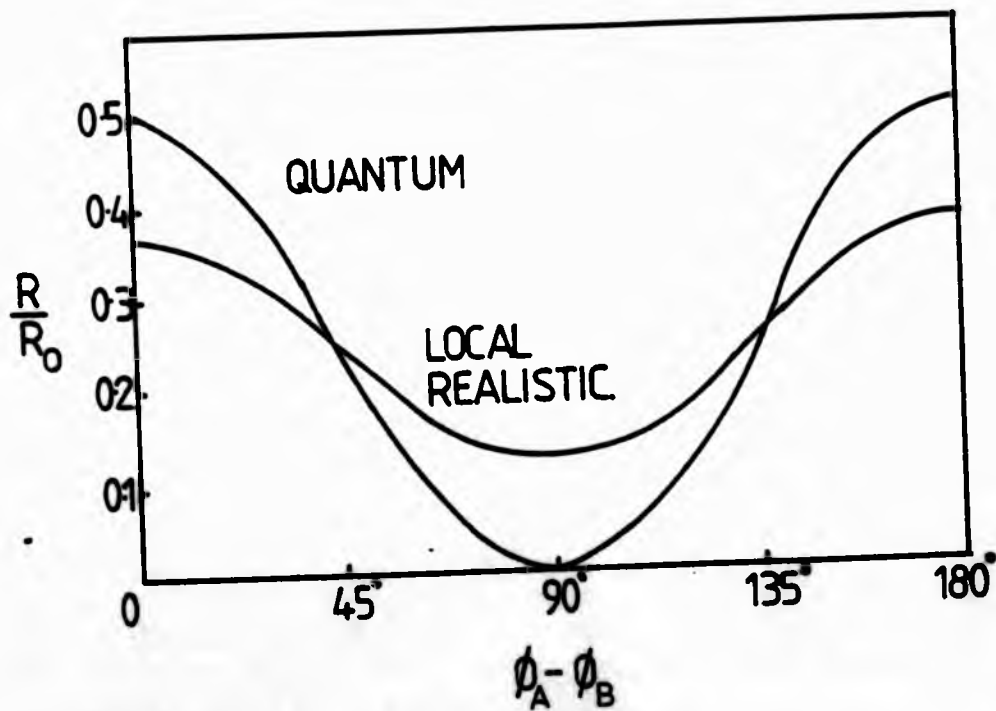


FIG. 10. COMPARISON OF LOCAL REALISTIC AND QUANTUM MECHANICAL PREDICTIONS FOR IDEAL CASE. R_0 IS COINCIDENCE RATE WITH POLARISERS REMOVED.

CHAPTER III : APPARATUS

III.3 Introduction

A schematic diagram of the apparatus is shown in fig. 11. Protons (deuterons) are extracted from a radio-frequency ion source and focussed by an einzel lens into a caesium charge-exchange cell producing a neutral beam of atomic hydrogen (deuterium) which is collimated before entering the detection region. Here, the beam is observed by two symmetrically positioned u.v. transmitting optical systems consisting of a vacuum window, lens, pile-of-plates polariser and fast photomultiplier. The photomultiplier tubes are coupled to a delayed coincidence circuit which monitors the distribution of arrival time differences of pulses from the photomultiplier anodes.

The metastable flux is monitored by quenching in an electric field and the resulting Lyman alphan radiation detected by a photomultiplier with an oxygen window.

Finally, the atomic beam enters the magnet tank and is collected by a neutral current detector/Faraday cup. With the caesium cell off, the charged components of the resulting ion beam can be analysed by a mass separating magnet and collected in a Faraday cup.

A set of electric field plates prior to the observation region is used to quench the metastables periodically so that the background may be monitored.

III 3.1 Vacuum System

The vacuum system consists of three main stainless steel chambers, individually pumped, designated from the source as Rectangular Tank, Vacuum Generators chamber I (VG1) and Vacuum Generators chamber II (VGII). These chambers could be isolated from their respective pumping systems by quarter swing butterfly valves, pneumatically controlled.

The Rectangular Tank is pumped by a six-inch Edwards E06 oil filled

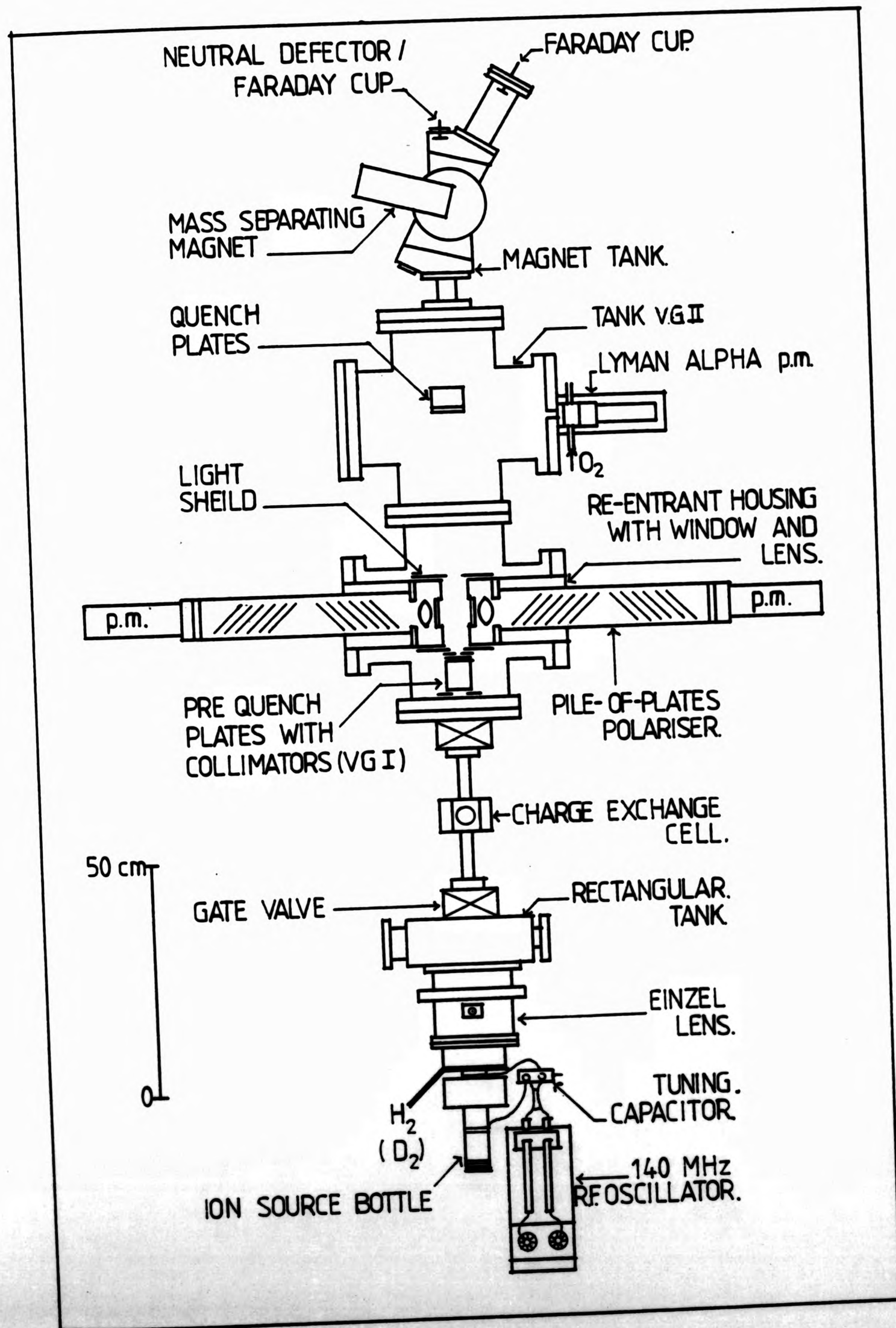


FIG. 11 SCHEMATIC DIAGRAM OF APPARATUS

diffusion pump (1350 l s^{-1}) with water cooled chevron baffle and backed by a two-stage oil filled rotary pump, type ED660 with a displacement of 660 l min^{-1} . Typical pressure in this chamber was 3.10^{-7} torr with the ion source off and 4.10^{-6} torr with the source running.

Chambers VGI and VGII are identical 8 inch UHV crosspieces bolted together and pumped by 6 inch E06 diffusion pumps with thermo-electric and water cooled chevron baffles respectively. The pressure in these tanks was $2.0.10^{-7}$ torr, the presence of the atomic beam making little difference. Backing was provided by an ISC 450B single-stage oil filled rotary pump with a displacement of 550 l min^{-1} .

Santovac 5 pumping fluid is used throughout because of its exceptional high vacuum performance, in particular, its chemical and thermal stability, its extremely low vapour pressure (2.10^{-10} torr at 20°C) and its breakdown products being electrically conducting.

Bolted to the end of tank VGII is the magnet tank with a short beam line attached, pumped via tank VGII.

A combination of copper and rubber gaskets are used to seal the chambers and each chamber has a VIG 21 ionisation gauge head with thorium coated iridium filaments (non burn-out) and a measuring range of $10^{-2} - 10^{-10}$ torr.

III 3.2 Rectangular Tank

The design of this vacuum chamber arose out of a number of important requirements. Firstly, it had to support and align the ion source assembly; it had to minimise the physical separation along the beam line between source and charge exchange cell (in an attempt to achieve high atomic beam densities) and finally, to pump effectively the gas load from the RF ion source.

A rectangular design was chosen whose dimensions were approximately $27.5 \times 25.5 \times 10.5$ cm with a matching section below it to the pump

orifice. From the tank dimensions, the calculated conductance $C = 1106 \text{ ls}^{-1}$, sufficiently high such that its effect on the pumping speed would be to reduce it by less than 20%. Three ports were included in the design, one for a roughing line, the second for pressure monitoring and the third spare - to be used, for example, for the insertion of a retractable Faraday cup.

III 3.3 Pumping Speed at Source

It is important to show that the effective pumping speed is adequate to handle the required gas load from the source.

The gas consumption, at full source output is quoted to be $10 \text{ cm}^3 \text{ hour}^{-1}$ at one atmosphere ($2.10^{-3} \text{ torr ls}^{-1}$) while the pressure in the "source pumping chamber" should not exceed 2.10^{-5} torr . At this pressure, the gas load is 100 ls^{-1} , hence the effective pumping speed S_{eff} should be $> 100 \text{ ls}^{-1}$.

The conductance of the einzel lens (EL) and rectangular tank (RT) were calculated, from their geometry, to be,

$$\begin{aligned} C_{\text{EL}} &= 150 \text{ ls}^{-1} && (\text{air}) \\ C_{\text{RT}} &= 1106 \text{ ls}^{-1} \end{aligned}$$

The system conductance C_{T} is therefore given by,

$$\frac{1}{C_{\text{T}}} = \frac{1}{C_{\text{EL}}} + \frac{1}{C_{\text{RT}}} \quad 3.1$$

hence $C_{\text{T}} = 132 \text{ ls}^{-1}$ for air at 300° K .

For Hydrogen (deuterium), the system conductance is higher by a factor 3.8 (2.7) and so $C_{\text{T}} = 500 \text{ ls}^{-1}$ (306 ls^{-1}). The pumping speed for H_2 (D_2) of a six inch diffusion pump with butterfly valve and baffle is $S = 970 \text{ ls}^{-1}$ (680) and so the effective pumping speed S_{eff} is given by,

$$\frac{1}{S_{\text{eff}}} = \frac{1}{C_{\text{T}}} + \frac{1}{S} = \frac{1}{500} + \frac{1}{970} \left(\frac{1}{360} + \frac{1}{680} \right) \quad 3.2$$

Thus $S_{\text{eff}} = 330 \text{ ls}^{-1}$ (240) > gas load, as required.

The gas load from the caesium cell was estimated to be 2 ls^{-1} at a pressure $p \sim 10^{-5}$ torr and therefore negligible in the above calculation.

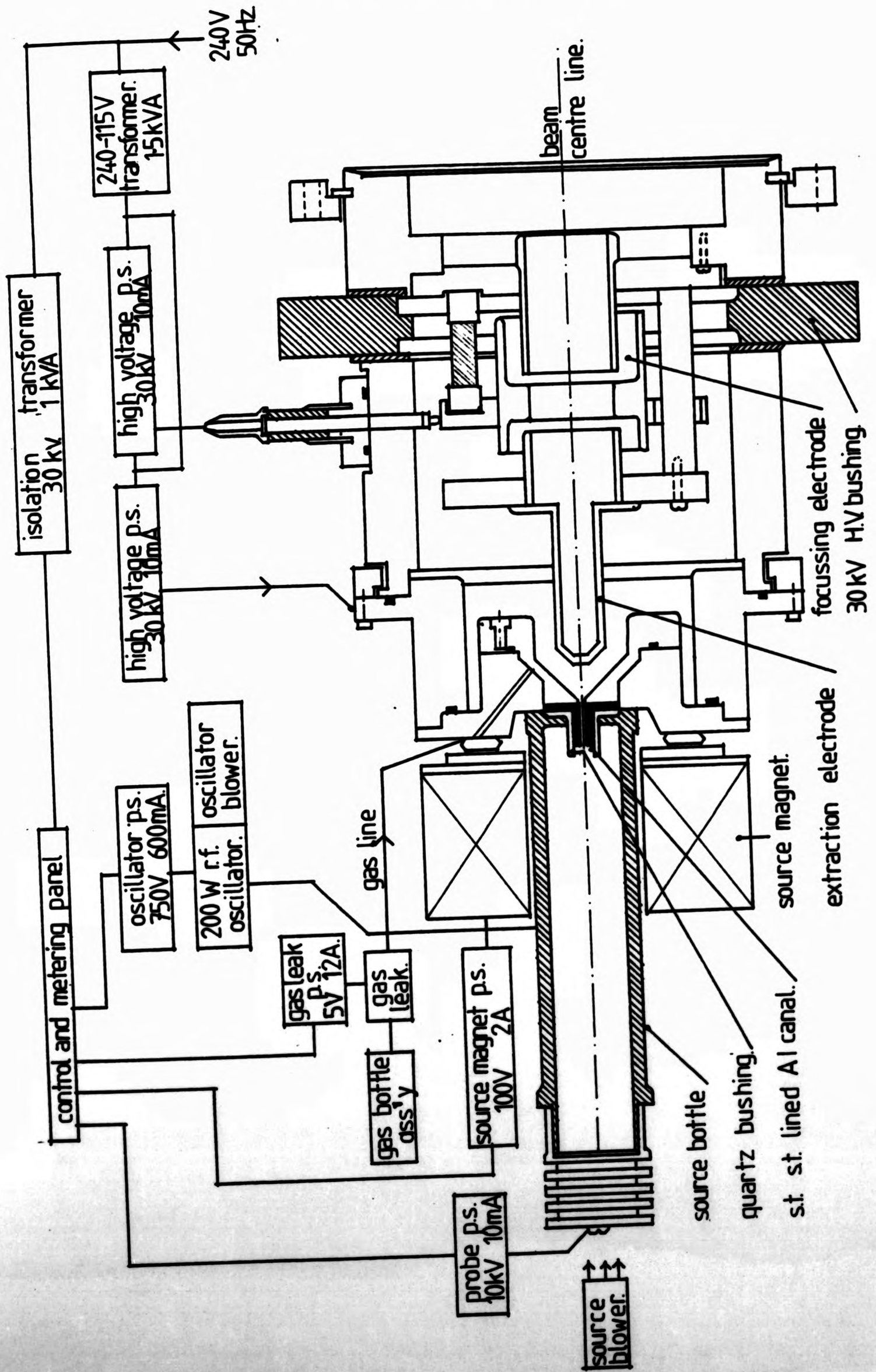
III 4.1 The Ion Source

This is a Thoneman type radio-frequency ion source, model C-SO-173 produced by High Voltage Engineering Corporation, Burlington, Massachusetts. It is a heavy duty, prolific source of hydrogen and other ions. A beam energy of up to 35keV, (30kV acceleration and 5kV probe) with total hydrogen ion current approaching 2mA and proton fraction >0.75 is possible.

The source bottle, made from quartz contains hydrogen at a pressure of $\sim 10^{-2}$ torr which is excited by a 140MHz radio-frequency oscillator, capacitively coupled to the gas, Fig 12. The plasma is confined by an axial magnetic field and the base of the source is fitted with a stainless steel lined aluminium canal (surrounded by a quartz bush) through which ions are extracted. Source output is optimised by control of the source gas pressure, magnetic field, oscillator loading and acceleration voltages.

A 200W self-exciting oscillator, type B-TE-78 containing two 4CX 250B air cooled electron tubes is used to excite the discharge. The oscillator plate and screen power supply provides 750V, 600mA DC. The RF output is fed via two plate lines (exciter lines) to a 300 Ω twin lead transmission line and is coupled to the source bottle by external electrodes placed on either side of the magnet, which in turn is powered by a 100V, 2A DC power supply. Loading adjustment is achieved by altering the height of the clips on the twin feeder line above the shorted end of the exciter line and source tuning is accomplished using a 1.6 pF, 1.5kV variable capacitor connected in parallel with the electrodes and located on the source base mounting flange.

FIG. 12. ION SOURCE AND POWER SUPPLIES



Hydrogen (deuterium) flows from a small cylinder to a palladium leak heated by a 5V, 12A AC supply, the leak temperature controlling the flow rate and hence the pressure in the source. Source pressure was monitored in the adjacent rectangular vacuum chamber.

The source bottle and RF oscillator are both air cooled by fans producing a throughput of $90\text{ft}^3 \text{min}^{-1}$ (2430l min^{-1}) at one atmosphere. The source output is very stable for periods of several weeks, after which time the hydrogen cylinder needs re-filled.

The canal and bottle lifetimes are quoted to be, 100 and 700 hours, respectively, at full source output. By operating the source at low energies, we have obtained lifetimes greater by at least an order of magnitude.

III 4.2 Extraction, Acceleration and Focussing

The probe electrode, coupled to a 10kV, 10mA DC supply biases the plasma with respect to the extraction canal, 2mm diameter and 16mm long, which is surrounded by an insulating quartz sleeve. As the probe voltage is raised, a sheath region develops between the canal tip and the body of the discharge, forming a roughly spherical plasma surface over the mouth of the quartz sleeve. This acts as a lens, focussing ions through the canal (to a beam waist at its centre) and acceleration to their final energy takes place in the region between the canal and the grounded snout of the einzel lens, immediately downstream. This "gap lens" thus controls the initial beam divergence. The einzel lens is operated in the "decel-accel" mode with the central electrode positive and so requires a voltage $V_{\text{focus}} = V_{\text{probe}} + V_{\text{accel}}$ to focus the beam on target.

The RF source and einzel lens are mounted in a 6 inch diameter bushing assembly, a section of which is insulated for 30kV. Alignment between source head and lens assembly is pre-determined and repeatable.

The elements of the einzel lens are supported, aligned and insulated on porcelain insulators.

III 4.3 Observations on the Extracted Ion Beam

During the early stages of the apparatus construction, interest centred naturally on the ion source performance. With a large deep, Faraday cup (20mm entrance aperture) bolted directly to the rectangular tank, the total ion current extracted at a beam energy $E = 5\text{keV}$ and focussed into the cup was measured to be I_+ (total) = $430\mu\text{A}$. This compared well with the quoted "LAB TEST STAND" figure of $450\mu\text{A}$. The source perveance P which relates the extracted current I to the accelerating potential V , is given by

$$P = I / V^{3/2} \quad 3.3$$

$$= 1.2 \cdot 10^{-3} \mu\text{AV}^{-3/2}$$

The beam profile was observed with the aid of a quartz window (covered by a high transmission earthed grid) which fluoresces under ion bombardment. At a distance $d \sim 35\text{cm}$ from the end of the einzel lens (near the centre of the charge-exchange cell when later installed), a 5keV beam was observed to focus to a uniform circular spot $\approx 1.0\text{cm}$ diameter. Taking the object to be half way along the extraction canal (diameter 2.1mm), the overall magnification $M \approx 5$ at this position - approximately that expected on the basis of geometrical optics. It is this magnification which is important in determining the metastable density which is achieved during charge-exchange.

Fig 13 shows the total beam current as a function of energy extracted from the RF source and focussed into a 1cm diameter retractable Faraday cup in tank VGI (detection region). Secondary electrons were suppressed using a biased grid at a potential of -45volts . The total beam energy is set by the sum of probe and acceleration voltages and the output initially follows the Langmuir $V^{3/2}$ law. Evidently, the probe determines

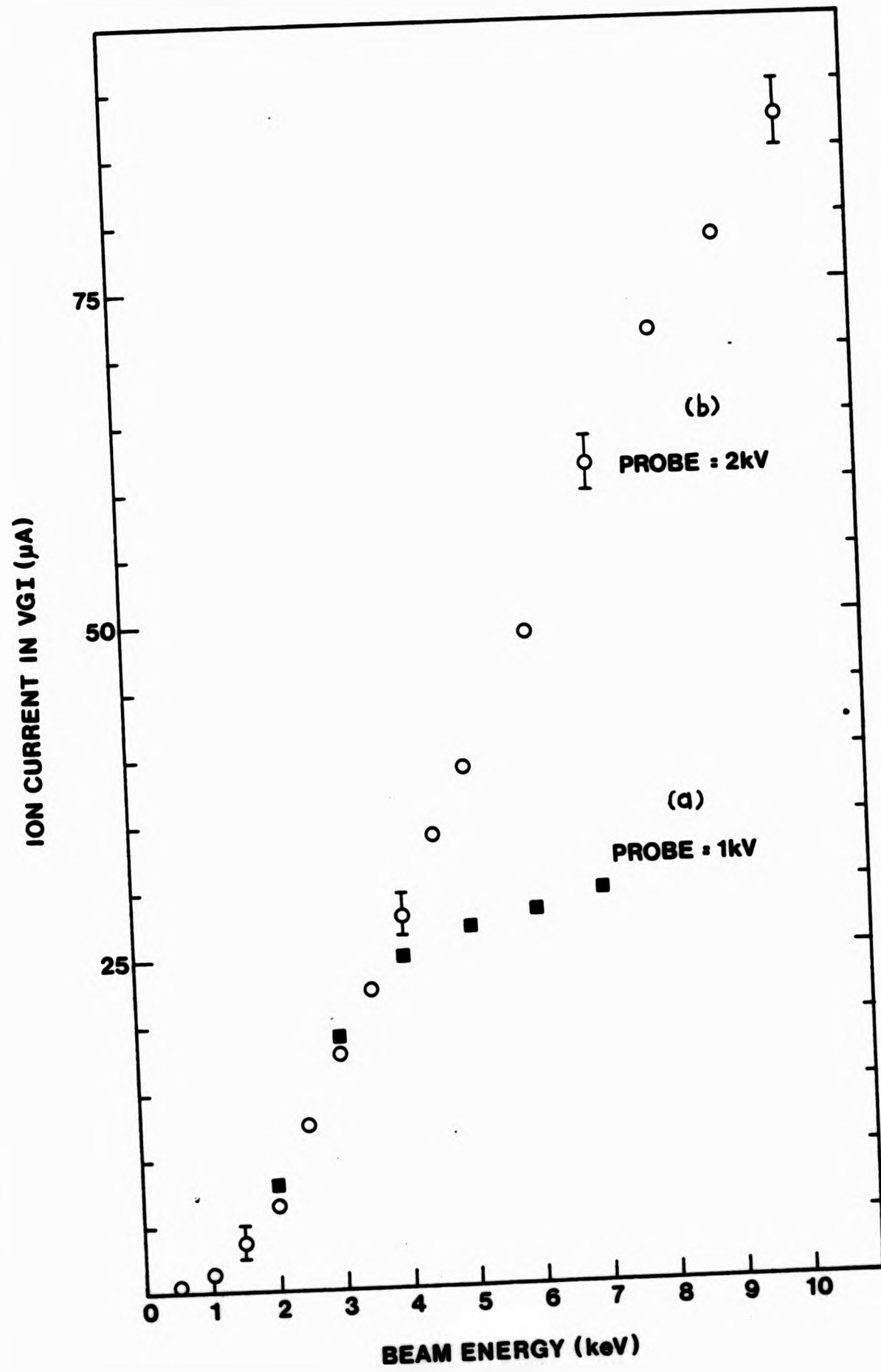


FIG.13. TOTAL BEAM CURRENT AS A FUNCTION OF ENERGY FOCUSED INTO VGI FARADAY CUP. ENTRANCE APERTURE $\phi = 1$ CM.

the total ion flux emanating from the source bottle, while increasing the acceleration, for a given probe voltage, increases the ion beam intensity at the target by decreasing the beam emittance in the acceleration region.

III 4.4 Magnetic Separation

The source output was mass analysed at the end of the apparatus using a C-type electromagnet (cut from soft iron) capable of producing a field $B \approx 0.05$ Tesla between its pole pieces, which are 12.5cm diameter, spaced by 3 cm and designed to fit neatly into the recesses above and below the magnet tank. The ions were deflected 30° and the beam was collimated by a 4mm diameter aperture at the entrance to the magnet tank.

With hydrogen in the source, the proton fraction was measured to be $f_p \sim 0.65$, slightly lower than expected. Deuterium was introduced giving an improved deuteron fraction $f_D = 0.75$ which with continuous operation of the discharge, rose to 0.88, Fig 14. Since cleanliness of the source bottle is the main factor affecting monatomic ion yield, the discharge evidently "cleans up" the bottle presumably by ion bombardment.

III 5.1 Caesium Cell

The design of the caesium charge-exchange cell used is similar to that of Bacal et al.⁶⁶ This design achieves a low loss rate of caesium by,

- (1) reducing to a low level, the flux of alkali metal atoms lost via the cell ports through an appropriate choice of cell geometry, and
- (2) continuously returning to the central evaporator the alkali metal condensed on the cell walls, using capillary action.

The central region of the cell (evaporator) is heated to $\sim 100^\circ\text{C}$ at which a vapour pressure of 10^{-3} torr is achieved. As the melting point of caesium is 28.5°C , a constant temperature in the range $30 - 40^\circ\text{C}$ is maintained at all the extremities of the cell by temperature

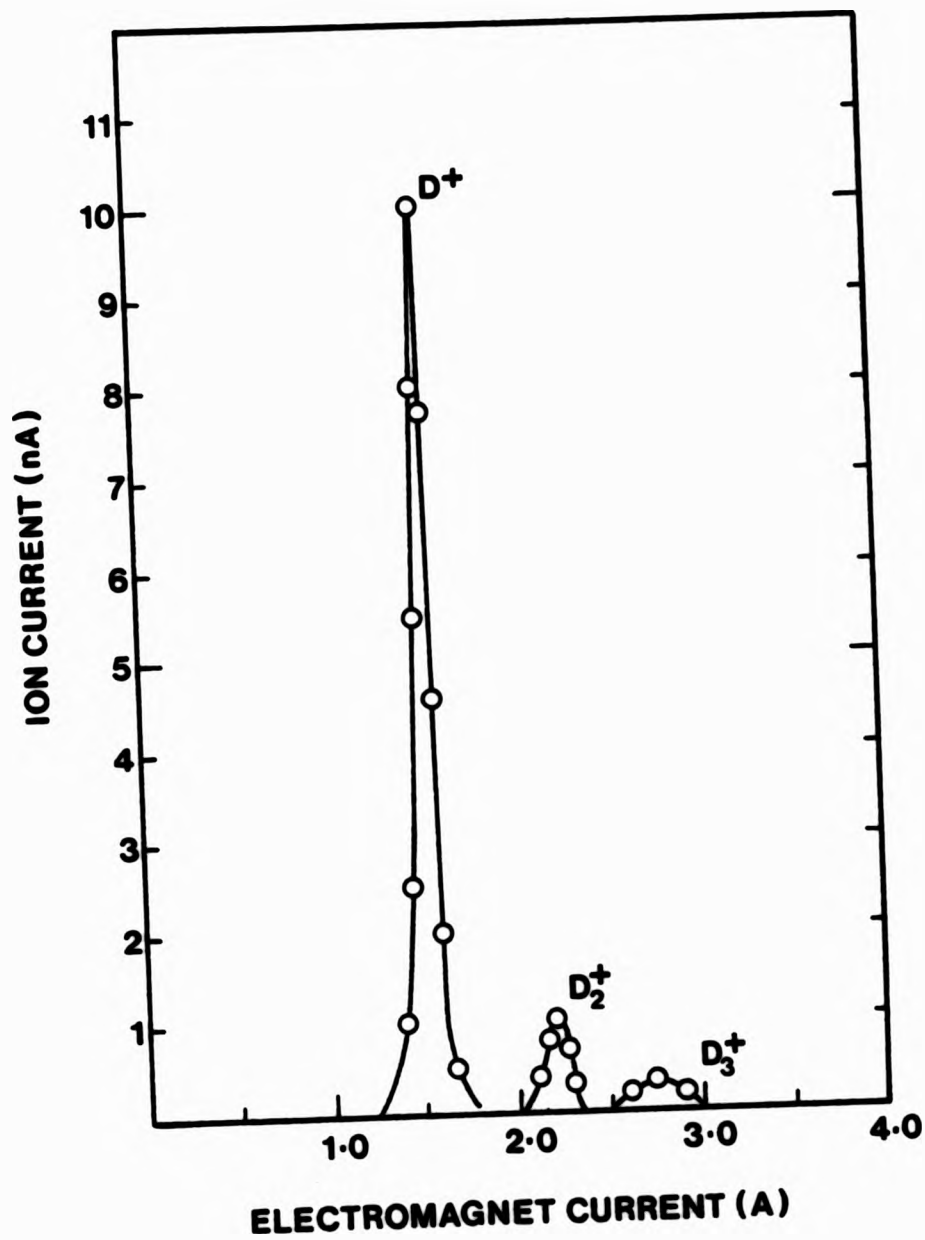


FIG. 14. MASS ANALYSIS OF ION BEAM EXTRACTED FROM RF ION SOURCE

controlled circulating water. Therefore, outside the central isothermal region, an important temperature gradient exists.

In order to return the liquid condensate back to the central evaporator, the internal surface of the cell is lined with several layers of stainless steel gauze wound on to a rigid wick which fits tightly against the inner surfaces of the cell. The caesium which condenses on this is spread out by capillary action and does not get a chance to "ball up" and block the beam. The caesium thus circulates in a closed cycle, purifying itself in the process.

⁶⁶ Bacal measured the caesium atom flux density through the cell ports to be $1.5 \cdot 10^{14}$ atoms $\text{cm}^{-2} \text{s}^{-1}$ for an evaporator temperature $T = 110^\circ\text{C}$ and a condenser temperature $T = 32^\circ\text{C}$. This is equivalent to a total loss rate of $6.1 \cdot 10^{-4}$ g hour⁻¹. We have observed that a 5 gram ampoule of caesium will last a few months, in reasonable agreement with this observed loss rate. In practice, the evaporator and condenser temperatures were regulated to within $\pm 0.5^\circ\text{C}$ using thermocouples connected to temperature controllers.

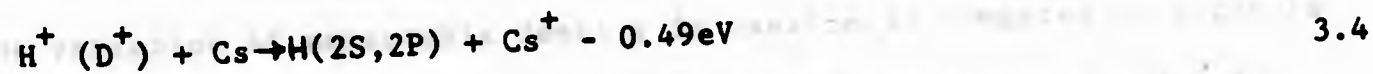
The cell has three ports, one of which supports a needle valve for flushing the cell with argon when filling with caesium. The cell can be isolated from the vacuum system by gate valves at either end. The important physical dimensions of the cell are as follows;

- (i) Overall length = 30cm
- (ii) Internal diameter with wicks in place, 1.8cm.

III 5.2 Production of the Metastable Beam

Experiments involving charge-exchange of protons in gas targets (N_2 , H_2 , Ar, Kr,....) to produce metastable hydrogen atoms have shown that the cross-sections σ_{+m} are small and reach a maximum at relatively high energies. For nitrogen and argon, for example, $\sigma_{+m}(\text{max}) = 3.3 \cdot 10^{-17} \text{cm}^2$ and $2.9 \cdot 10^{-17} \text{cm}^2$, respectively, at an energy $E = 25\text{keV}$.⁶⁷

In the present experiment, a dense beam of metastable atomic hydrogen is produced by the near-resonant charge-exchange of protons in caesium vapour, as the small energy defect of the reaction,



ensures a large cross section at low energy for production of metastables.

This process was first studied by Donally et al in 1964 and later by others.⁶⁸

⁶⁹ Pradel measured the cross-section for the above charge-exchange reaction

and found $\sigma_{+m}(\text{max}) = 6 \cdot 10^{-15} \text{cm}^2$ at an energy $E = 600\text{eV}$.

The fractional metastable yield f_m in the outgoing beam was found to reach a maximum of 0.31 at an energy $E = 500\text{eV}$ and a target thickness $\pi = 1.2 \cdot 10^{14}$ atoms cm^{-2} .

It is interesting to note that at low energy $E < 1\text{keV}$ and at high target thickness, $\pi \approx 10^{15}$ atoms cm^{-2} , caesium also provides the highest conversion efficiency among the alkali metals for the production of D^+ ions (by double electron capture by D^+) for use in fusion research.

III §.3 Charge-Exchange Observations

With a proton beam of constant energy passing through caesium vapour, fig. 15 shows how the Lyman-alpha monitor count rate varies as a function of cell temperature. As expected, a peak occurs around an evaporator temperature $T = 110^\circ\text{C}$. This is the optimum operating temperature for the production of metastables and is found to be (within a few degrees) the same for proton and deuteron beams, independent of beam energy.

Fig 16 shows the relative metastable density measured as a function of energy for charge-exchange of protons in caesium vapour, and for comparison, that obtained in argon. (With the cell cool, argon was leaked via a needle valve mounted on the cell).

These curves demonstrate clearly why caesium is used in the low keV region to produce dense metastable atomic hydrogen beams. In caesium, the metastable density reaches a maximum around an energy $E \approx 5\text{keV}$, then falls off, while in argon, the density rises almost linearly over the energy range investigated. Presumably, the significant difference in the variation of metastable density in caesium as compared to argon is due to the fact that the cross-section for metastable production is resonant in caesium while it is non-resonant in argon.

Clearly, at energies above 10keV , there is little advantage in using caesium as opposed to argon or some other target gas for the production of metastables.

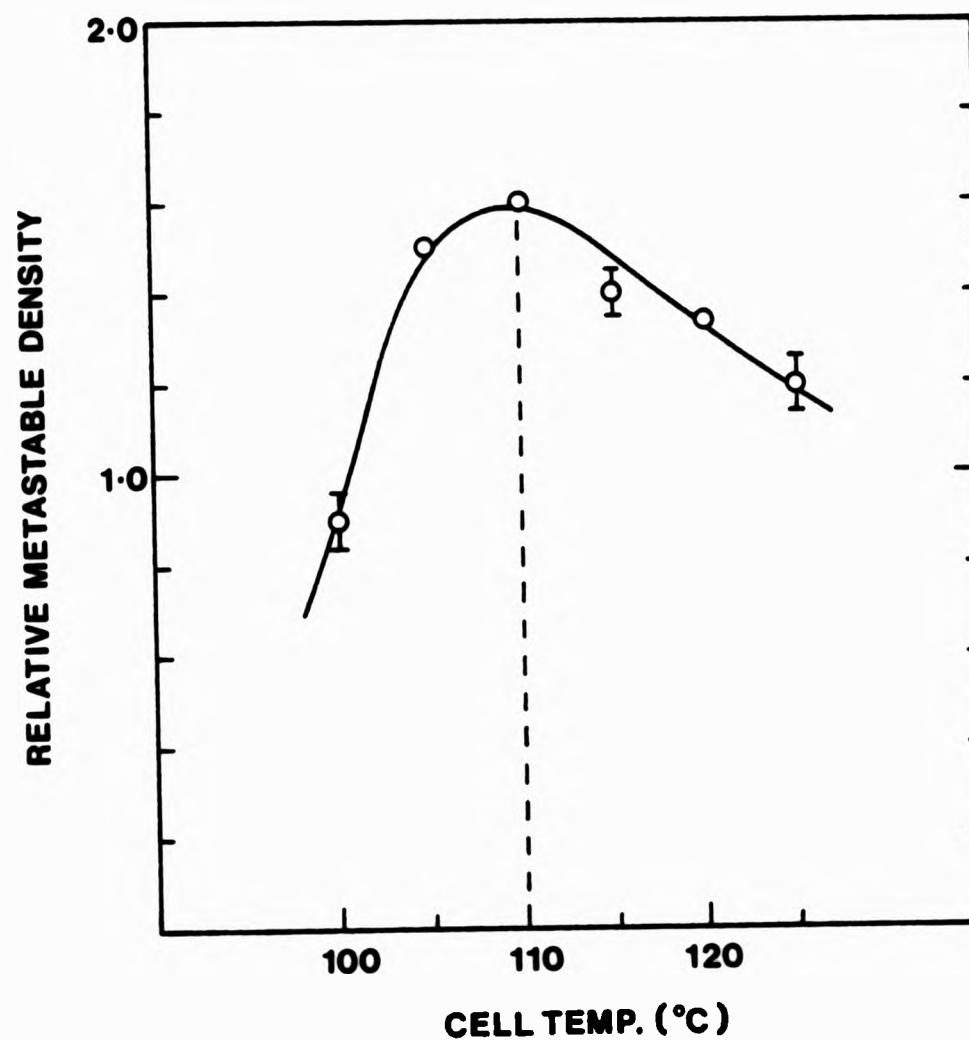


FIG. 15 LYMAN-ALPHA MONITOR COUNT RATE VERSUS CELL TEMPERATURE.
BEAM ENERGY $E = 5\text{keV}$

The absolute metastable density at the maximum in fig. 16 can be estimated approximately from the equation,

$$n(\text{H}_{2s}) = \frac{f_+ I_+ f_m}{e v A} \quad 3.5$$

where I_+ is the incident ion current measured in the VGI Faraday cup with the charge-exchange cell off, f_+ is the proton fraction, f_m is the metastable fraction in the outgoing beam after charge-exchange, e is electronic charge, v is the beam velocity and A is the beam cross-section.

From fig 13(b), $I_+ = 40\mu\text{A}$ at $E = 5\text{keV}$ or a velocity $v = 10^8\text{ cm s}^{-1}$, the proton fraction $f_+ \approx 0.65$ and the beam cross-section $A \approx 0.79\text{ cm}^2$.

Pradel measured the metastable fraction in the outgoing beam (at a target thickness $\pi = 1.2 \cdot 10^{14}\text{ atoms cm}^{-2}$) over the energy range 0.5 - 2.5 keV and extrapolated to an energy $E = 5\text{keV}$ gives $f_m \approx 0.05$. Using the above values, the metastable density,

$$n(\text{H}_{2s}) = 1.1 \cdot 10^5\text{ cm}^{-3} \quad 3.6$$

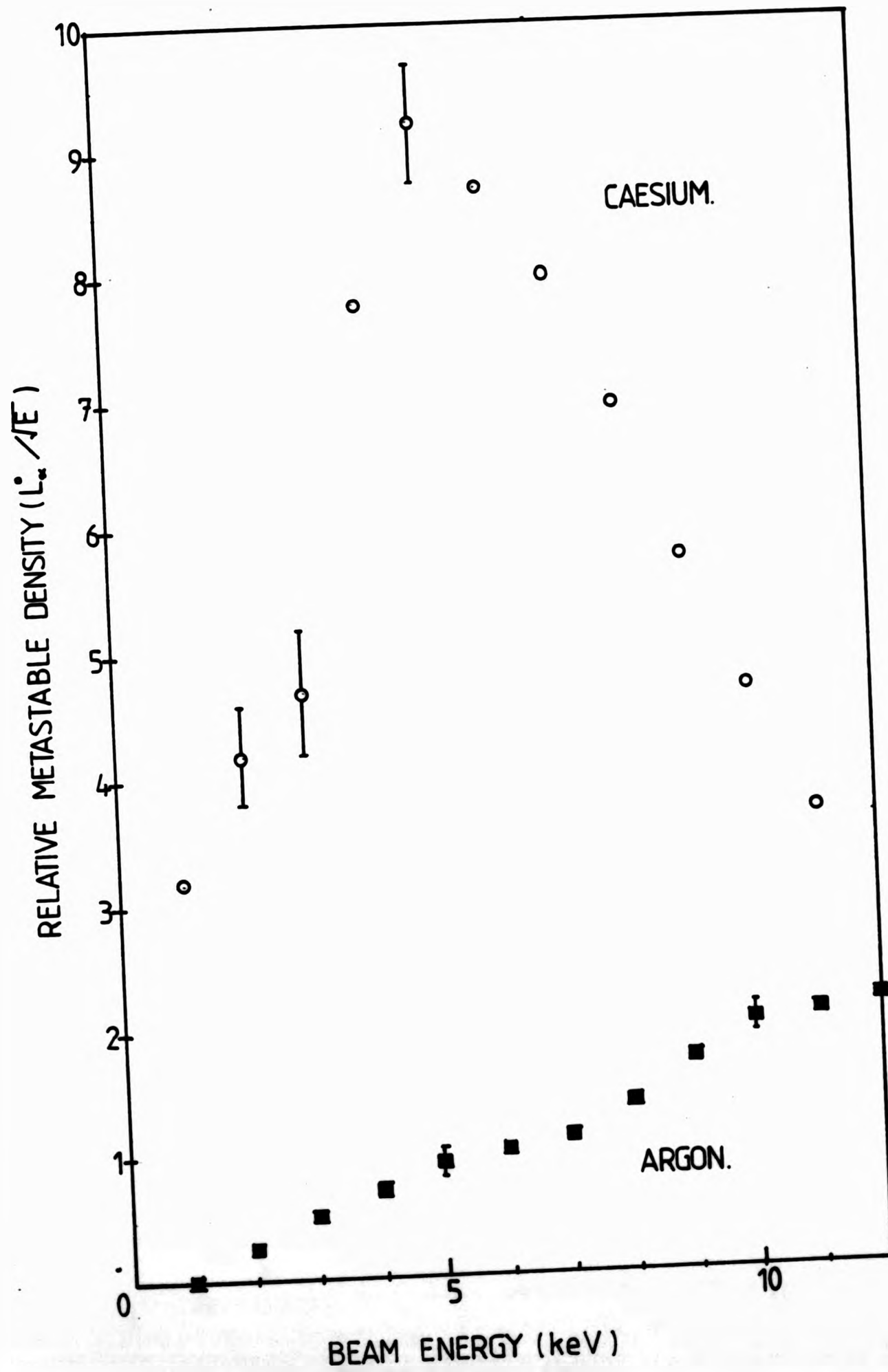


FIG. 16. RELATIVE METASTABLE DENSITY AS A FUNCTION OF BEAM ENERGY FOR CHARGE-EXCHANGE IN CAESIUM AND ARGON.

while the metastable flux,

$$\phi = nv = 8.8 \cdot 10^{12} \text{ cm}^{-2} \text{ s}^{-1} \quad 3.7$$

at an energy $E = 5\text{keV}$.

However, the region in which the best statistical accuracy for the observation of a two-photon signal was found at an energy $E \approx 1\text{keV}$, and can be attributed to the behaviour at the background radiation generated by the interaction of the atomic beam in the apparatus. This will be discussed in greater detail in sections III.10 and IV 4.2

III.6 System Interlock

The experiment was interlocked to prevent system damage in the event of malfunction, and in particular to protect the radio-frequency ion source under the following conditions;

- 1) Mains Power failure.
- 2) Pressure failure (vacuum)
- 3) Water failure (diffusion pump cooling)
- 4) High Voltage penetration (RF source)

Logic gates lend themselves ideally to this type of application where a change of state is to be detected. CMOS 4011B integrated circuits containing quad 2-input Nand gates were wired as a series of flip-flops whose outputs Q and \bar{Q} are complementary, Fig 17. With the interlock switch closed, and R momentarily brought low (reset), \bar{Q} is high, Q is low, B is high so that transistor $T1$ switches on and the relay changeover contacts are operated.

If the interlock sensor now goes open circuit (failure) Q goes high (\bar{Q} low) and the transistor switches off. To re-set the circuit to its initial state, the interlock switch must be closed and reset R brought low momentarily.

Each flip-flop is used to control a separate function and clearly the radio-frequency ion source can be operated only when the vacuum

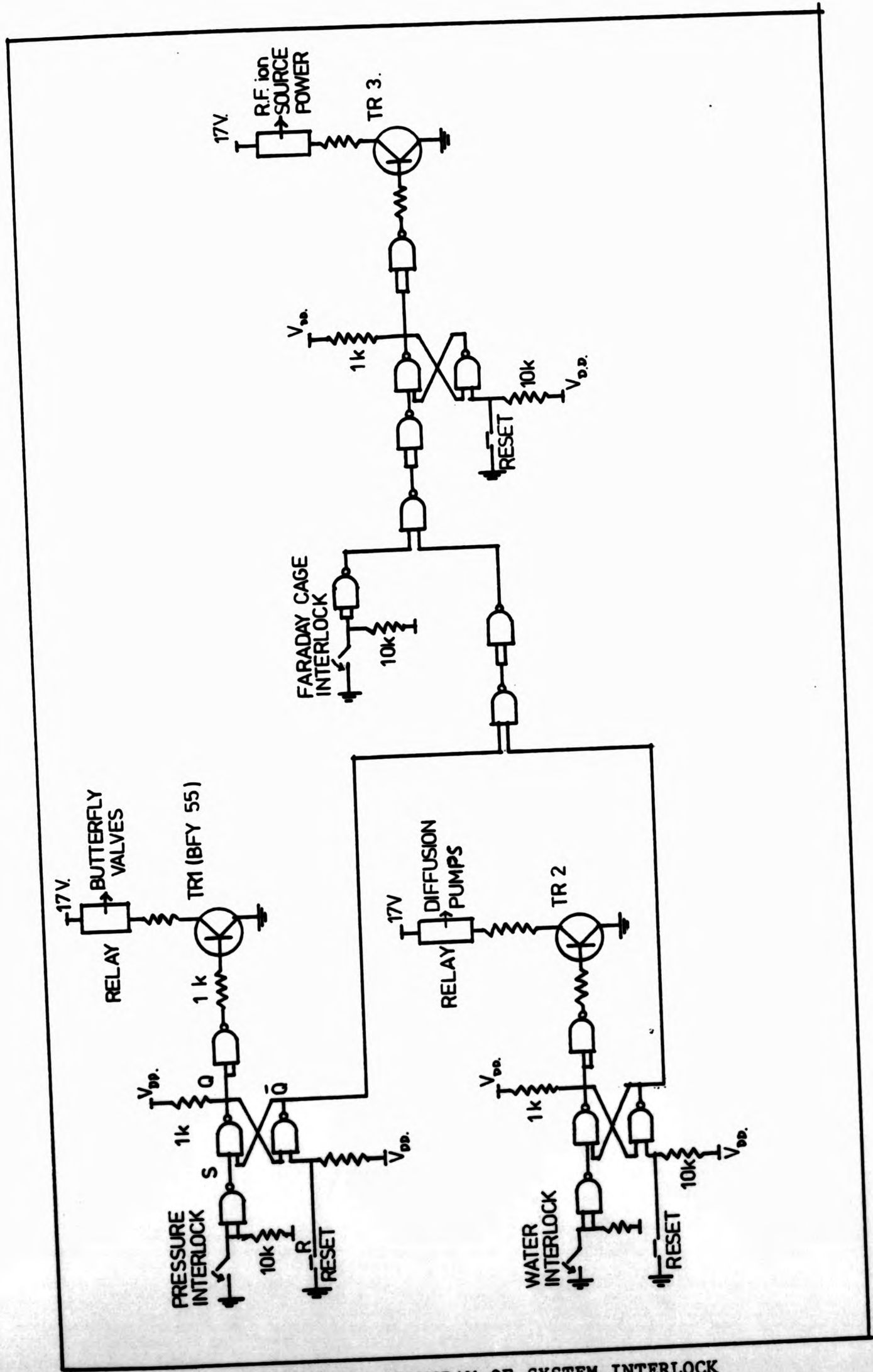


FIG. 17. DIAGRAM OF SYSTEM INTERLOCK

is satisfactory, the diffusion pumps are cooled, and the Faraday cage door is closed. More importantly, the protection of personnel from high voltage shock was ensured by the Faraday cage interlock microswitch.

The mains power interlock was achieved using a latch relay, which in the event of a sudden mains failure, isolates all power to the experiment.

Two power supplies were included in the overall design; a 17V, 0.5A DC supply for the relays and a regulated 15V DC supply for the CMOS logic circuits, chosen for their relatively low switching speeds and high noise immunity.

III. 7 Metastable Monitor System

To detect metastables, advantage is taken of the low value of the Lamb shift. An applied electric field Stark mixes the radiative 2P states with the 2S state inducing a quenching transition with the subsequent emission of a Lyman alpha photon.

The quenching system consists of a set of four plates similar to a design of Spiess et al.⁸⁰ The inner plates, biased at opposite potentials with respect to earth are 65mm long and spaced 40 mm apart. A distance 3mm outside these plates are a set of image plates, longer by 4 mm which reduce the fringe fields significantly so that quenching of the metastables takes place in a small region in front of the detector. Fig. 18 shows how the metastable monitor count rate varies as a function of the applied quench voltage and indicates that $\pm 250V$ is adequate to quench the metastable beam completely. A voltage of $\pm 250 V$ therefore was permanently applied to these plates.

The Lyman alpha photons were detected by an EMR 542 G-08-18 photo-multiplier tube with a LiF window. This tube is solar blind with a spectral response covering 105-220nm peaking at the Lyman-alpha wavelength, 121.6nm. A sealed LiF window covered by a 1 mm diameter aperture is mounted on chamber VGII and dried molecular oxygen whose flow rate was

FIG. 18. LYMAN ALPHA COUNT RATE VERSUS PRE-QUENCH VOLTAGE
BEAM ENERGY E = 791eV

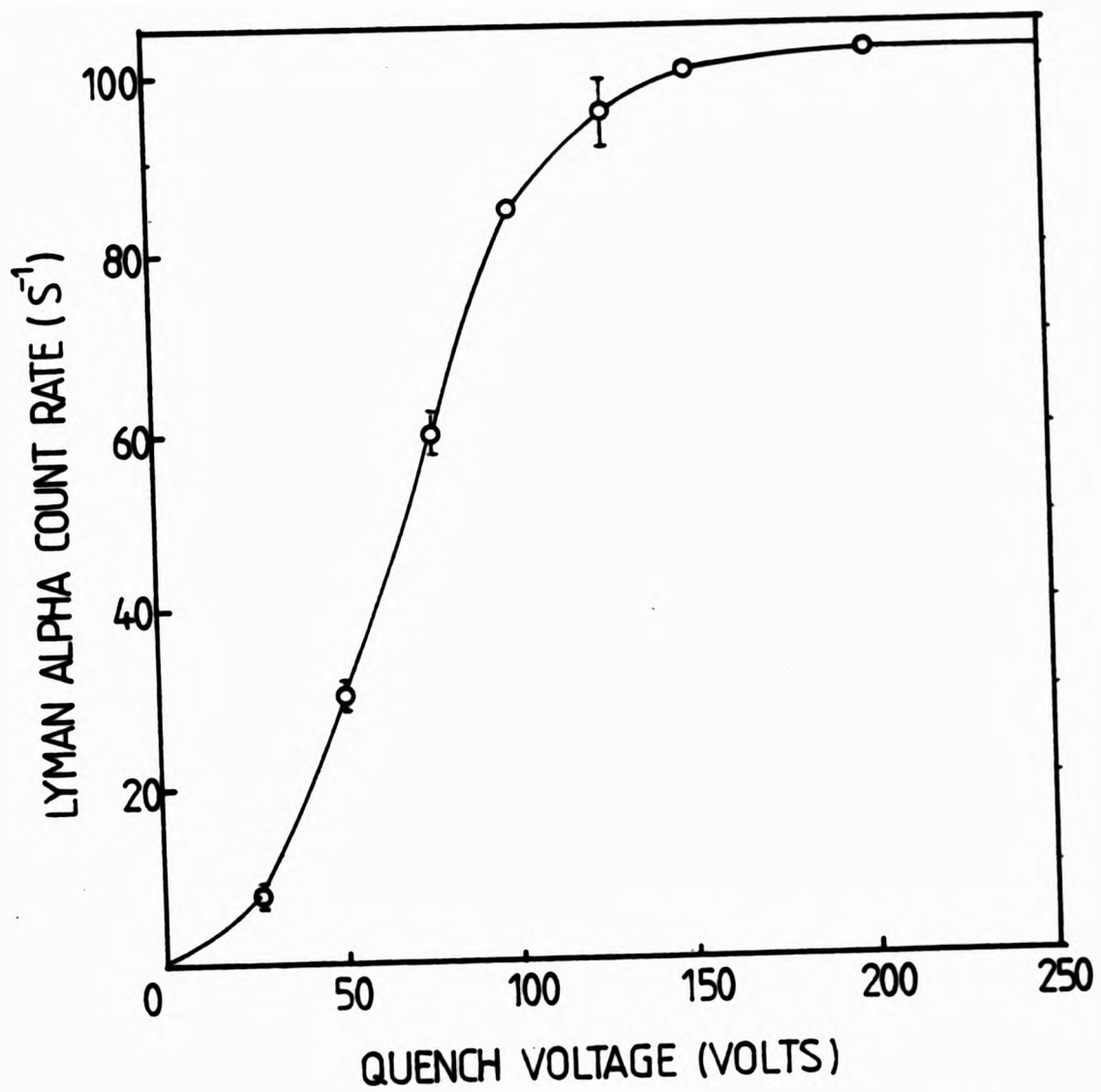


FIG. 18. LYMAN ALPHA COUNT RATE VERSUS QUENCH VOLTAGE.
BEAM ENERGY $E = 795eV$.

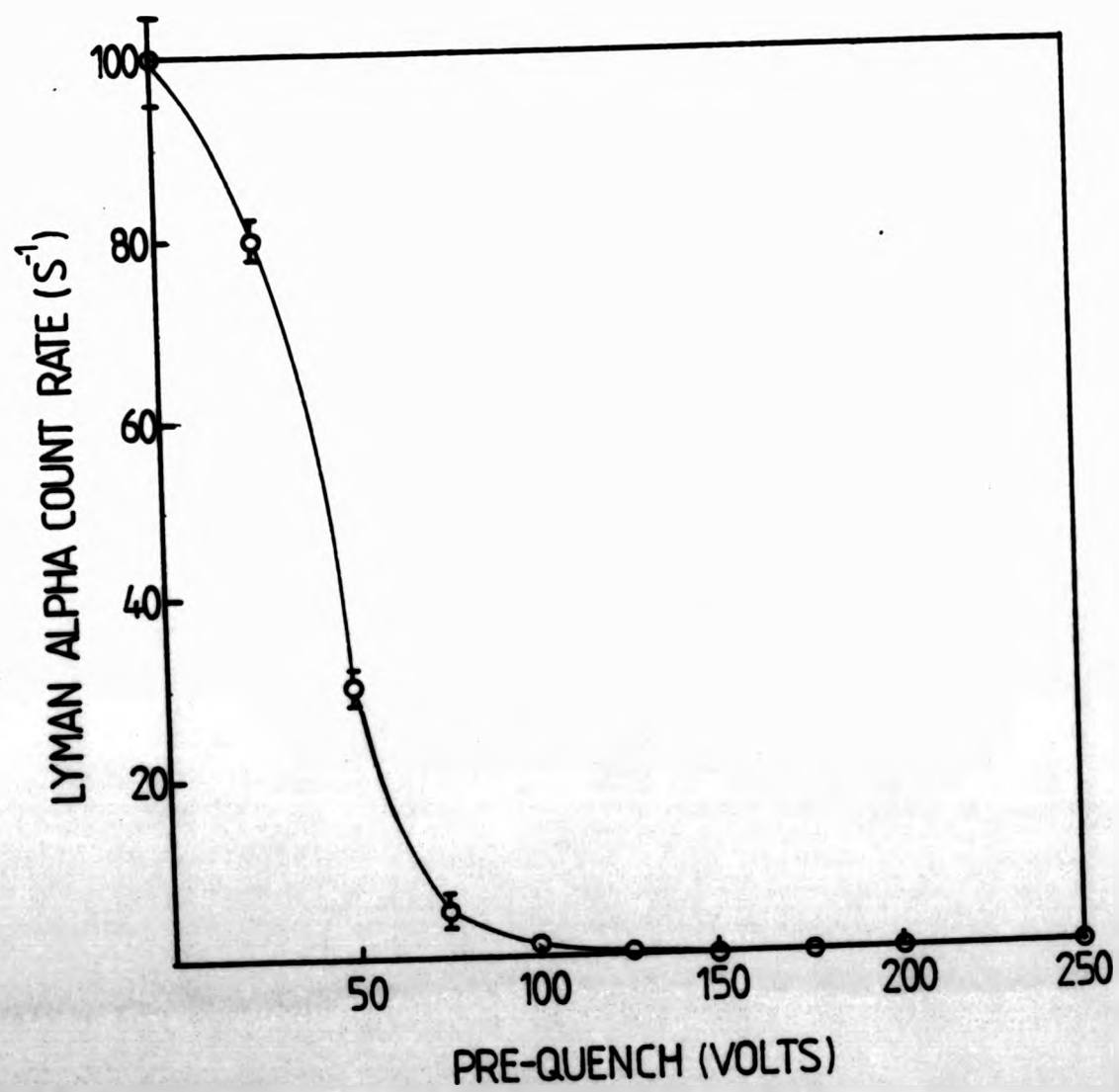


FIG. 19. LYMAN ALPHA COUNT RATE VERSUS PRE-QUENCH VOLTAGE
BEAM ENERGY $E = 795eV$

carefully monitored was allowed to flow between this window and the PM tube acting as a filter for the L_{α} radiation. Molecular oxygen has a very narrow transmission window at the L_{α} wavelength.⁷⁰

III. 8 Pre-Quench Plates

These plates, 11.0cm long separated by a 2.5 cm are used to quench the metastable component of the beam so that the background can be monitored. The end plates, which ensure a rigid construction have 1cm diameter apertures used to collimate the atomic beam immediately ahead of the detection region. Ideally, these plates should be very long with a low field applied, sufficient to deflect any remaining ions in the beam without quenching a significant fraction of the metastables. However, physical space was limited in the detection region and therefore their maximum length was determined by other constraints. The observed Lyman alpha count rate as a function of pre-quench voltage is shown in Fig. 19.

A voltage of $\pm 200V$ is adequate to quench a fraction $f > 99.5\%$ of the metastable flux and the pre-quench plate voltages were switched alternately between $\pm 200V$ and $0V$ to separate the radiation due to the metastables from the other components of the beam.

It was felt important to ensure that the metastables decayed in as near a zero field region as possible. It is easy to show that (using Gauss' law) the field experienced by the metastables due to the remaining ions in the beam is $E < 0.01Vcm^{-1}$. On the other hand it was estimated that a voltage of $\pm 40V$ on the pre-quench plate which was necessary to remove the remaining ions, would quench 60% of the metastable flux and may have caused a leakage field in the interaction region $E \sim 0.5Vcm^{-1}$. In this case significant reduction in two-photon signal and hence statistical accuracy would have been unacceptable.

The motional electric field experienced by the atoms in the Earth's magnetic field, (vertical component)

$$|E| = |\underline{v} \times \underline{B}| = vB_{\perp} \\ = 0.2Vcm^{-1}$$

$$\begin{cases} B_{\perp} = 0.5 \cdot 10^{-4} \text{ T} \\ v = 4 \cdot 10^5 \text{ ms}^{-1} \end{cases} \quad 3.8$$

so that the leakage field mentioned above would have caused little trouble in reality.

III.9 Coincidence Photomultipliers

These photomultipliers, obtained from EMI, type 9883QA (selected) and 9883QB are fast linear focussed tubes for timing applications with an output pulse risetime of 2.2 ns and a gain of $3 \cdot 10^8$. The photocathodes, which are Bi-alkali with a quartz window, have a spectral sensitivity covering the range 180-600 nm and a quantum efficiency $\eta = 28\%$ at $\lambda = 420\text{nm}$. They combine good spectral matching to the two-photon radiation with low dark counts, typically 40s^{-1} (9883QA) and 150s^{-1} (9883QB) respectively. These tubes have a high d_1^* gain stage which results in a well resolved single electron response (S.E.R.) giving good discrimination against low amplitude background not derived from the photocathode. Fig.20 shows the optimised pulse height distribution for tube 9883QB, obtained by shaping the fast photomultiplier pulses in an amplifier, type NE4603 and feeding the inverted output pulses to a multichannel analyser.

Fig 21 shows how the S.E.R. (defined as the peak - to- valley ratio) varies with the cathode to d_1 voltage $V(k - d_1)$ for tube 9883QA and it is clear that no significant improvement in resolution is obtained by operating the first stage beyond 300 volts, where the S.E.R. = 3.2 (d_1 gain = 14 at 300V). The well defined S.E.R. confines the thermionic background, ensuring very little "statistical spill out" beyond 3 photoelectrons equivalent.

Both photocathodes were operated at ground potential to avoid field gradients across the P.M. windows which might introduce some sensitivity to polarisation.

* d_1 is first dynode

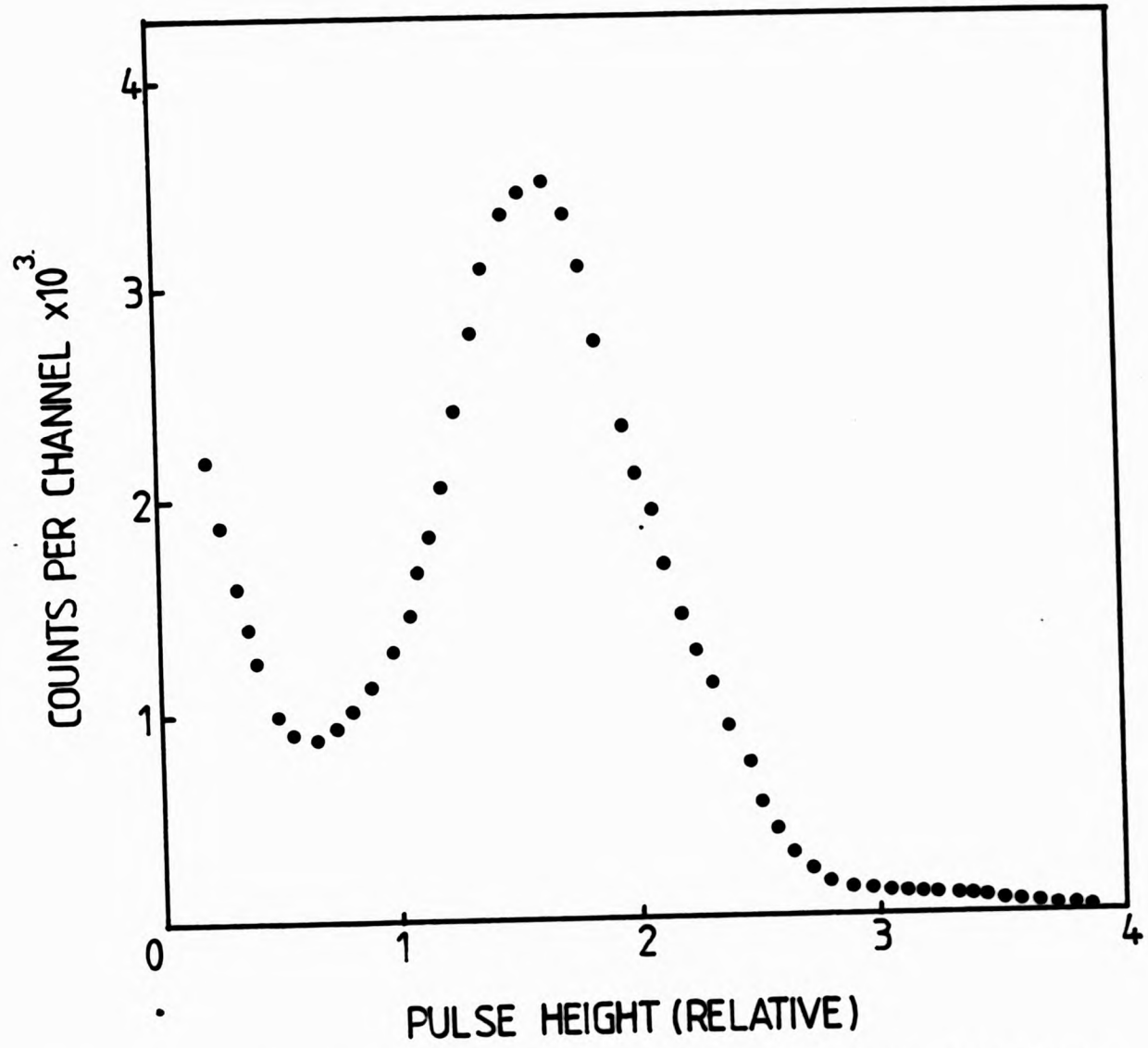


FIG. 20. OPTIMISED PULSE HEIGHT DISTRIBUTION FOR PM 9883QB.
 $V(k-A) \approx 2300$ V.

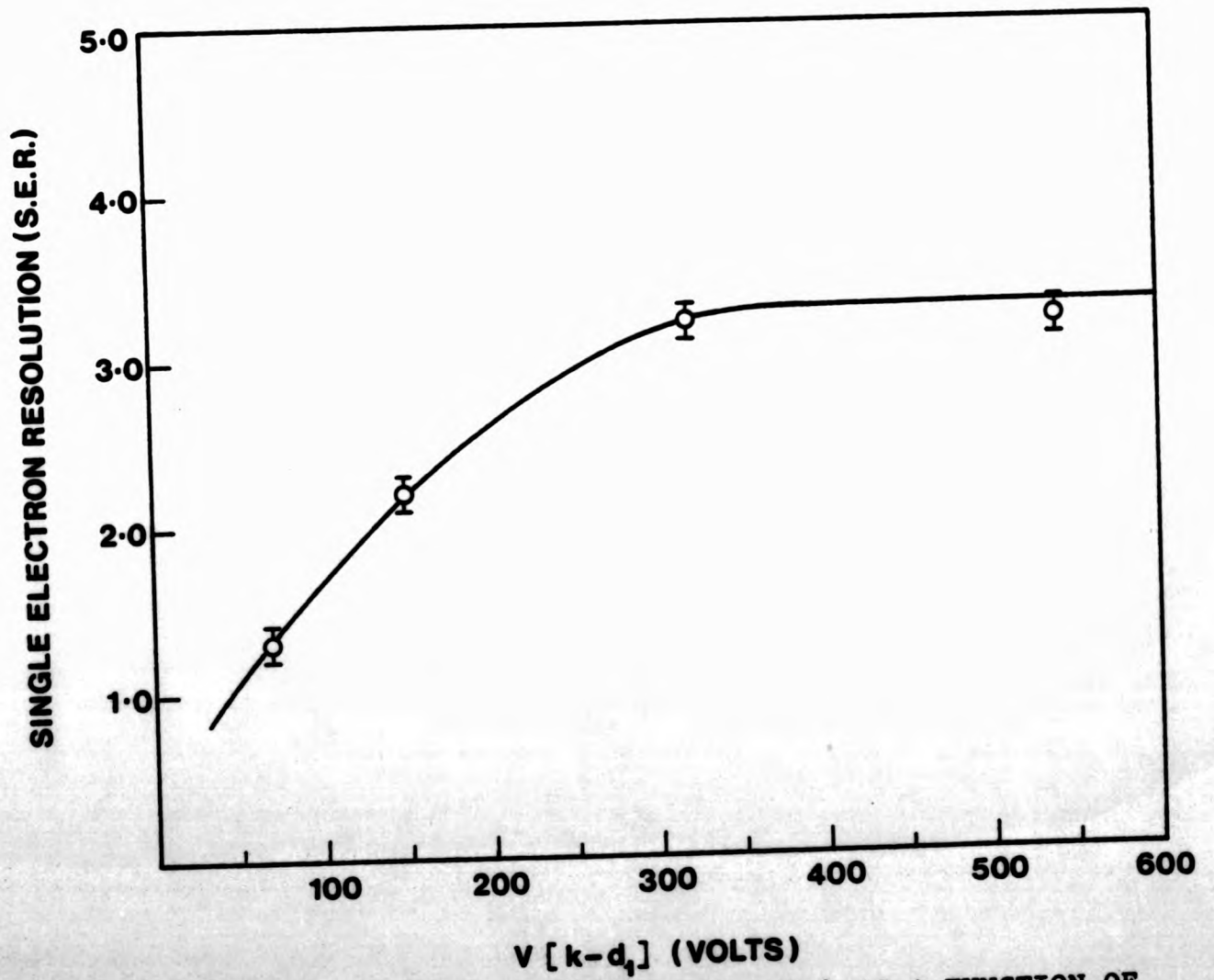


FIG. 21. SINGLE ELECTRON RESOLUTION (S.E.R.) AS A FUNCTION OF VOLTAGE ON FIRST DYNODE D1 FOR TUBE 9883QA. OVERALL TUBE GAIN FIXED.

III.9.1 Detection Electronics

The electronic system is designed to have the best practical timing resolution so that matched 50Ω cables are used throughout and the PM anodes were naturally matched to the cable. Since the photocathodes were operated at ground potential, the anodes were AC coupled.

As expected, the operation of the detection system in the absence of an atomic beam gave rise to a spurious coincidence peak, most probably due to cosmic rays and natural radioactivity in the environment. (Cross-talk between channels was eliminated as far as possible by separating each amplifier/discriminator channel into different NIM bins). The magnitude of the spurious effect was reduced considerably by the large physical separation of the P.M. tubes (1.1m). Similar effects have been observed by Novick,⁷¹ King et al⁷² and O'Connell et al.⁴⁴

In order to compensate for this effect, the metastable beam was modulated by a DC electric quenching field while synchronously switching the detection system. This procedure, of course, doubled the measurement period.

Fig.22 shows a schematic diagram of the electronic system. Pulses from the coincidence photomultipliers anodes were amplified in fast amplifiers, type LRS 333 with a 2ns risetime and a maximum gain of $\times 10$. The output pulses were then fed to a constant fraction differential discriminators, ORTEC type 583. One discriminator output is taken directly to the Start input of a time-to amplitude converter (TAC) while the other is taken through a variable delay to the Stop input. The TAC produces an output pulse whose amplitude is proportional to the arrival time difference of the start and stop pulses.

The TAC output is taken directly to the input of a multi-channel pulse height analyser (MCPHA), an Intertechnique DIDAC 800. The subgroup of the MCPHA memory being addressed by the TAC output is determined by a

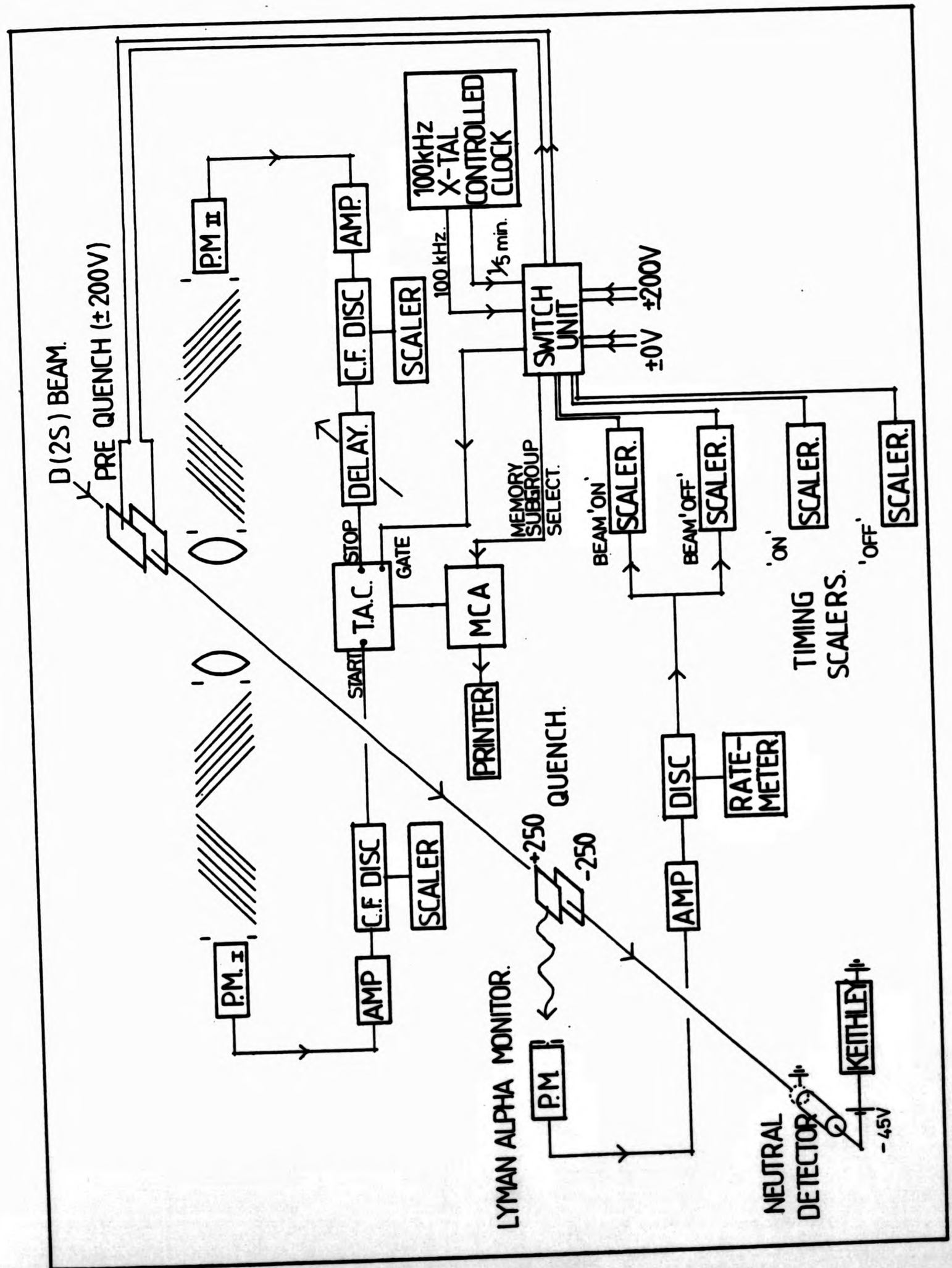


FIG. 22. SCHEMATIC OF ELECTRONIC SYSTEM

switch unit so that the time spectra for the beam with metastable component present, then quenched are stored separately. The difference spectrum then represents the true signal due only to two-photon decay.

When the voltage on the pre-quench plates is being changed, the TAC output is gated off by the switch unit to avoid the possibility of spurious coincidences being generated.

The metastable monitor, which counts the Lyman alpha photons emitted by the metastable beam on entering the quench field is coupled to a slow shaping amplifier, type NE 4603 and integral discriminator type NE 4623. The discriminator output is fed to a ratemeter and two scalars which are gated alternately on and off by the switch unit. One scalar monitors the metastable beam and the other the background. The difference of these two readings gives a measure of the integrated metastable current used in the normalisation procedure

III.9.2 Switch Unit

The timing of the switch unit is controlled by a 100kHz 0.1% accuracy crystal controlled clock. The switch unit fulfills six separate functions as follows;

- (1) it switches the pre-quench field high and low,
- (2), it routes the metastable monitor output to a corresponding scalar depending on whether the pre-quench field is high or low,
- (3), it routes the TAC output to the appropriate subgroup of the multichannel analyser memory,
- (4), it continuously monitors the timing of the beam on/beam off periods.
- (5), it gates the TAC off during a pre-quench field switching operation for a precise time, (0.655s)
- (6), it switches the read/store function on the MCPHA.

The clock unit was set to produce one output pulse every five minutes

and on arrival at the switch unit initiates a change in the level of the pre-quench field, provided the start button has been pressed. When, during a run, the stop button is pressed, the unit changes to a stop condition only after a switching cycle is complete thus preserving equal beam on/ beam off times.

A detailed circuit diagram of this unit has been described previously.³²

III.10 Background Radiation

The spectral distribution of the background radiation in the presence of the beam in the detection region was investigated with the aid of a Macpherson vacuum ultraviolet monochromator whose 2400 grooves/mm grating was blazed for a wavelength $\lambda = 300\text{nm}$. Light from the atomic beam was focussed on to the entrance slit by a suprasil lens (λ cut off = 160nm). To obtain sufficient intensity at the slit, a beam energy $E \geq 3\text{keV}$ was required and so the distribution of the background around 1keV where the two-photon signal was observed can only be inferred from the present work. The main features of this radiation background were as follows:

- (1) A strong Balmer spectrum, converging with rapidly decreasing intensity to the Balmer limit at 365nm.
- (2) A weak molecular band whose head lies at approximately $\lambda = 303.2 \pm 0.3\text{nm}$ and is degraded to the red. Lack of intensity prevented resolution of the vibration - rotation structure but from a table of persistent band heads, a possible candidate is NH i.e. excitation of nitrogen in the background gas.
- (3) A faint continuum observed over the entire spectral range investigated from 180 - 500nm. This radiation is possibly produced by dissociation of excited molecular hydrogen created through charge-exchange of the small H_2^+ (D_2^+) fraction in the beam. It is well known that the $1s\sigma 2s\sigma^3 \Sigma_g^+$ state in mole-

cular hydrogen decays to the repulsive $1s\sigma 2p\sigma^3 \Sigma_u^+$ state with the emission of a continuum over the spectral region 160-500nm. Recent measurements of the products from the charge-transfer of D_2^+ (H_2^+) ions in a caesium vapour have confirmed this possible source of continuous radiation.⁷³

Observation of the RF discharge with a hand held spectroscope also confirmed the presence of a faint continuum whose intensity increased with increasing pressure in the source.

- (4) The fraction of the total light intensity below the Balmer limit was found to be 3% and independent of energy over the range 3-10keV. By applying $\pm 200V$ to the pre-quench plates, the intensity of the Balmer lines reduced in total by a factor ~ 0.5 .

At a beam energy of 1keV, the observed ratio of single rates from the coincidence photomultipliers with the metastable component present, then quenched was found to be ~ 0.7 . This result, along with that obtained in (4) above indicates that the Balmer lines, even at 1keV probably constitute the main source of background radiation. Note that the Balmer alpha line is beyond the spectral sensitivity of the coincidence photomultipliers and hence is assumed to make a negligible contribution to the background. It was noted that with the caesium cell off, the resulting ion beam produced single background rates an order of magnitude lower than with the neutral atomic beam present. Hence the random background due to the remaining small ionic component in the "neutral beam" constitutes $< 1\%$ of the total random background.

The level of background radiation in the detection region due to beam surface collisions etc, was reduced with the aid of a shield consisting of a cylindrical aluminium "can" with 15 and 20 mm diameter holes for the passage of the atomic beam, avoiding direct collisions. This slid neatly over the stainless steel inserts in VGI and was carefully aligned.

with the 1cm diameter collimating apertures on the pre-quench plates. Its internal surfaces were sooted to reduce reflections.

Also, very importantly, the shield was effective in preventing contamination of the vacuum windows with caesium emanating from the ends of the charge-exchange cell.

III.11.1 Optical System

An efficient u.v. transmitting optical system was achieved using optical elements made from the best commercially available synthetic fused silica, Suprasil I, which has a cut-off wavelength $\lambda = 160\text{nm}$. This material offers a number of excellent optical properties, such as; extreme homogeneity and freedom from striae or inclusions; high resistance to radiation darkening from u.v., x-ray and other radiations; low dispersion, reducing chromatic aberration and very low fluorescence levels (0.1% that of natural quartz excited at $\lambda = 254\text{nm}$.)

An ideal lens system would attempt to produce a well collimated beam of light through each polariser. However, the continuous nature of the source radiation complicates any proper optical design in which spherical and chromatic aberrations are minimised. (This can be achieved more easily for a single wavelength). Moreover, the relatively low signal strength necessitated the use of a source region significantly larger than an ideal "point source".

As a result, a simple approach was adopted, Fig. 23 which shows one channel of a necessarily symmetric optical system. On each side of the atomic beam, light passes through a 50mm diameter, 5mm thick vacuum window and is collected by an f/1 bi-convex lens of focal length $f = 50\text{mm}$. The lens focusses the light through a pile-of-plates polariser forming a magnified image ($\sim \times 10$) at the PM photocathode.

The window and collecting lens are supported on a re-entrant stainless steel housing which also supports one end of the polariser on a tight

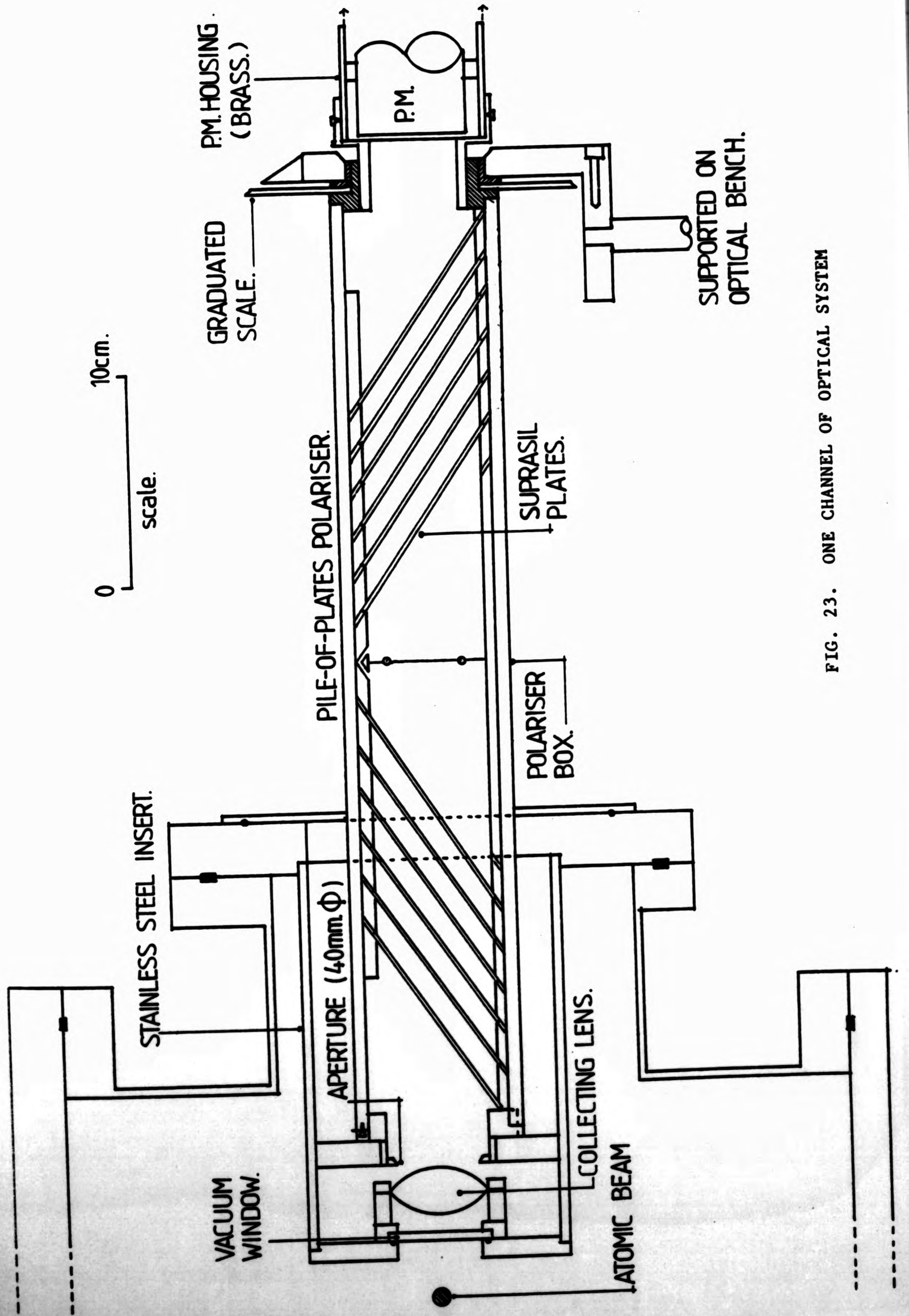


FIG. 23. ONE CHANNEL OF OPTICAL SYSTEM

fitting rotatable teflon bearing. The other end of the polariser (which has a graduated 0 - 360° scale) and the PM housing were supported on an Oriel 1.5m long optical bench and coupled together by a light tight aluminium bearing. The optical benches were positioned, aligned and supported on 2 metre long aluminium tables, bolted at right angles to the main framework of the experiment.

Great care was taken in aligning the windows, lenses and polarisers to a common optic axis. This was achieved with the aid of a He-Ne laser.

III.11.2 Focal length of lenses in the U.V.

While the focal length of the lenses is 50mm at a design index $n = 1.4585$ ($\lambda = 587.6\text{nm}$), the focal length at the centre of the two-photon spectral distribution ($\lambda = 243\text{nm}$) is significantly smaller due to dispersion, and was easily re-calculated to be $f(243) = 44.9\text{mm}$. This focal length and knowledge of the image distance $s' \approx 480\text{mm}$, fixed by the physical size of the polariser determined the object distance from the lenses, $s = 49.5\text{mm}$. The principal planes are located 6.9mm within the lens surfaces and thus allowed reasonably accurate positioning of the collecting lenses with respect to the centre of the atomic beam for $\lambda = 243\text{nm}$. In the spectral region of interest (185-355nm), chromatic aberration for such lenses is significant, as one can see by comparing the focal lengths for example between 200 and 300nm, table 1.

This dispersion causes "over focussing" of the light below $\lambda = 243\text{nm}$ producing an image within the polarisers while that above 243nm is "defocussed" producing an image which lies well beyond the P.M. photocathode. This effect naturally reduces the overall detection efficiency.

III.11.3 Effective Observation Volume

The effective source size which contributes to the observed two-photon signal is determined by two factors:-

- (i) the collimation of the atomic beam ($\phi = 10\text{mm}$)

λ (nm)	f (mm)	S (mm)	S' (mm)	M = S'/S
200	42.7	49.5	310.8	6.3
<u>243</u>	44.9	49.5	480	<u>9.6</u>
300	47.2	49.5	1015.8	20.5

TABLE 1
VARIATION OF FOCAL LENGTH AND MAGNIFICATION AS A FUNCTION OF WAVELENGTH IN THE RANGE $200 < \lambda < 300\text{nm}$.

(ii) the magnification of the optical system.

Fig. 24 shows the relevant geometry which considers extreme rays undeviated through the lenses making an angle α with the optic axis. These rays just reach the outer edge of the photocathode whose effective diameter $\phi = 40 \text{ mm} = h'$. Since the magnification,

$$M = s'/s \approx 10 = h'/h \quad (243\text{nm}) \quad 3.9$$

then $h = 4\text{mm}$ is the effective dimension of the observation volume in the x-direction selected by the lenses. Clearly, source points in the x-z plane outside the region defined by the intersection of the extreme rays and the atomic beam cross-section would not be expected to contribute significantly to the detected coincidence signal.

By rotational symmetry, the source region selected from the atomic beam by the lens will approximate to a cylinder 4mm in diameter and 10mm long. Hence the volume of this cylinder,,

$$V = \pi \frac{h^2}{4} d \approx 126\text{mm}^3 \quad 3.10$$

The cross-sectional area of that part of the beam contributing to the detected two-photon signal $A \sim 40\text{mm}^2$, approximately half that of the atomic beam in the detection region. Thus, a significant fraction of the metastable flux which contributes to the normalisation procedure does not contribute to the detected 2-photon signal. This problem and its resolution is discussed in section IV.4.7

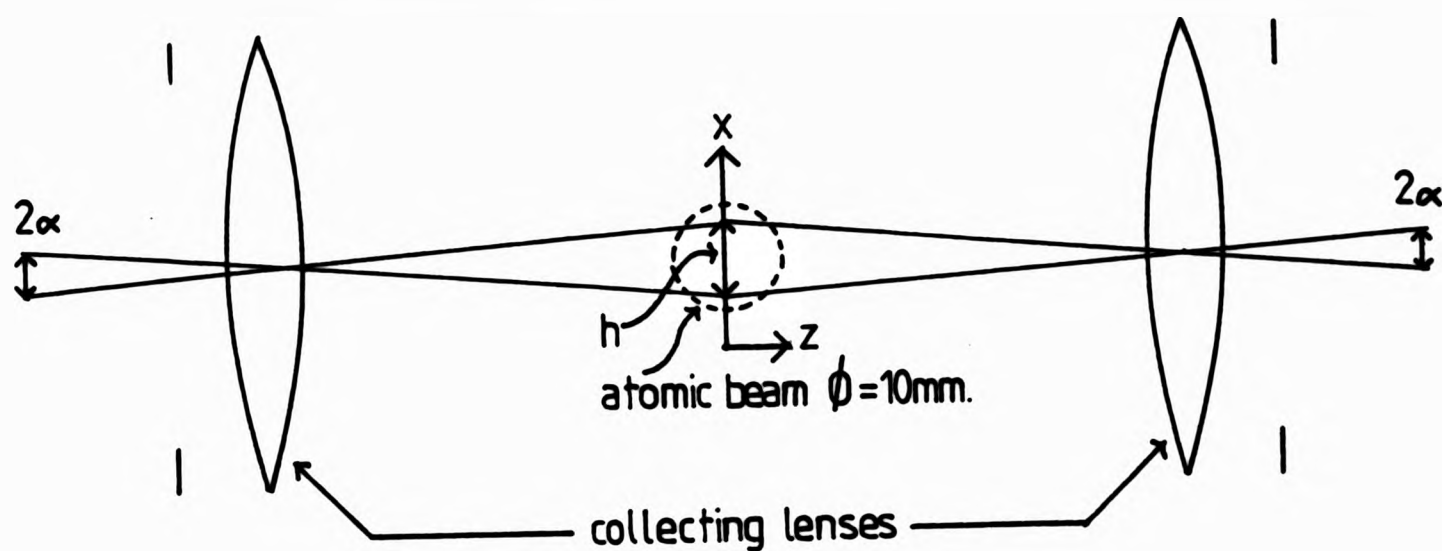


FIG. 24 EFFECTIVE SOURCE SIZE SELECTED BY LENS SYSTEM. EXTREME RAYS MAKES ANGLES $\pm\alpha$ TO OPTIC AXIS.

III. 11.4 Pile of Plates Polarisers

Efficient transmission pile-of-plates polarisers for the u.v. were each constructed from 12 Suprasil plates oriented at Brewster's angle $\theta_B = 56.5^\circ$ to the incident light ($\lambda = 243 \text{ nm}$). The plate dimensions are $100 \times 60 \times 2 \text{ mm}$ polished to 2λ per face at $\lambda = 243 \text{ nm}$ and stacked in two complementary sets of 6 plates to cancel transverse ray displacements.

Essentially, light polarised in the plane of incidence (p-component) has a reflection coefficient $R_p = 0$ at Brewster's angle while light polarised perpendicular to the plane of incidence (s-component) is partially reflected at each interface and hence attenuated. The emerging light is therefore largely p-polarised.

Fig. 25 shows the reflection coefficients for the p and s components determined from Fresnel's equations when unpolarised light is incident upon a di-electric surface.

The higher the refractive index n , the higher is the reflection coefficient R_s and hence fewer plates would be required to achieve a reasonable degree of polarisation. Pile-of-plates polarisers can achieve a very high degree of polarisation. However, with regard to a test of Bell's theorem, it is the absolute transmission for the p-component ϵ_M

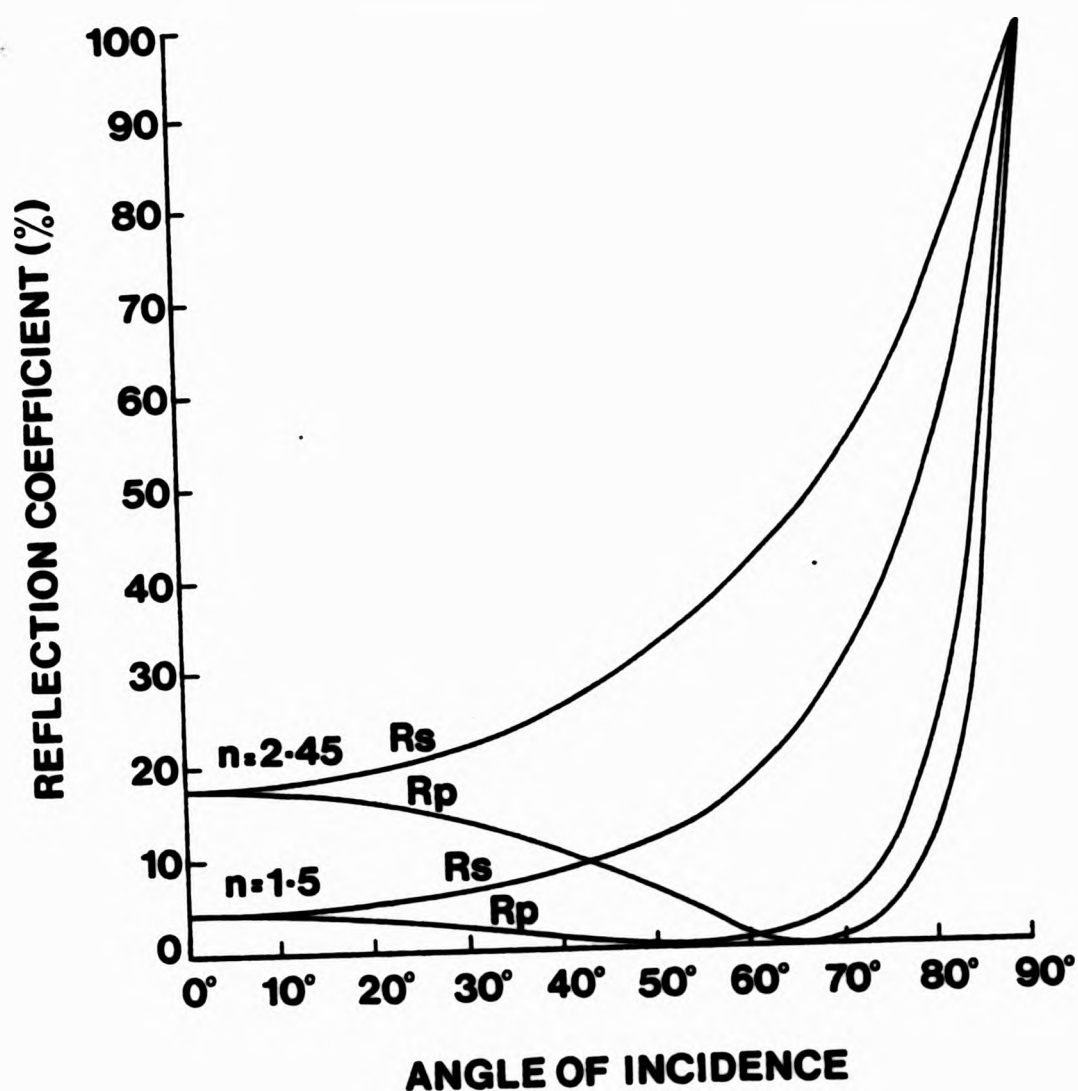


FIG. 25 REFLECTION COEFFICIENTS FOR P AND S COMPONENTS FOR TRANSMISSION OF UNPOLARISED LIGHT AT A DIELECTRIC SURFACE. AT BREWSTER'S ANGLE $\theta_B = \tan^{-1} n$, $R_p = 0$.

which is the critical factor in the design of a decisive experiment.⁴

We now consider both these factors.

- (1) In order to achieve a reasonable degree of polarisation, we require the intensity of the s-component to be reduced to the order of a few percent. Consider unpolarised light incident on a single non-absorbing plate at Brewster's angle. Assuming no interference within the plate (which is reasonable as the phase differences between interfering components can be regarded as randomly distributed, the coefficients for reflected and transmitted intensities R and T , respectively, are given by the Airy expressions (in terms of refractive index n),⁷⁴

$$R = (n^2 - 1)^2 / n^4 + 1$$

$$T = 1 - R = 2n^2 / n^4 + 1$$

3.11

Hence at $\lambda = 243\text{nm}$, where $n = 1.511$ for Suprasil, $T_s = 0.735$ for a single plate and the transmission through m plates, (neglecting reflections between plates),

$$T_s^m = (0.735)^m \quad 3.12$$

Thus to reduce the s-component to $< 5\%$ requires $m > 10$. We chose $m = 12$ and so expect $T_s^{12} = (0.735)^{12} = 0.025$. The degree of polarisation, then, since $T_p = 1$ at Brewster's angle should be,

$$P = \frac{1 - T_s^{12}}{1 + T_s^{12}} = 0.95 \quad 3.13$$

Although multiple reflections between plates can occur, diverting a proportion of the unwanted radiation back into the transmitted beam, thus reducing the expected polarisation, Conn and Eaton,⁷⁴ have shown however, that provided only a small number of such rays reach the detector, no significant reduction in P would be expected. With the plate spacing used, ($D = 16\text{mm}$) and 40mm apertures either end of the polarisers, only two such rays at most can contribute to the observed intensity of the s-component. We estimate the increased transmission of the s-component to be $\sim 1.8 T_s^{12} = 0.04$ ($\lambda = 243\text{nm}$)

- (2) The Transmission $T_p = \frac{\epsilon_M}{\epsilon_m}$ for the p-component must be very high
 Clauser et al⁴ have shown that in the design of a decisive experiment to test for hidden variables, a lower limit for ϵ_M is given approximately by the inequality,

$$2F(\theta) + 1 > 2/\epsilon_M \quad 3.14$$

where $F(\theta)$ is the geometrical factor slightly less than unity related to the collection half angle of the lenses. This inequality can also be derived from equation 2.31 Chapter II by setting $(\epsilon_- / \epsilon_+)^2 = 1$ and $\epsilon_+ = \epsilon_M + \epsilon_m \approx \epsilon_M$.

Hence from inequality 3.14, since for our geometry, $F(\theta) = 0.996$,

λ	Absorption Coefficient α	$\xi_M = 10^{-12}\alpha d$
200	0.013 cm ⁻¹	0.931
204	0.01 cm ⁻¹	0.946
243	0.002 cm ⁻¹	0.989
248	0.00126 cm ⁻¹	0.993
306	0.00049 cm ⁻¹	0.997

TABLE 2
 ABSORPTION COEFFICIENT (CM⁻¹) FOR SUPRASIL I AT VARIOUS WAVELENGTHS
 AROUND 243NM. VALUES QUOTED BY MELLES GRIOT (AMERSIL INC).

$$T_p = \xi_M > 0.83$$

3.15

Clearly, any losses through (i) absorption and (ii) scattering due to surface imperfections will serve to reduce ξ_M . The plate flatness, 2λ per face should be adequate to reduce surface scatter to a minimum.

Absorption, of course, can be reduced by using very thin plates. However plates with thickness $d < 0.2$ cm could not be obtained owing to the risk of breakage during polishing. The absorption coefficient for Suprasil I in the spectral region around $\lambda = 243$ nm is shown in table 2 along with the calculated transmission at Brewster's angle through 12 plates.

It would appear then that although significant absorption occurs in the region below 200nm, we should expect to obtain, on averaging over the two-photon spectral distribution (185-355nm) a value for $\langle \xi_M \rangle$ significantly higher than the lower limit set by inequality 3.14.

III.11.5 Angular Acceptance of Polariser

In order to achieve a reasonable two-photon signal through the polarisers, the angular acceptance was relaxed to $\theta = \theta_B^+ = 4.8^\circ$, determined by the physical length of the polarisers and the apertures used. This will have the effect

of reducing the expected value of ϵ_M further. However, for small variations in the angle of incidence close to θ_B (fig. 25), R_p passes through a minimum and varies slowly so that the reduction in ϵ_M should not be too significant.

III 11.6 Transverse Ray Displacements

It is very important with regard to a test of Bell's inequality to make sure that all rays which pass through the polariser with the plates out also pass through when the plates are in.

The lateral displacement suffered by a ray passing through m plates is given simply by,

$$D_m = mt \sin (\theta_i - \theta_r) / \cos \theta_r \quad 3.16$$

where t = plate thickness

θ_i = angle of incidence ($\theta_i = \theta_B \pm 5^\circ$)

θ_r = angle refraction within plate

The maximum deviation occurs at $\theta = \theta_B + 5^\circ = 61.5^\circ$ then $\theta_r = 35.5^\circ$ ($\lambda = 243$) and the displacement due to a stack of 6 plates is,

$$D_6 (\text{max}) = 6.5\text{mm}$$

The 40mm aperture used at the polariser entrance ensured a clearance of 7mm to the top edge of the plates, thus ensuring the above condition.

III 11.7 Measured Transmittances ϵ_M, ϵ_m at $\lambda = 254\text{nm}$

With the polarisers in situ, the transmittances for a pile-of-plates polariser were measured in a subsidiary experiment, as follows. The photomultiplier was removed from one detection arm and the radiation from a mercury lamp passed through a pin-hole and thin paper screen to produce a diffuse diverging light source which was made to converge through a u.v. dichroic linear polariser (Polacoat PL40) and 254nm interference filter before entering the first pile-of-plates polariser.

The transmission axis of the dichroic polariser was aligned parallel to that of polariser I to produce a highly polarised beam entering polariser

II, (which is under test). For the dichroic film, the transmittance for light polarised parallel and perpendicular to the transmission axis is, $\epsilon'_M = 0.3$, $\epsilon'_m = 0.01$ respectively, while for pile-of-plates polariser I, we expect, (see section 2.4), $\epsilon_M \gg 0.9$, $\epsilon_m \approx 0.04$.

Hence the resulting degree of polarisation will be,

$$P = \frac{\epsilon'_M \epsilon_M - \epsilon'_m \epsilon_m}{\epsilon'_M \epsilon_M + \epsilon'_m \epsilon_m} \geq 0.997 \quad 3.17$$

which is very satisfactory. With the converging lens positioned to give maximum intensity at the PM tube, we assume that an image of the source is formed at the photocathode and a secondary diverging source of light formed mid-way between the collecting lenses at the position normally occupied by the atomic beam. In this case the convergence of the light in polariser II is assured and under similar conditions to that when the atomic beam is present.

The measured values of transmittance when polariser II is rotated parallel and perpendicular to the polarised beam were;

$$\epsilon_M = 0.936 \pm 0.008 = I(0^\circ) / I_0 \quad 3.18$$

$$\epsilon_m = 0.031 \pm 0.001 = I(90^\circ) / I_0$$

where I_0 is the intensity measured with the plates removed. In fact, no significant variation in the extinction coefficient ϵ_m / ϵ_M was observed when the convergence of the radiation was altered. Since the polarisers are identically constructed, we assume that the corresponding transmittances in each polariser are almost equal, i.e.

$$\epsilon_M^1 = \epsilon_M^2 = \epsilon_M \quad 3.19$$

$$\epsilon_m^1 = \epsilon_m^2 = \epsilon_m$$

With regard to the two-photon spectral distribution, the measured values of ϵ_M , ϵ_m above must be corrected for a slight absorption in Suprasil below $\lambda = 243\text{nm}$. By using the quoted values of the absorption coefficient in table 2 and extrapolating below 200nm, this effect has been estimated by averaging α over the effective two-photon spectrum

(185-355nm where $\lambda = 185\text{nm}$ corresponds to the oxygen cut-off.)

This results in a correction factor, which when applied to the measured values at $\lambda = 254\text{nm}$, (where there is negligible absorption), yields finally,

$$\begin{aligned}\epsilon_M &= 0.908 \pm 0.013 \\ \epsilon_m &= 0.0299 \pm 0.0020\end{aligned}\quad 3.20$$

III.11.8 Quarter Wave Plates

Quarter wave plates in conjunction with the pile-of-plates polarisers were used to investigate the circular polarisation correlation of the photon decay of metastable atomic deuterium, (see section IV.4). The $\lambda/4$ plates are achromatic over the spectral range 180-300nm (matching the 2-photon spectrum very well) and the accuracy of the path difference is $\pm 10\%$ with an incident ray deviation $\delta\theta < 1^\circ$ to the normal. These are produced by Halle Nachfl of Berlin.

The retarders consist of a combination of four elements - two double plates of crystal quartz and MgF_2 with air spacing between the single plates. All are cut parallel to the optic axis, polished to $\lambda/10$ and mounted in a cylindrical holder engraved with the fast axis. The aperture is 19.5mm ϕ .

The cylindrical holder was mounted in a teflon sleeve which recessed neatly into the front end of the polariser housing (nearest the lens). The relative angle between the $\lambda/4$ plate fast axis and the transmission axis of the polariser could be set with the aid of a graduated scale (22.5° intervals) marked on the teflon bearing supporting this end of the polariser.

CHAPTER IV RESULTS

IV.4.1 Measurement Method

Since coincidence runs last typically around 20 hours to achieve an acceptable statistical accuracy ($< 10\%$), all experimentally relevant parameters were carefully monitored throughout each run to check and correct if necessary for drifts. The performance of the RF ion source in this respect excelled all expectations giving a very stable output for long periods so that constant source conditions and hence stable beam conditions could be maintained.

The parameters monitored throughout each run apart from the beam energy and source conditions were: the integrated beam "on"/beam "off" times, the integrated Lyman alpha counts (beam "on"/beam "off") so that the difference of these scaler readings can be used to normalise each run, the singles rates and the integrated singles counts from the coincidence photomultipliers, the neutral beam current, the Lyman alpha count rate and the oxygen flowrate to the Lyman alpha monitor.

IV 4.2 Optimum Conditions for Best Statistical Accuracy

The most favourable conditions under which to observe a two-photon signal were estimated as follows. If $S_{2\gamma}$ is the two-photon signal, then,

$$S_{2\gamma} \propto n(D_{25}) \propto \dot{L}_\alpha / \sqrt{E} \quad 4.1$$

where $n(D_{25})$ is the metastable density, \dot{L}_α is the observed Lyman alpha count rate, and E is the beam energy.

If $\dot{N}_1(\gamma)$, $\dot{N}_2(\gamma)$ are the observed singles rates from the coincidence photomultipliers, then the random error in a coincidence spectrum, is

$$R \propto \sqrt{\dot{N}_1 \dot{N}_2} \quad 4.2$$

Hence an indication of the best operating conditions can be obtained by observing the ratio,

$$S_{2\gamma} / R \propto \dot{L}_\alpha / \sqrt{\dot{N}_1 \dot{N}_2} E \quad 4.3$$

as beam energy and source conditions are altered, Fig. 26 shows how S_{28}/R varies with beam energy and indicates an optimum around a beam energy $E \approx 800\text{eV}$ for deuterium.

This analysis breaks down at low energy since then the background coincidence peak becomes troublesome. It was observed that an increase in beam energy of only a few hundred eV above the optimum in fig. 26 reduced the statistical accuracy significantly in agreement with this crude analysis. Consequently, the beam energy for coincidence runs was selected close to $E = 800\text{eV}$.

IV 4.3 Linear Polarisation Correlation

Fig. 27 shows how the measured coincidence rate varies with the relative angle between the transmission axes of the polarisers (in the range $0 \leq \phi \leq 180^\circ$) along with a least squares fit of the form $A + B \cos^2 \phi$ since this is the QM predicted form of the correlation in the case of non-ideal polarisers, equation 2.41. One can see that the data and the fitted curve are in good agreement. The raw data for these runs are given in appendix III.

These results indicate a strong correlation in linear polarisation between the detected photons and that the transition probability is indeed proportional to $(\hat{e}_1 \cdot \hat{e}_2)^2$ in agreement with the prediction of the theory of spontaneous two-photon decay.²¹

Fig. 28 shows a typical coincidence spectrum which is the difference of two spectra stored in separate subgroups of the MCPHA memory - one with the metastables present and the other with the metastables quenched so that the small contribution from the background (cosmic rays, radioactivity and electrical pick-up) has been subtracted out. The peak FWHM ~ 3 channels or 2.5ns, approximately equal to the timing resolution of the electronic system. (This is in fact limited by the transit time spread in the photomultipliers, typically 1 ns for each tube.) The symmetric nature of the coincidence peak is consistent with the obser-

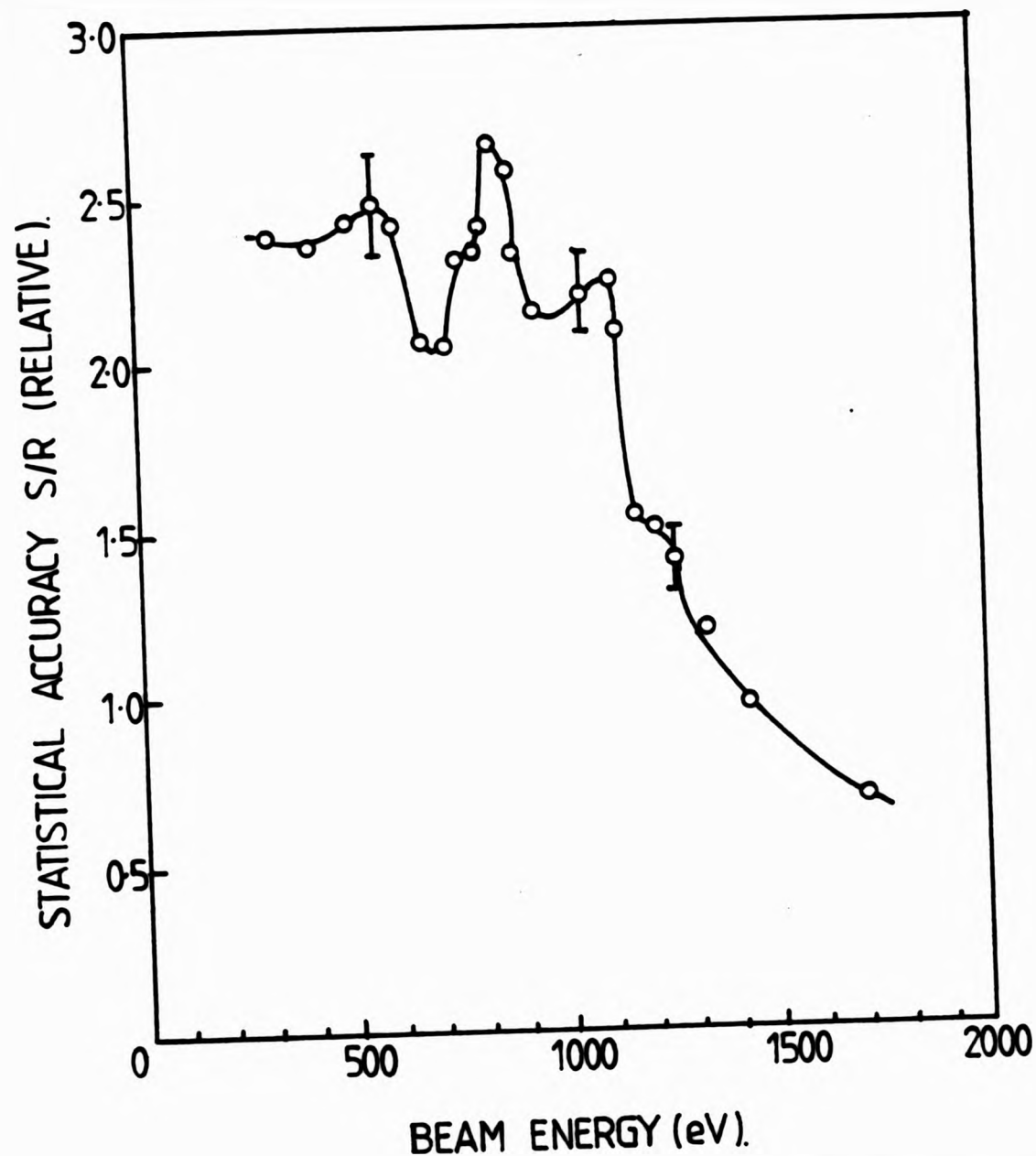


FIG. 26 ESTIMATED STATISTICAL ACCURACY TO BE EXPECTED FOR OBSERVATION OF TWO-PHOTON SIGNAL WHEN BEAM ENERGY IS VARIED.

vation of a fast radiative process, as in two-photon emission.

Finally, the observed strong polarisation correlation eminently confirms the correctness of the two-photon state vector equation 1.42 and hence the suitability of the two-photon decay of metastable atomic hydrogen (deuterium) for a test of Bell's theorem.

IV 4.4 Test of Bell's Inequality

From the linear polarisation data, appendix 4, a decisive test for local realistic theories can be performed assuming the Clauser-Horne⁵³ no-enhancement hypothesis is valid. In Chapter II, we derived Bell's inequality, and assuming the rotational invariance of the coincidence rate $R(\phi)$, this inequality contracts to the simplified form,

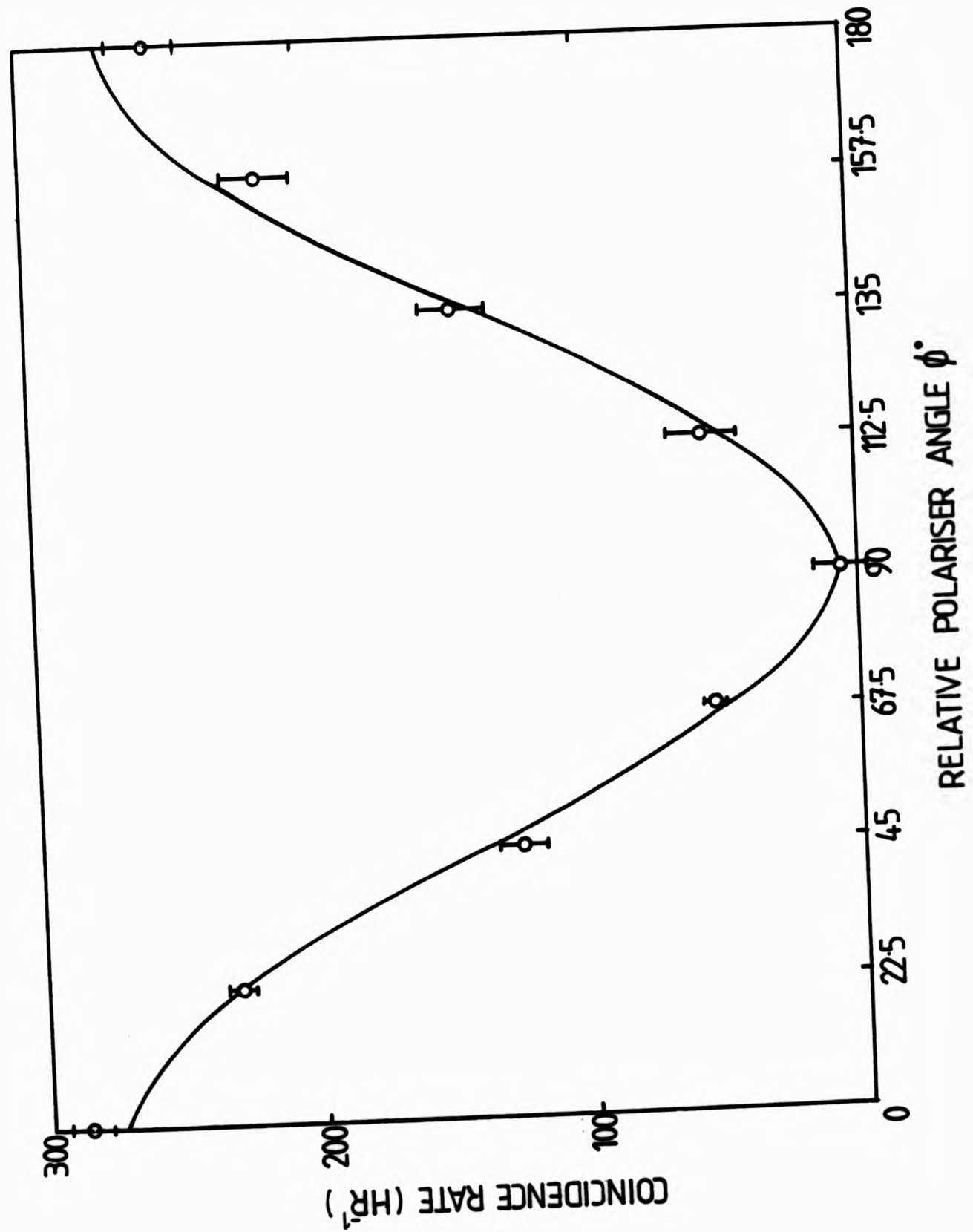


FIG. 27. LINEAR POLARISATION CORRELATION IN THE TWO-PHOTON DECAY OF METASTABLE ATOMIC DEUTERIUM. A LEAST SQUARES FIT OF THE FORM $A + B\cos^2\phi$ IS SHOWN TO AGREE WELL WITH THE OBSERVED DATA (APPENDIX 3). ERROR BARS SHOW ONE STANDARD DEVIATION. FROM FIT, $A = 264.8 \pm 7.4$, $B = 7.0 \pm 4.8$ WHERE THE QUOTED ERRORS ARE AGAIN ONE STANDARD DEVIATION.

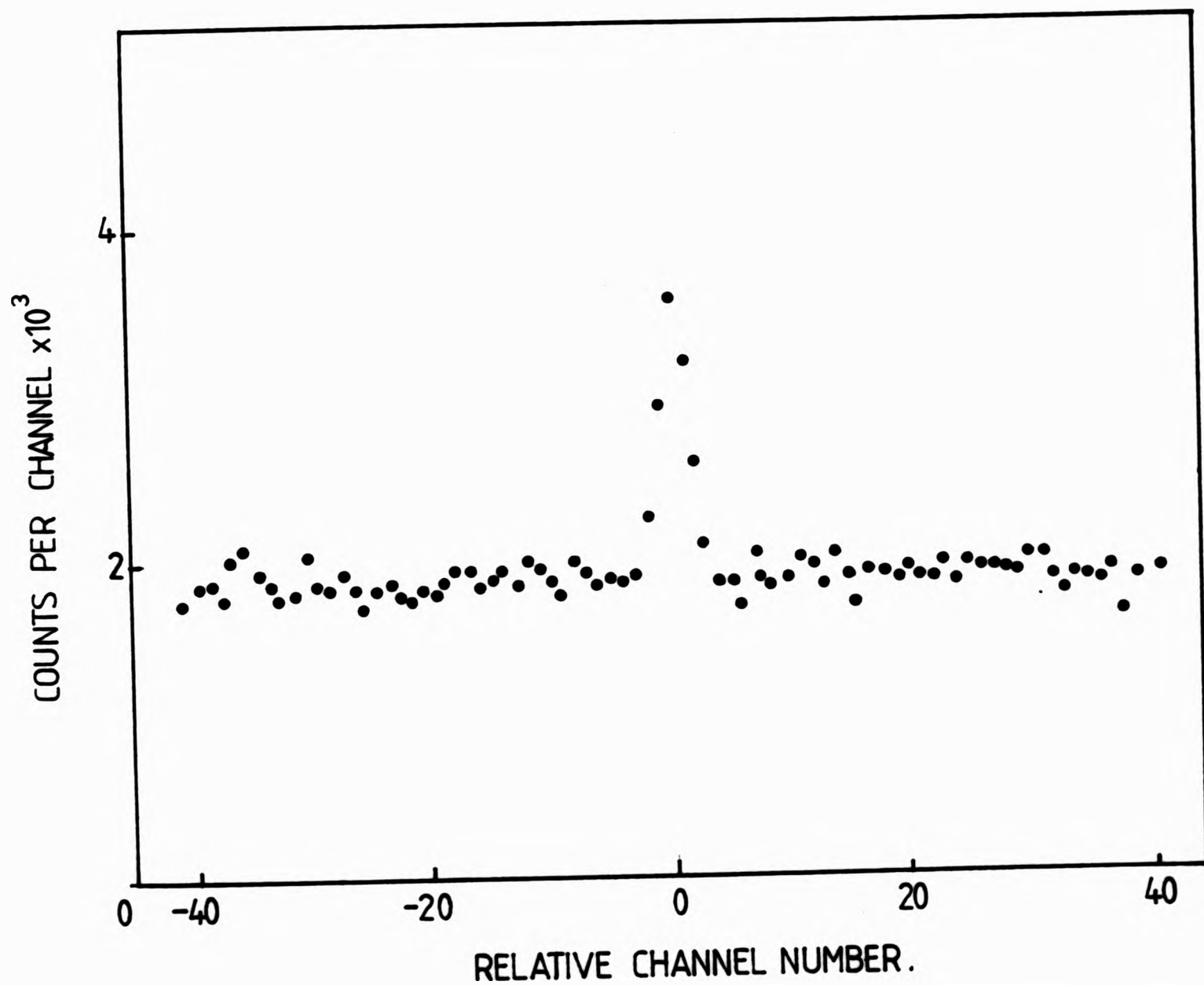


FIG. 28. A TYPICAL TIME-CORRELATION SPECTRUM AFTER SUBTRACTION OF THE SPECTRUM OBTAINED WITH THE METASTABLE COMPONENT OF THE BEAM QUENCHED. POLARISER PLATES ARE REMOVED. TIME DELAY PER CHANNEL IS 0.8 ns. TOTAL COLLECTION TIME IS 21.5 HR. SINGLES RATES WITH METASTABLES PRESENT (QUENCHED) ARE ABOUT $1.15 \cdot 10^4 \text{ s}^{-1}$ ($0.85 \times 10^4 \text{ s}^{-1}$). TRUE TWO-PHOTON COINCIDENCE RATE IS $490.5 \pm 16.2 \text{ HR}^{-1}$. LYMAN ALPHA COUNT RATE $\langle L_{\alpha}^{\circ} \rangle = 70.51 \text{ s}^{-1}$.

equation 2.37. Thus, all local realistic theories predict that the quantity,

$$\delta = |R(22.5^\circ) - R(67.5^\circ)| / R_0 \leq 0.25^* \quad 4.4$$

where $R(22.5^\circ)$, $R(67.5^\circ)$ are the normalised coincidence rates at $\phi = 22.5^\circ$, 67.5° respectively and R_0 is the coincidence rate with the polariser plates removed. Using the data in appendix III, we obtain

$$\delta = .267 \pm 0.010 (1\sigma) \quad 4.5$$

violating inequality 4.4 by 1.7 standard deviations. The Quantum Mechanical predictions for our experiment can be calculated from equation 2.41, Chapter II,

$$\left[\frac{R(\phi)}{R_0} \right]_{QM} = \frac{1}{4} [(\epsilon_M + \epsilon_m)^2 + (\epsilon_M - \epsilon_m)^2 F(\theta) \cos 2\phi] \quad 4.6$$

The measured polariser efficiencies at $\lambda = 254\text{nm}$ corrected for a slight absorption in the plates are, $\epsilon_M = 0.908 \pm 0.013$, $\epsilon_m = 0.0299 \pm 0.0020$ while the geometrical factor $F(\theta) = 0.996$ (appendix II)

Thus,

$$\left[\frac{R(\phi)}{R_0} \right]_{QM} = 0.028 + 0.384 \cos^2 \phi \quad 4.7$$

Fig 29 shows this absolute QM prediction along with the measured values of $R(\phi) / R_0$ over $0^\circ \leq \phi \leq 90^\circ$ where one can see that the agreement is satisfactory. From the predicted values at $\phi = 22.5^\circ, 67.5^\circ$ we obtain,

$$\delta_{QM} = 0.272 \pm 0.008 \quad 4.8$$

in good agreement with the observed value, equation 4.5. Note that the error bars show one standard deviation and vary from point to point because of the different total counting times allocated to different angles. The data at $\phi = 22.5, 67.5^\circ$ were accumulated over a counting period of around 240 hours for each point.

IV 4.5 Circular Polarisation Correlation

With the aid of achromatic quarter wave plates (described earlier) mounted ahead of the linear polarisers, the circular polarisation

* In contrast in the ideal case, $\delta_{QM} = 0.354$

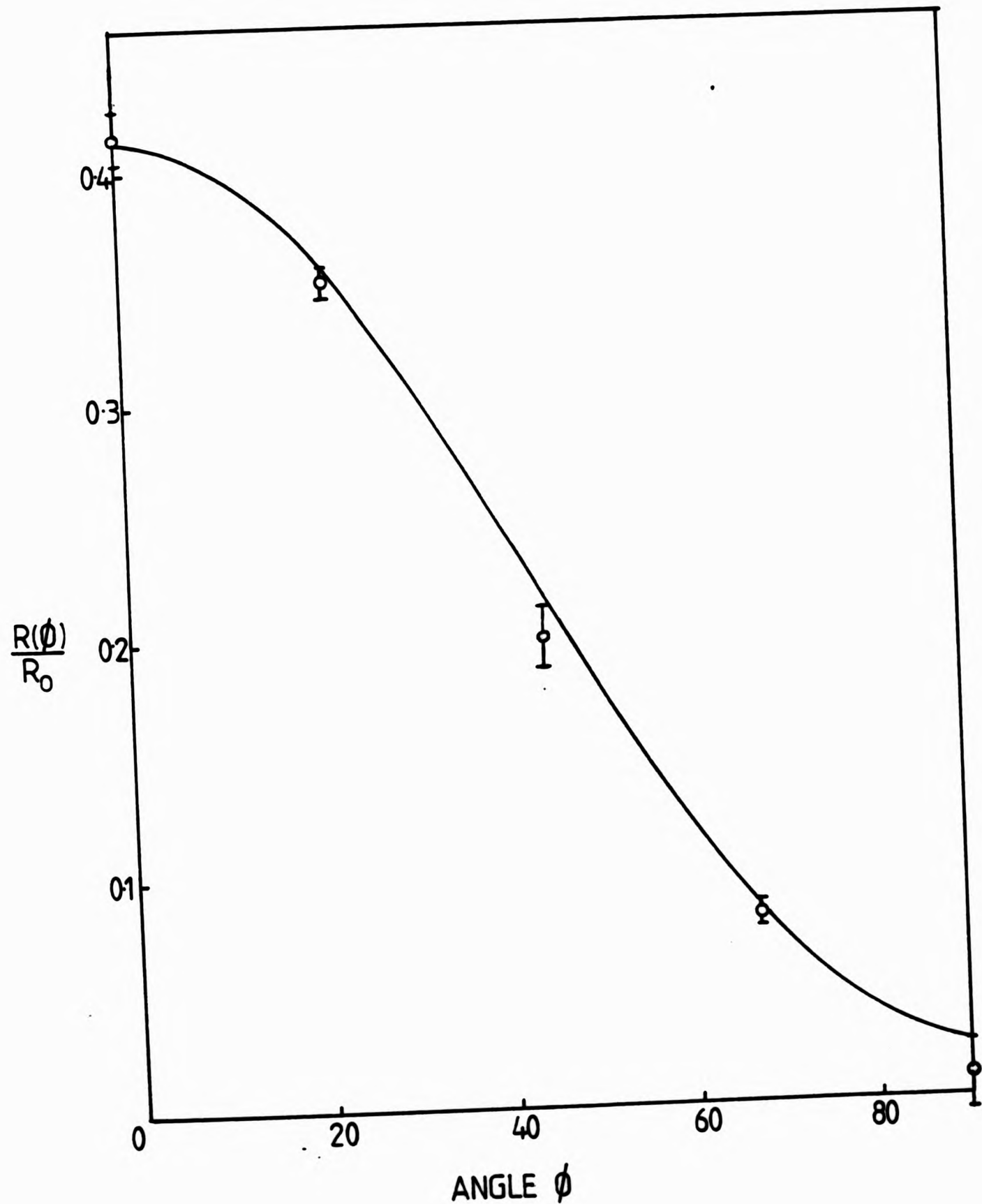


FIG. 29. COINCIDENCE SIGNAL AS A FUNCTION OF THE ANGLE ϕ BETWEEN THE TRANSMISSION AXES OF THE POLARISERS, RELATIVE TO R_0 , THE COINCIDENCE SIGNAL WITH THE POLARISER PLATES REMOVED. THE SOLID CURVE REPRESENTS THE QM PREDICTION OF EQUATION 4.7, WHERE THE MEDIAN VALUES OF ϵ_M , ϵ_m HAVE BEEN USED.

correlation of the two-photon decay was investigated, and the results are shown in Fig.30. In this case, one channel was set to detect right hand circularly polarised light $|R\rangle$ while the $\lambda/4$ plate fast axis in the other channel was rotated to an angle ϕ with respect to the transmission axis of the linear polariser. Hence at one extreme ($\phi = -45^\circ$) the second polariser detects right hand circularly polarised light $|R\rangle$, while at the other extreme ($\phi = +45^\circ$) it detects left hand circularly polarised light $|L\rangle$. A least squares fit of the form $\alpha + \beta \cos^2(\phi + \pi/4)$ which is the QM prediction is also shown and reasonably agrees with the observed data. The low coincidence rates in this case compared to the linear polarisation results, Fig. 27 are due mainly to the reduction in the collection solid angle. (The external transmission of the $\lambda/4$ plates is 70% due mainly to reflection losses at the plate surfaces).

The collimation of the incident light on the $\lambda/4$ plate has an average deviation to the optic axis of $\sim \pm 1.8^\circ$ corresponding to a retardation $\lambda/4 \pm \sim 15\%$.

The measurements of circular polarisation are important since they directly confirm the conservation of angular momentum along the common axis of detection.

The appropriate two-photon state vector equation 1.41 was derived by considering conservation of angular momentum and parity during the emission process. As a result of a measurement, we expect the state vector to collapse to $|R_1\rangle |R_2\rangle$ or $|L_1\rangle |L_2\rangle$ for which we have $L_z = 0$ in each event and thus $\langle L_z \rangle = 0$ for the ensemble.

Fig 31 (i - iv) shows the coincidence spectra obtained when the polarisers are set to detect $|R_1\rangle |R_2\rangle$, $|L_1\rangle |L_2\rangle$, $|R_1\rangle |L_2\rangle$ and $|L_1\rangle |R_2\rangle$ photon pairs and these spectra clearly support angular momentum conservation. Within statistical error, the coincidence rates

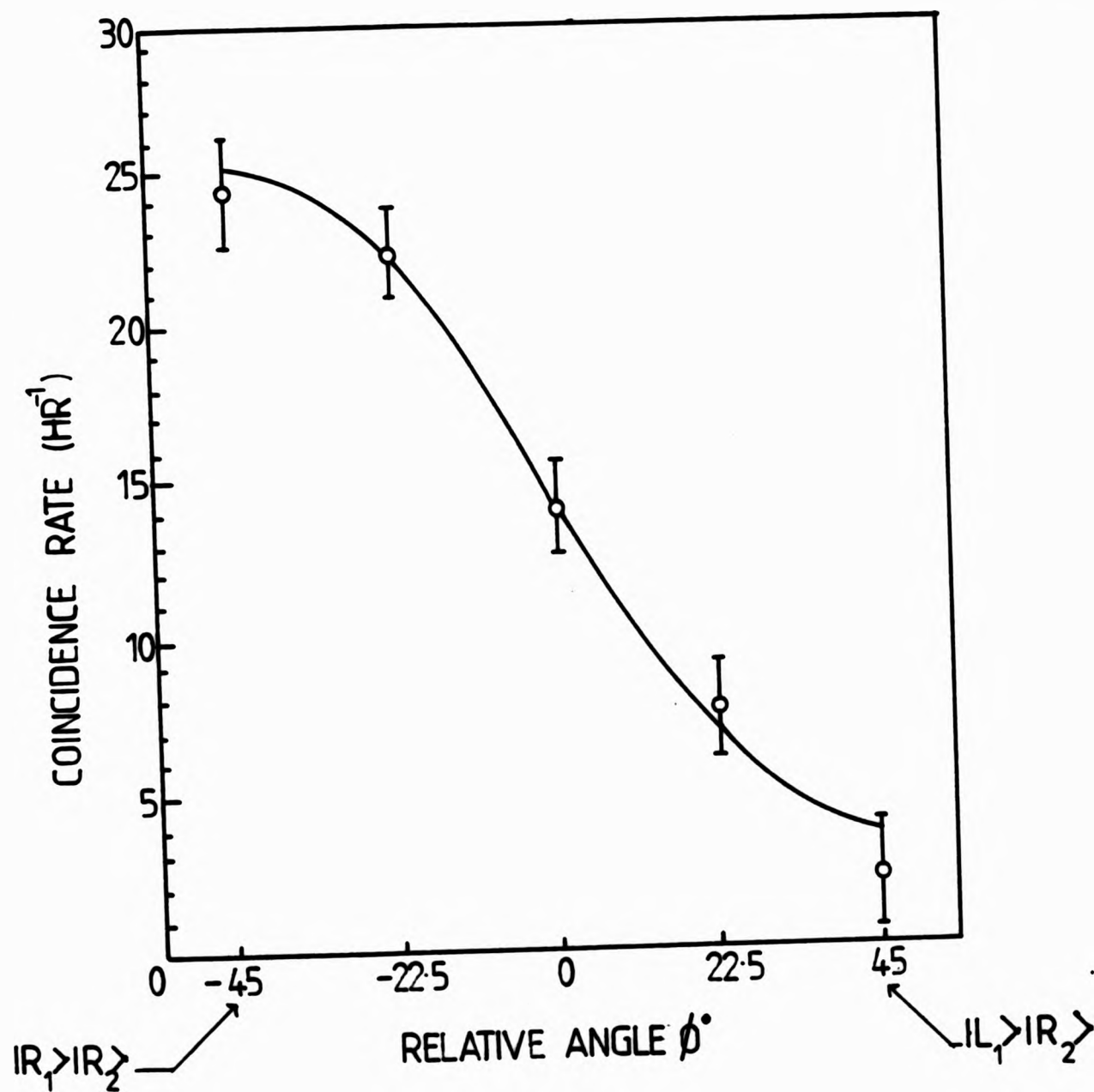


FIG.30. CIRCULAR POLARISATION CORRELATION IN THE TWO-PHOTON DECAY OF METASTABLE ATOMIC DEUTERIUM. ϕ IS THE RELATIVE ANGLE BETWEEN THE FAST AXIS OF THE QUARTER WAVE PLATE AND THE TRANSMISSION AXIS OF POLARISER I. THE OTHER QUARTER WAVE PLATE WAS SET TO $\phi = -45^\circ$ RELATIVE TO THE TRANSMISSION AXIS OF POLARISER II, THUS DETECTING RIGHT HAND CIRCULARLY POLARISED LIGHT. A LEAST SQUARES FIT OF THE FORM $\alpha + \beta \cos^2(\phi + \pi/4)$ IS ALSO SHOWN TO FIT THE DATA FAIRLY WELL. ERROR BARS SHOW 1 S.D. FROM FIT, $\alpha = 21.7 \pm 3.7$, $\beta = 3.6 \pm 2.3$ (1 S.D.).

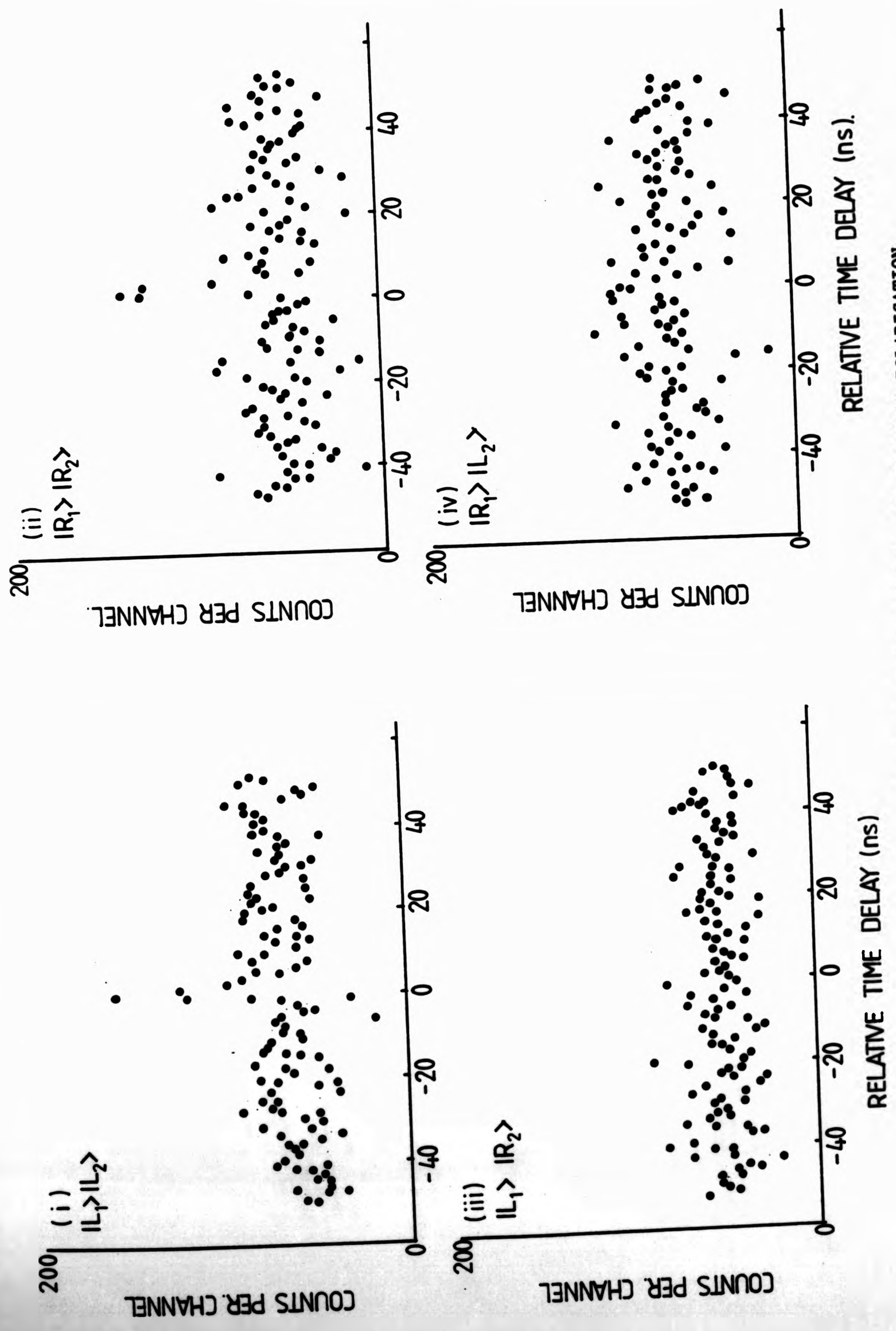


FIG. 31. COINCIDENCE SPECTRA FOR CIRCULAR POLARISATION.

for detection of $|R_1\rangle |R_2\rangle$ and $|L_1\rangle |L_2\rangle$ pairs were found to be equal, as expected. (Similarly for $|L_1\rangle |R_2\rangle$ and $|R_1\rangle |L_2\rangle$ pairs.)

IV 4.6 Check for Rotational Symmetry of Optical System

It is important to show that the optical elements preceding the polarisers do not introduce any significant polarisation in the transmitted radiation which could lead to a loss of rotational invariance. This is particularly important with regard to a test of Bell's inequality in the "Freedman" form, equation 4.4 .

In this experiment, a stable neutral atomic beam was used as the source and the response of the coincidence photomultipliers monitored as each pile-of-plates polariser was rotated. The PM's were rotated with the polarisers avoiding any effects from sensitivity to polarisation which might exist in the P.M. photocathodes.

The results are shown in Fig 32. From the spread in observed singles rates, we obtain,

$$\text{Polariser I , } \langle N_1 \rangle = (2.17 \pm 0.05) \cdot 10^3 \text{ s}^{-1} , \sigma[\langle N_1 \rangle] / \langle N_1 \rangle = 0.023$$

$$\text{Polariser II, } \langle N_2 \rangle = (1.66 \pm 0.04) \cdot 10^3 \text{ s}^{-1} , \sigma[\langle N_2 \rangle] / \langle N_2 \rangle = 0.023$$

while the variation in beam current $\sigma[I_0] / I_0 = \frac{0.01}{0.50} = 0.020$

Hence the spread of the data is consistent with the observed fluctuation in beam current. The results indicate that the optical system is indeed rotationally invariant, as required.

IV 4.7 Normalisation Procedure

The two-photon signal should be proportional to the metastable density so that variations from run to run must be taken into account through normalisation.

The metastable monitor output gives a measure of the metastable flux, proportional to the density when the beam energy is constant. When there are also slight variations in beam energy E between runs, this can be taken into account through the normalisation factor, equation 4.1,

$$\langle L_i \rangle / \sqrt{E}.$$

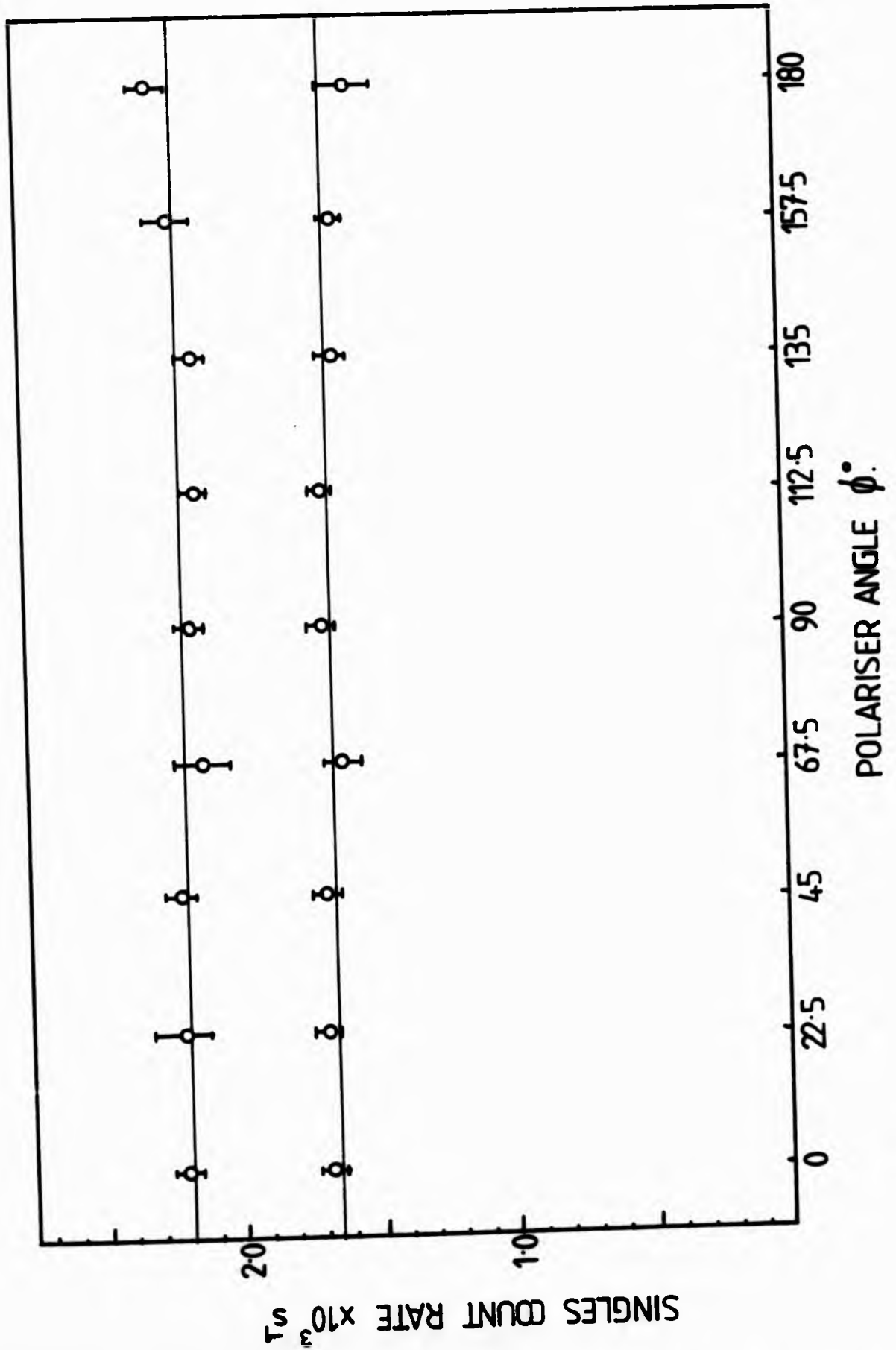


FIG. 32. CHECK ROTATIONAL INVARIANCE OF EACH ARM OF THE OPTICAL SYSTEM. POINTS SHOW MEASURED SINGLES RATES FROM THE COINCIDENCE PM'S AS EACH POLARISER WAS ROTATED. SOURCE OF RADIATION WAS A STABLE NEUTRAL ATOMIC BEAM OF INTENSITY $I_0 = 0.50 \pm 0.01 \cdot 10^{-8} \text{ A}$ EQUIVALENT. ERROR BARS SHOW ONE STANDARD DEVIATION.

Each series of runs (linear, circular polarisation) were normalised to a typical Lyman alpha count rate and beam energy although in practise the effect of variations in beam energy on normalisation were almost negligible.

The linearity between the observed two-photon signal and the Lyman alpha monitor count rate was investigated and the results are shown in Fig. 33. When the incident ion beam is strongly focussed to give the highest metastable densities, the results indicate a spread somewhat larger than would be expected statistically and thus, some additional influence appears to be present. However, when the beam is de-focussed producing lower currents and densities a highly linear region is observed.

This effect may be due partially to the collimation employed which allows a fraction of the metastable flux to reach the metastable monitor system which may not contribute significantly to the observed two-photon signal - this problem was hinted at in section III 23. Also, a focussed beam will have a non-uniform current density (probably Gaussian) so that slight beam instabilities, could result in shifts of the observation volume with respect to the collecting lenses and hence to a variation in the measured coincidence rate.

By de-focussing the incident ion beam into the charge-exchange cell, a much more uniform density parallel atomic beam probably results reducing the atomic beam dimensions at the quench plates and improving linearity as observed. We can regard this procedure as tuning a parallel beam. In general, the beam was de-focussed until the Lyman alpha count rate $\dot{L}_\alpha \leq \frac{1}{2} \dot{L}_\alpha^{\text{(max)}}$ as indicated in Fig. 31. It was under these conditions that the data for linear and circular polarisation were taken.

IV 4.8 Spurious (Background) Coincidence Rate

The rate at which spurious true coincidences are detected depends on the "optical coupling" between the coincidence P.M. photocathodes and

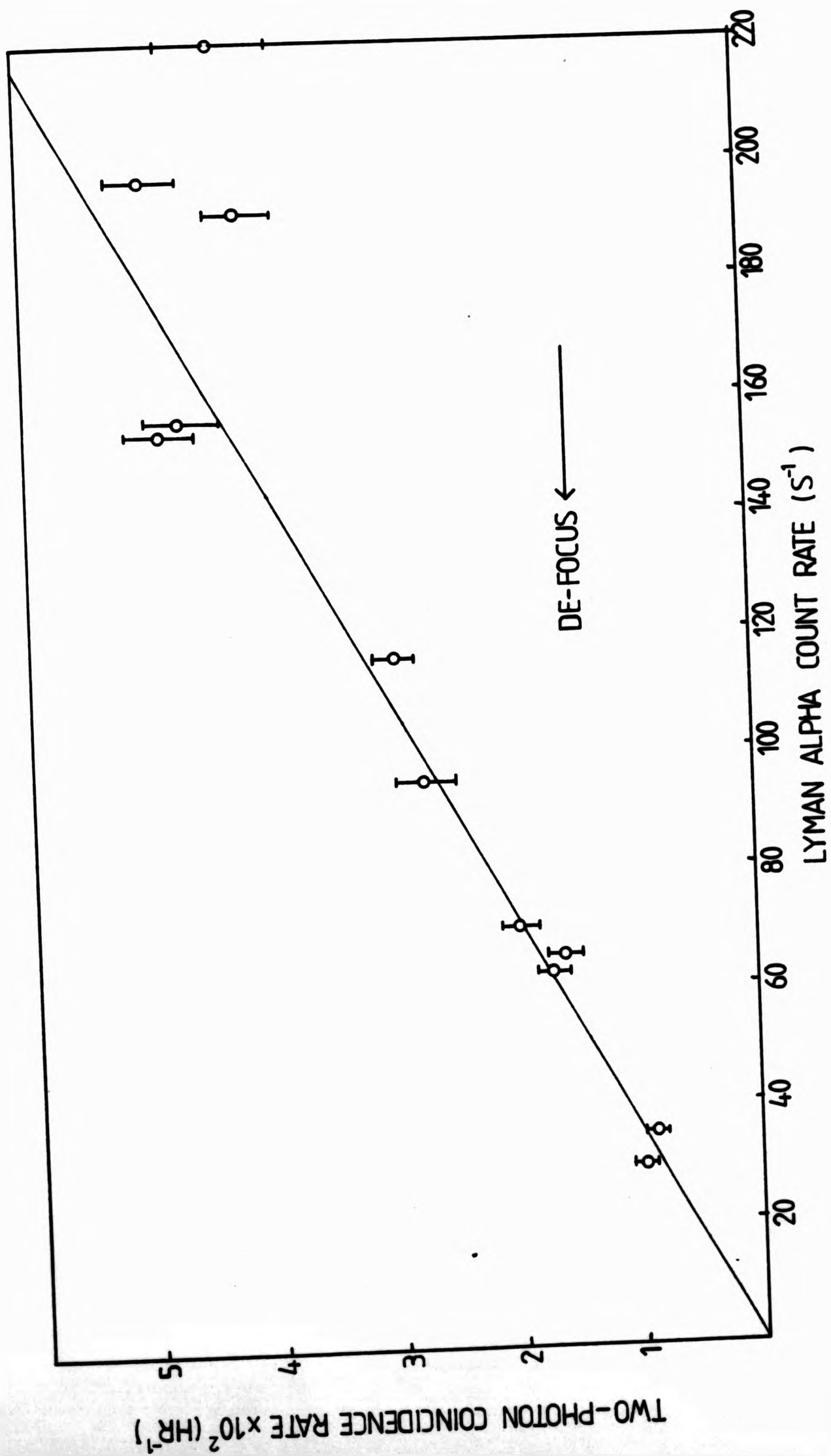


FIG. 33. OBSERVED TWO-PHOTON COINCIDENCE RATE VERSUS LYMAN ALPHA COUNT RATE (METASTABLE DENSITY), VARIED BY DE-FOCUSING THE ION BEAM INTO THE CHARGE EXCHANGE CELL.

decreases as the physical separation between the PM's increases. With the polarisers in place, the P.M. photocathodes are 1.06m apart and the detected background coincidence rate was around $0.5 \cdot 10^{-2} \text{ s}^{-1}$ ($\sim 18 \text{ hr}^{-1}$) most probably due to cosmic rays, radioactivity and electrical pick-up. Thus, the background coincidence rate was almost always considerably less than the two-photon coincidence rate except when the polariser transmission axes were orthogonal. In the case of circular polarisation measurements, the detected background coincidence rate fell considerably to around 2 hr^{-1} due to the reduced apertures on the $\lambda/4$ plates.

Cosmic rays are known to produce large amplitude pulses from the P.M. anodes and the use of differential c.f. discriminators was effective in reducing this contribution to the background by almost 60%.

CHAPTER V: DISCUSSION AND CONCLUSIONS

An atomic beam system capable of producing intense metastable hydrogen and deuterium beams with densities approaching 10^5 atoms cm^{-3} has been constructed using a radio-frequency ion source and caesium charge-exchange cell.

The two-photon decay of the metastable 2S state in deuterium has been investigated in great detail by observing for the first time in a spontaneous second order radiative process, the linear and circular polarisation correlation of the emitted photons.

While previous measurements on the 2S state in the hydrogenic isoelectronic series have confirmed the continuous nature of the two-photon radiation as well as the decay rates and angular correlation of the photons, observation of the polarisation correlation in the present experiment complements and extends previous measurements of this fundamental radiative process.

In particular, the strong linear polarisation correlation demonstrates directly that fine and hyperfine structure have no effect during the simultaneous emission of two photons, in accord with the theoretical predictions while the observed circular polarisation correlation has confirmed the conservation of angular momentum along the common axis of detection.

In addition, the highly correlated state of polarisation of the emitted photons has also given us a rare opportunity to test the predictions of quantum mechanics against those of local realistic ("hidden variable") theories in the form of Bell's Inequality which constrains the correlations between spatially separated systems. The linear polarisation results violate Freedman's form of Bell's Inequality significantly and agree with the QM predictions.

The majority of previous related experiments used to test for the existence of hidden variables i.e. those using annihilation radiation

from positronium and those using visible photons from atomic cascades have also given results in agreement with Q.M. While the results from annihilation quanta, through the lack of efficient polarisers for 0.5MeV photons, cannot test Bell's Inequality directly, nevertheless no reduction in the azimuthal asymmetry for Compton scattering has been observed for source-detector separations up to 24 m ,⁷⁶ confirming that spontaneous localisation has not been observed even when the photon wave-packets are extremely well separated. Such a localisation process might be expected since all known interactions (gravitational, weak, electromagnetic and strong) decrease with distance and hence the physical connections between two microscopic systems should go to zero as their mutual separation increases.

The atomic cascade experiments have the advantage of good signal intensities compared to the present experiment. However, the simultaneous emission of two photons is arguably conceptually closer to the EPR-Bohm Gedanken experiment.¹¹ The simultaneous emission also ensures that the detection events for the two photons are space-like separated in the relativistic sense. With a timing resolution $\tau \approx 2.5\text{ ns}$ this condition is fulfilled if the photodetector separation $d > c\tau$. In the present experiment, where the detectors are separated by a distance $d \approx 1.06\text{ m}$, this condition $d > c\tau$ ($\approx 0.75\text{ m}$) is satisfied.

As in most previous experiments of this nature, the static set-up with fixed polariser orientations during a run has the disadvantage that conceivably, Bell's locality condition might not apply, since the analyser settings are made sufficiently in advance to allow them "to reach some mutual rapport by exchange of signals with velocity less than or equal to light", and hence influence the outcome of measurements without in any way violating causality. If such interactions existed, Bell's theorem would of course no longer apply for static experiments.

This loophole was effectively eliminated in a most impressive recent experiment by Aspect, Dalibard and Roger using the correlated photon pairs from a $J = 0-1-0$ cascade in calcium. They switched their polariser orientations in a time (10ns) significantly shorter than the transit time of the photons (40ns), using acousto-optic switches driven at different frequencies. Although the switching was not truly random, but rather quasi-periodic, nevertheless it is natural to assume that they operated in an uncorrelated way. Their results still showed an impressive violation of Bell's Inequality (by 5σ).

The only remaining loophole for the proponents of local realistic theories lies in the denial of the no-enhancement hypothesis of Clauser and Horne which has to be introduced due to the low efficiency of the photon detectors. Local realistic models with enhancement have been found which can reproduce to a high degree the QM predictions for photon correlation experiments, and in such cases, the hidden variables may play a role at the point of detection so that some photons are detected with higher probabilities than others. It is therefore important to attempt experiments for which the no-enhancement hypothesis is not required and for which local realistic photon models predict significant deviations from quantum theory. An experiment of this type proposed recently by Selleri in which the normal pile-of-plates polarisers are followed by $\lambda/2$ plates could now be attempted with the present apparatus.

A feasible experiment in which this loophole could be eliminated has also been suggested by Lo and Shimony.

Consequently no experiment to date has been performed which can give a completely unequivocal rejection of local realistic theories.

Hence, the debate between the QM and local realistic descriptions of nature is set to continue, fifty years after Einstein, Podolsky and

Rosen first concluded that objective reality is incompatible with the assumption that Quantum Mechanics is complete.

The difficulties regarding the conceptual foundations of quantum theory have troubled many great physicists. No one has contributed more to the exposition and understanding of quantum theory than the late P.A.M. Dirac who wrote in 1975,⁷⁹ "... I think it might turn out that ultimately Einstein will prove to be right, because the present form of QM should not be considered as the final form. There are great difficulties..... in connection with the present QM. It is the best that one can do till now. But, one should not suppose that it will survive indefinitely into the future. And I think that it is quite likely that at some future time, we may get an improved QM in which there will be a return to determinism and which will, therefore, justify the Einstein point of view."

Appendix I

Von Neumann assumed that "dispersion free" states and so hidden variables are impossible. His essential assumption is;

"Any real linear combination of any two Hermitian operators represents an observable and the same linear combination of expectation values is the expectation value of the combination".

Hence for some microstate ψ, λ he assumed that if A and B are Hermitian operators, then

$$\langle A + B \rangle_{\psi, \lambda} = \langle A \rangle_{\psi, \lambda} + \langle B \rangle_{\psi, \lambda} \quad [I]$$

By way of a simple counter-example, Bell showed that dispersion free states have additive expectation values only for commuting operators.

In quantum mechanics,

$$\langle A + B \rangle_{\text{mix}} = \langle A \rangle_{\text{mix}} + \langle B \rangle_{\text{mix}} \quad [II]$$

since $\langle A \rangle_{\text{op}}$, happens to depend linearly even on non-commuting terms in A_{op} , but for dispersion free states, equation [I] is not true in general

Hence Bell showed that one of the axioms on which von Neumann had derived his famous theorem was not justified.

Appendix IIQM Predictions for Detection Probabilities and Geometrical Factors

These have been calculated by M.A.Horne in his Ph.D thesis, and are given as follows;

$$P_1 = \frac{1}{2} \eta_1 f_1(\theta) \xi_+^1$$

$$P_2 = \frac{1}{2} \eta_2 f_2(\theta) \xi_+^2$$

$$P_{12}(\phi) = \frac{1}{2} \eta_1 \eta_2 f_1(\theta) g(\theta) [\xi_+^1 \xi_+^2 + \xi_-^1 \xi_-^2 F_1(\theta) \cos n\phi]$$

$$P_{12}(a', \infty) = \frac{1}{2} \eta_1 \eta_2 f(\theta) \xi_+^1 \dots \dots \dots \text{Polariser II removed}$$

$$P_{12}(\infty, b) = \frac{1}{2} \eta_1 \eta_2 f(\theta) g(\theta) \xi_+^2 \dots \dots \dots \text{Polariser I removed}$$

$$P_{12}(\infty, \infty) = \eta_1 \eta_2 f(\theta) g(\theta) \dots \dots \dots \text{both Polarisers removed}$$

For photons, $n = 2$ and the function $f_1 = f_2 = f(\theta)$ (where θ is the half angle subtended by the collecting lenses) is the probability that the first photon (second photon) enters apparatus I (II) and is given by,

$$f(\theta) = \frac{1}{2} (1 - \cos \theta)$$

The angular correlation factor $g(\theta)$ is given by,

$$g(\theta) = \frac{3}{8} \frac{[G_2(\theta)]^2 + \frac{1}{2} [G_3(\theta)]^2}{1 - \cos \theta}$$

$$\text{The function, } F_1(\theta) = \frac{2[G_1(\theta)]^2}{[G_2(\theta)]^2 + \frac{1}{2}[G_3^2(\theta)]}$$

reflects a slight depolarisation effect due to the non-collinearity of the two photons and approaches unity for infinitesimal detector apertures ($\theta \rightarrow 0$).

The functions $G_1(\theta)$, $G_2(\theta)$, $G_3(\theta)$ are given by,

$$G_1(\theta) = \frac{1}{4} \left[\frac{4}{3} - \cos \theta + \sin^2 \theta - \frac{1}{3} \cos^3 \theta \right]$$

$$G_2(\theta) = \frac{2}{3} - \frac{1}{3} [\sin^2 \theta + 2] \cos \theta$$

$$G_3(\theta) = \frac{4}{3} - \cos \theta - \frac{1}{3} \cos^3 \theta$$

and are valid for a $J = 0-1-0$ cascade and for spontaneous two-photon

emission from the 2S state in hydrogen. The half-angle subtended by the collection lenses is $\theta = 22.6^\circ$ and hence, for our experiment, $F_1(\theta) = 0.996$.

The QM predictions for a $J = 0-1-1$ electric dipole cascade (and for a $J = 1-1-0$, provided the initial statistical state of the atom is isotropic) are obtained by replacing $F_1(\theta)$ with $-F_2(\theta)$, where

$$F_2(\theta) = \frac{2[G_1^2(\theta)]}{2G_2(\theta)G_3(\theta) + \frac{1}{2}[G_3^2(\theta)]}$$

APPENDIX III

DATA FOR LINEAR POLARISATION CORRELATION AND TEST OF BELL'S INEQUALITY) IS RELATIVE POLARISER ANGLES R(0) IS NORMALISED COINCIDENCE RATE, AND DIFFERENCE IN SIGMA APPLIES TO LEAST SQUARES FIT TO THE DATA (FIG.27). ∞ DENOTES REMOVAL OF POLARISER PLATES.

RUN	ϕ	OBS R(ϕ)	DIFF IN SIGMA.
155	22.5	221.2 \pm 16.1	- 0.7344
156	22.5	206.9 \pm 16.9	- 1.5458
157	22.5	230.8 \pm 8.7	- 0.2556
159	67.5	48.2 \pm 12.0	0.2015
160	67.5	26.5 \pm 10.8	- 1.7854
161	67.5	62.8 \pm 11.4	- 1.4928
162	22.5	224.3 \pm 9.6	- 0.9087
163	67.5	61.7 \pm 12.9	1.2340
164	67.5	41.1 \pm 16.3	- 0.2872
165	∞	652.7 \pm 38.2	-
166	∞	637.3 \pm 27.5	-
167	∞	718.2 \pm 29.2	-
170	∞	679.2 \pm 37.6	-
171	∞	624.7 \pm 20.6	-
172	∞	664.0 \pm 22.2	-
173	22.5	218.8 \pm 10.8	- 1.3170
174	67.5	45.4 \pm 10.1	- 0.0378
175	∞	696.1 \pm 41.6	-
176	∞	743.1 \pm 24.9	-
177	22.5	266.4 \pm 17.6	1.8964
179	22.5	280.2 \pm 16.4	2.8766
180	67.5	29.2 \pm 16.7	- 0.9929
181	67.5	52.1 \pm 16.2	0.3900
182	0	279.7 \pm 27.5	0.2872
183	0	276.4 \pm 22.6	0.2034
184	22.5	271.3 \pm 21.9	1.7478
185	45.0	119.9 \pm 21.1	- 0.9243
187	0	329.0 \pm 26.1	2.1915
189	0	275.9 \pm 21.9	0.1871
190	45	136.8 \pm 17.8	- 0.1462
191	45	125.4 \pm 18.0	- 0.7779
192	90	19.5 \pm 14.0	0.8927
193	135	171.1 \pm 20.9	1.5166
201	0	281.6 \pm 40.3	0.2431
202	0	278.7 \pm 21.4	0.3223
205	135	135.0 \pm 21.4	- 0.2057
206	180	262.2 \pm 37.3	- 0.2574
207	180	233.0 \pm 22.0	- 1.7638
208	157.5	203.6 \pm 19.6	- 1.5012
209	112.5	55.0 \pm 14.9	0.6187
210	90	-14.8 \pm 18.0	- 1.2113
211	45	119.6 \pm 21.0	- 0.9211
214	0	295.6 \pm 22.2	1.0720
216	0	285.2 \pm 18.4	0.7281
225	0	285.8 \pm 30.5	0.4589
228	180	257.9 \pm 22.1	- 0.6291
231	180	292.8 \pm 30.0	0.6999
232	180	246.8 \pm 30.1	- 0.8307

APPENDIX CONTINUED

RUN	ϕ	OBS R(ϕ)	DIFF. IN SIGMA
233	157.5	234.0 \pm 22.0	0.0444
234	135	131.3 \pm 21.1	- 0.3982
235	90	5.8 \pm 18.3	- 0.0657
236	112.5	61.0 \pm 30.1	0.5056

237
 238
 239
 240
 241
 242
 243
 244
 245
 246
 247
 248
 249
 250
 251
 252
 253
 254
 255
 256
 257
 258
 259
 260

References

1. J.A. Wheeler, Ann. New York Acad. Sci. 48 219 (1946)
2. C.S. Wu and I Shakhov Phys. Rev. 77 136 (1950)
3. C.N. Yang, Phys Rev. 77 (1950)
4. J.F. Clauser, M.A. Horne, A Shimony, and R.A. Holt, Phys. Rev. Lett. 23 880 (1969)
5. A. Einstein, B. Podolsky, and N. Rosen, Phys. Rev. 47 777 (1935)
6. N. Bohr, Phys. Rev. 48, 696 (1935)
7. J. von Neumann, Mathematische Grundlagen der Quantummechanik. (Julius Springer-Verlag, Berlin, 1932), (English translation, Princeton University Press (1955).
8. D. Bohm, Phys. Rev. 85, 166, 180 (1952)
9. J.S. Bell, Rev. Mod. Phys. 38, 447 (1966)
10. J.S. Bell, Phys.1, 195 (1964)
11. D. Bohm, Quantum Theory (Prentice-Hall, Inc, Englewood Cliffs New Jersey, 1951) p. 614.
12. C.A. Kocher and E.D. Commins, Phys. Rev. Lett. 18, 575 (1967)
13. A. Aspect, P. Grangier, and G. Roger, Phys. Rev. Lett. 47, 460 (1981)
14. A.Aspect, P. Grangier, and G. Roger, Phys. Rev. Lett. 49, 91 (1982)
15. A.Aspect, J. Dallibard, and G. Roger, Phys. Rev. Lett. 49 1804 (1982)
16. T.W. Marshall, E. Santos, and F. Selleri, Phys. Rev. Lett. 98A, 5 (1983)
17. T.W. Marshall, E. Santos, and F. Selleri, Lett. Nuovo. Cim. 38, 417 (1983)
18. T.W. Marshall, Phys. Lett. 99A, 163 (1983)
19. T.W. Marshall, Phys. Lett. 100A, 225 (1984)

20. F. Selleri, Lett. Nuovo Cim. 39, 252 (1984)
21. G. Breit and E. Teller, Astrophys. J. 91, 215 (1940)
22. M. Goeppert-Mayer, Ann. Phys. 9, 273 (1931)
23. L. Spitzer and J.L. Greenstein, Astrophys. J., 114, 407 (1951)
24. J. Shapiro and E. Breit, Phys. Rev. 113, 179 (1959)
25. S. Klarsfeld, Phys. Lett. 30A, 382 (1969)
26. B.A. Zon and L.P. Rapaport, Sov. Phys. - JETP 7, 52 (1968)
27. W.R. Johnson, Phys. Rev. Lett. 29, 1123 (1972)
28. S.P. Goldman and G.W.F. Drake, Phys. Rev. A. 24 (1981)
29. F.A. Parpia and W.R. Johnson, Phys. Rev. A. 26, 1142 (1982)
30. P.L. Knight and L. Allen, Concepts of Quantum Optics, Pergamo press, Headington Hill Hall, Oxford, 1982) p.27
31. D. Marcuse, Engineering Quantum Electrodynamics, Harcourt Brace and World Inc, New York (1970)
32. D. O' Connell, Ph.D. thesis, Stirling University, 1975 (unpublished).
33. G. Baym, Lectures on Quantum Mechanics, W.A. Benjamin Inc. Reading, Massachusetts, (1977).
34. R.W. Schmeider, and R. Marrus, Phys. Rev. Lett., 25, 1612, (1970)
35. C.A. Kocher, J.E. Clendin, and R. Novick, Phys. Rev. Lett., 29, 615, (1972)
36. M.H. Prior, Phys. Rev. Lett, 29, 611, (1972)
37. R. Marrus and R.W. Schmeider, Phys. Rev. A., 5, 1160 (1972)
38. H. Kruger and A. Oed, Phys. Lett. 54A, 251 (1975)
39. C.L. Cocke, B. Curnutte, J.R. McDonald, J.A. Bednar, and R. Marrus, Phys. Rev. A. 9, 2242 (1974)
40. E.A. Hinds, J.F. Clendenin, and R. Novick, Phys. Rev. A. 17, 670 (1978)
41. H. Gould and R. Marrus, Phys. Rev. A. 28, 2001 (1983)
42. M. Liples, R. Novick, and N. Tolk, Phys. Rev. Lett, 15, 690, (1965)

20. F. Selleri, Lett. Nuovo Cim. 39, 252 (1984)
21. G. Breit and E. Teller, Astrophys. J. 91, 215 (1940)
22. M. Goeppert-Mayer, Ann. Phys. 9, 273 (1931)
23. L. Spitzer and J.L. Greenstein, Astrophys. J., 114, 407 (1951)
24. J. Shapiro and E. Breit, Phys. Rev. 113, 179 (1959)
25. S. Klarsfeld, Phys. Lett. 30A, 382 (1969)
26. B.A. Zon and L.P. Rapaport, Sov. Phys. - JETP 7, 52 (1968)
27. W.R. Johnson, Phys. Rev. Lett. 29, 1123 (1972)
28. S.P. Goldman and G.W.F. Drake, Phys. Rev. A. 24 (1981)
29. F.A. Parpia and W.R. Johnson, Phys. Rev. A. 26, 1142 (1982)
30. P.L. Knight and L. Allen, Concepts of Quantum Optics, Pergamo press, Headington Hill Hall, Oxford, 1982) p.27
31. D. Marcuse, Engineering Quantum Electrodynamics, Harcourt Brace and World Inc, New York (1970)
32. D. O' Connell, Ph.D. thesis, Stirling University, 1975 (unpublished).
33. G. Baym, Lectures on Quantum Mechanics, W.A. Benjamin Inc. Reading, Massachusetts, (1977).
34. R.W. Schmeider, and R. Marrus, Phys. Rev. Lett., 25, 1612, (1970)
35. C.A. Kocher, J.E. Clendin, and R. Novick, Phys. Rev. Lett., 29, 615, (1972)
36. M.H. Prior, Phys. Rev. Lett, 29, 611, (1972)
37. R. Marrus and R.W. Schmeider, Phys. Rev. A., 5, 1160 (1972)
38. H. Kruger and A. Oed, Phys. Lett. 54A, 251 (1975)
39. C.L. Cocke, B. Curnutte, J.R. McDonald, J.A. Bednar, and R. Marrus, Phys. Rev. A. 9, 2242 (1974)
40. E.A. Hinds, J.F. Clendenin, and R. Novick, Phys. Rev. A. 17, 670 (1978)
41. H. Gould and R. Marrus, Phys. Rev. A. 28, 2001 (1983)
42. M. Liples, R. Novick, and N. Tolk, Phys. Rev. Lett, 15, 690, (1965)

43. C.J. Artura, N. Tolk, and R. Novick, *J. Astrophys.*, 157, L181 (1969).
44. D. O'Connell, K.J. Kollath, A.J. Duncan, and H. Kleinpoppen, *J. Phys. B*, 8, L214, (1975).
45. J.F. Clauser and A. Shimony, *Rep. Prog. Phys.* 41, 1881, (1978)
46. T.W. Hänsch, L. Schalow, and G.W. Series, *Sci. American*, March 1979. See also V.Dose, *Contemp. Phys.*, 23, 129, (1982)
47. B. d'Espagnat, Conceptual Foundation of Quantum Mechanics Benjamin, Menlo Park, California (1971)
48. E. Merzbacher, Quantum Mechanics, J. Wiley and Sons Inc. (1967)
49. N. Bohr, *Phys. Rev.* 48, 696 (1935)
50. F.J. Belinfante, "A Survey of Hidden Variable Theories", Pergamon Press, (1973)
51. J.M. Jauch, and C. Piron, *Helv. Phys. Acta* 36, 827 (1963)
52. A.M. Gleason, *J. Math and Mech.* 6, 885 (1957)
53. J.F. Clauser, and M.A. Horne, *Phys. Rev.* D10, 526 (1974)
54. D.Bohm, and Y. Aharonov, *Phys. Rev* 108, 1070 (1957)
55. P.J. Bussey, *Phys. Lett.* 90A, 9, (1982)
56. E. Schrödinger, *Proc. Comb. Phil. Soc.* 31, 555 (1935)
57. W.H. Furry, *Phys. Rev.* 49, 393 (1936)
58. J.F. Clauser and A. Shimony, *Rep. Prog. Phys.*, 41, 1881, 1978
59. M.A. Horne, Ph. d. Thesis, Boston University, 1970.
60. S.J. Freedman, and J.F. Clauser, *Phys. Rev. Lett.*, 28, 938 (1972)
61. R.A. Holt, and F.M. Pipkin, unpublished. See also R.A. Holt, Ph. D. Thesis, Harvard University (1973)
62. J.F. Clauser, *Il Nuovo Cimento* 33, 740 (1976)
63. E.S. Fry and R.C. Thomson, *Phys. Rev. Lett.* 37 465 (1976)

64. J. Freedman, Lawrence Berkley Laboratory Report No. LBL - 391, 1972 (unpublished)
65. J.F. Clauser, Phys. Rev. A, 6, 49 (1972)
66. M. Bacal, A. Truc, H.J. Doucet, M. Lamain, and M. Chretien, Nucl. Instr. Meth., 114, 407, (1974). See also M. Bacal and W. Reichelt, Rev. Sci. Inst., 20, 769 (1974).
67. R.L. Fitzwilson and E.W. Thomas, Phys. Rev. A, 3, 1305 (1971)
68. B.L. Donnally, T. Clapp, W. Sawyer and M. Schultz, Phys. Rev. Lett., 12, 502 (1964)
69. P. Pradel, F. Roussel, A.S. Schlachter, G. Spiess, and A. Valance Phys. Rev. A, 10, 797 (1974)
70. J.D. Carriere and F.J. de Heer, J. Chem. Phys., 56, 2993, (1972)
71. R. Novick, Physics of the One and Two-Electron Atoms, edited by F. Bopp and H. Kleinpoppen, North Holland, Amsterdam (1969)
72. G.C. King, F.H. Read and R.E. Imhof, J. Phys. B 8, 665 (1975)
73. J.R. Peterson and Y.K. Bae, Phys.Rev.A 30, 2807 (1984). See also D.P. de Bruijn, J. Neutelboom, V. Sidis and J. Los, Chem. Phys., 85 715 (1984)
74. G.K.T. Conn and G.K. Eaton, J. Opt Soc., Am., 44, 553 (1954)
75. A.J. Duncan, private communication
76. D,K. Butt, Birkbeck College, University of London , private communication
77. F. Selleri, Phys. Lett, 108A, 197 (1985)
78. T.K. Lo and A. Shimony, Phys. Rev. A 23, 3003 (1981)
79. P.A.M. Dirac, "Directions in Physics", edited by H. Hora and J.R. Shepanski (Sidney, 1976).
80. G. Spiess, A. Valance, and P. PRadel, Phys Rev. A, 6 746, (1972).